STUDIES OF THE RELATIONSHIP BETWEEN THE SURFACE ELECTROMYOGRAM, JOINT TORQUE AND IMPEDANCE

by

Chenyun Dai

A Thesis
Submitted to the Faculty
of the
WORCESTER POLYTECHNIC INSTITUTE
in partial fulfillment of the requirements for the
Degree of Doctor of Philosophy
in
Electrical and Computer Engineering,
2016

APPROVED:

Professor Edward A. Clancy, Major Advisor, WPI ECE

Professor Donald R. Brown, Committee Member, WPI ECE

Todd R. Farrell, Ph.D., Committee Member, Liberating Technologies, Inc., Holliston, MA

Denis Rancourt, Ph.D., Committee Member, Université de Sherbrooke, Canada

Abstract

This compendium-format dissertation (i.e., comprised mostly of published and in-process articles) primarily reports on system identification methods that relate the surface electromyogram (EMG)—the electrical activity of skeletal muscles—to mechanical kinetics. The methods focus on activities of the elbow and hand-wrist. The relationship between the surface EMG and joint impedance was initially studied. My work provided a complete second-order EMG-based impedance characterization of stiffness, viscosity and inertia over a complete range of nominal torques, from a single perturbation trial with slowly varied torque. A single perturbation trial provides a more convenient method for impedance evaluation. The RMS errors of the EMG-based method were 20.01% for stiffness and 7.05% for viscosity, compared with the traditional mechanical measurement.

Three projects studied the relationship between EMG and force/torque, a topic that has been studied for a number of years. Optimal models use whitened EMG amplitude, combining multiple EMG channels and a polynomial equation to describe this relationship. First, we used three techniques to improve current models at the elbow joint. Three more features were extracted from the EMG (waveform length, slope sign change rate and zero crossing rate), in addition to EMG amplitude. Each EMG channel was used separately, compared to previous studies which combined multiple channels from biceps and, separately, from triceps muscles. Finally, an exponential power law model was used. Each of these improvement techniques showed better performance ($P<0.05$ and ~0.7 percent maximum voluntary contraction (%MVC) error reduction from a nominal error of 5.5%MVC) than the current "optimal" model. However, the combination of pairs of these techniques did not further improve results. Second, traditional prostheses only control 1 degree of freedom (DoF) at a time. My work provided evidence for the feasibility of controlling 2-DoF wrist movements simultaneously, with a minimum number of electrodes. Results suggested that as few as four conventional electrodes, optimally located about the forearm, could provide 2-DoF simultaneous, independent and proportional control with error ranging from 9.0–10.4 %MVC, which is similar to the 1-DoF approach (error from 8.8–9.8 %MVC) currently used for commercial prosthesis control. The third project was similar to the second, except that this project studied controlling a 1-DoF wrist with one hand DoF simultaneously. It also demonstrated good performance with the error ranging from 7.8-8.7 %MVC, compared with 1-DoF control.

Additionally, I participated in two team projects—EMG decomposition and static wrist EMG to torque—which are described herein.

Acknowledgement

First and foremost, I shall greatly thank my academic advisor, Dr. Edward A. Clancy. He is not only a respectable and responsible person, but also provides valuable guidance and support to my research. I am looking forward to work with him in the future.

Thanks to my committee members, Dr. Donald R. Brown, Dr. Denis Rancourt, Dr. Todd Farrell for providing data and many good suggestions.

Thanks to my senior alumnus Lukai Liu, my senior alumna Pu Liu and my research partners Yejin Li and Ziling Zhu. They give me a lot of help on my research.

Thanks to my family. My parents Zhiyuan Dai and Jiangang Dai, the most important persons for me; give me life, love and whatever I want unconditionally. Also, my wife Yizhou Cao gives me much support in my life.

Table of Contents

Chapter 1: Introduction

The introduction includes two parts, a background and a description of the contributions of my Ph.D. work. The background part introduces some biomedical knowledge related with my projects and some signal processing techniques used. The contribution part introduces the current state of the research field for each project and gives an overall summary of my new contributions to the corresponding research field. And then, the final sub-section of this part summarizes my whole Ph.D. work and the main content of the rest of the dissertation chapters.

1.1 EMG and Its Signal Processing Background

In this part, some biomedical background and signal processing techniques are introduced. Sections 1.1.1, 1.1.2 and 1.1.3 describe the generation of the electromyogram (EMG) signal based on neuromuscular motor units, and an electrical engineering model of the EMG signal. Section 1.1.4 introduces the features we extract from the EMG signal, and the related signal processing methods.

1.1.1 Structure of Muscle and Motor Unit

EMG is the electrical signal generated by our muscles. When we walk or do exercise, our muscles always support us to produce these movements. Human muscle mainly contains a combination of two kinds of muscle fibers, which are respectively called slow twitch fibers (Type 1) and fast twitch fibers (Type 2). The slow twitch fibers are capable of sustaining low forceful contraction without too much fatigue for long periods; while the fast twitch fibers can generate a quicker and more forceful contraction, but fatigue much more rapidly. Both types of fibers cooperate with each other to fulfill different tasks. The detailed structure of skeletal muscle is depicted in Figure 1(a). One whole muscle usually consists of many parallel muscle fascicles, which are interspersed by connective tissues, blood vessels, sensory tissue, etc. Fascicles are a collection of parallel muscle fibers. These muscle fibers are innervated by branches of attached neurons. All fibers innervated by one neuron are near each other, but not necessarily adjacent. One motor unit is defined as one motor nerve and all innervated muscle fibers (Figure 1(b)). All muscle fibers in one motor unit are of the same type. And the contraction of one motor unit (in healthy muscle) obeys a rule called “all or nothing,” which means if one motor unit is activated, all of its innervated fibers will subsequently contract. One single muscle is comprised of a group of motor units which work together to coordinate different contractions, but the quantity of motor units

varies from muscle to muscle. Generally, muscles with larger size contain more motor units, but are less finely able to control force.

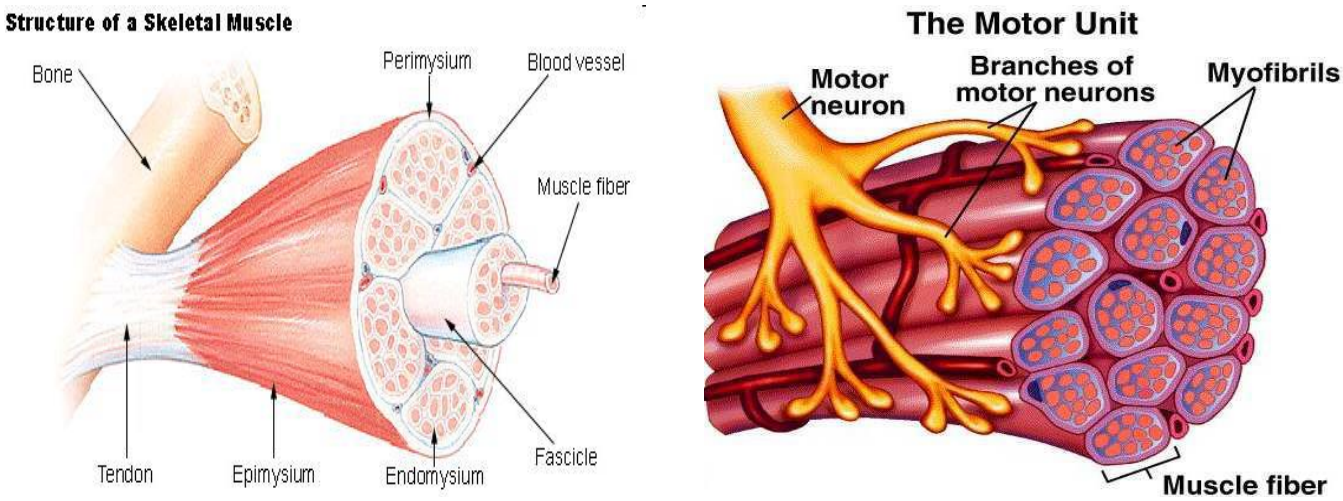

Figure 1: a) The structure of a skeletal muscle [1] b) The structure of a muscle fiber [2]

1.1.2 Muscle Electrical Activity and Its Engineering Model

When the central nervous system sends a command to a motor neuron, the motor neuron will electro-chemically activate muscle fibers. Then, those fibers depolarize, which leads to muscle contraction. After depolarization, the muscle fibers quickly repolarize to a rest state. This whole electrical process generates an electromagnetic field. The electromagnetic field can be recorded within muscle (indwelling EMG) or on the skin surface (surface EMG). Indwelling EMG is an invasive recording, which requires electrical needles/wires penetrating into human skin; while surface EMG is a non-invasive method to collect EMG signals. This thesis includes both indwelling EMG and surface EMG projects. Figure 2 shows the time course of depolarization-repolarization in one individual motor unit. The rest potential is often around –70 mV, which is based on the concentration of ions in body cells and fluid. When muscle fibers are activated, the action potential peaks around +30 mV. The duration of one action potential is usually 2–4 ms or longer. When the overall muscle continues to contract, the same motor unit will successively generate a series of action potentials with quite similar shape. Different motor units often produce different action potentials with different shapes. When humans perform different motions, the muscles require a different number of activated motor units to complete different tasks. The frequency of motor unit discharging is called firing rate. In general, a more forceful motion needs more activated motor units, and the firing rate of each motor unit also increases. The process of activating more motor units is called the recruitment of motor units. The force level is measured by

percent maximum voluntary contraction (%MVC) level. Usually, the firing rate is about 5–10 pulses per second when initially recruited and can be up to 20^{+} pulses per second at the highest force levels. The firing intervals are not perfectly periodic.

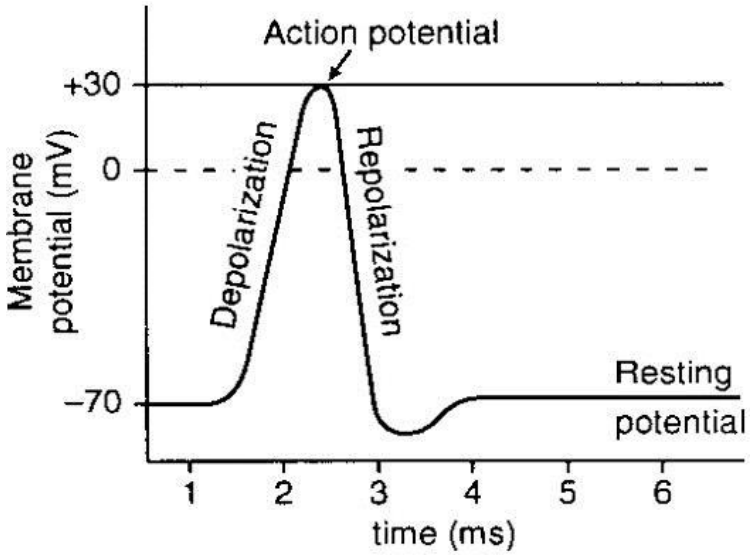

Figure 2: Electrical activity of one individual motor unit [3]

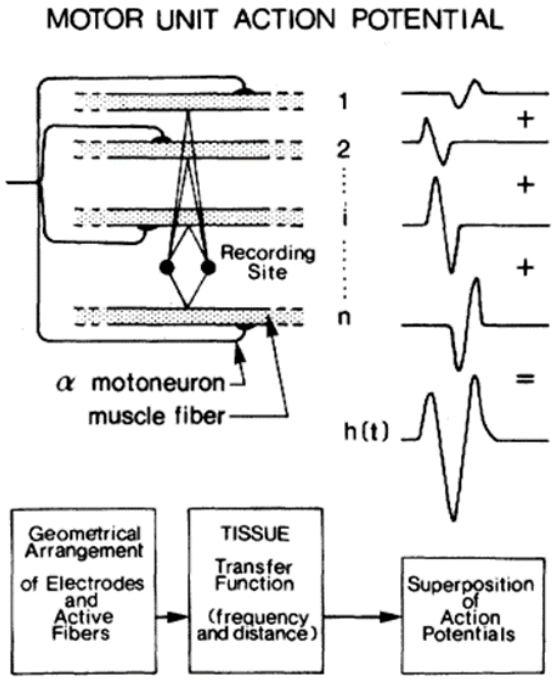

Figure 3: Schematic representation of the generation of the motor unit action potential [4]

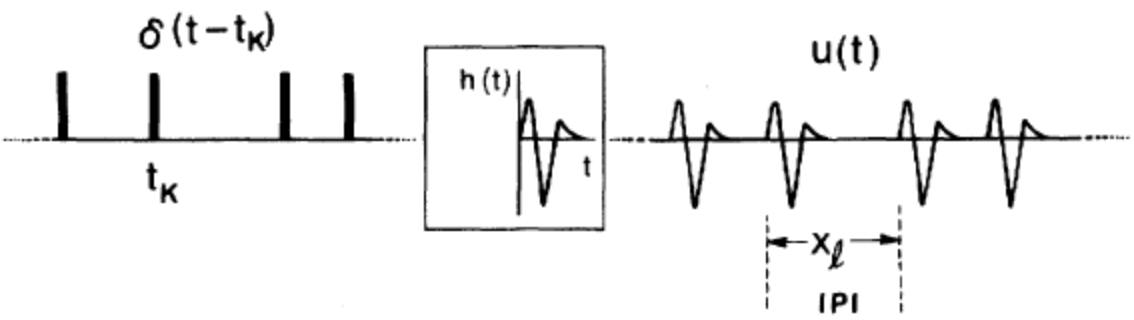

Figure 4: Schematic for the motor unit action potential train [4]

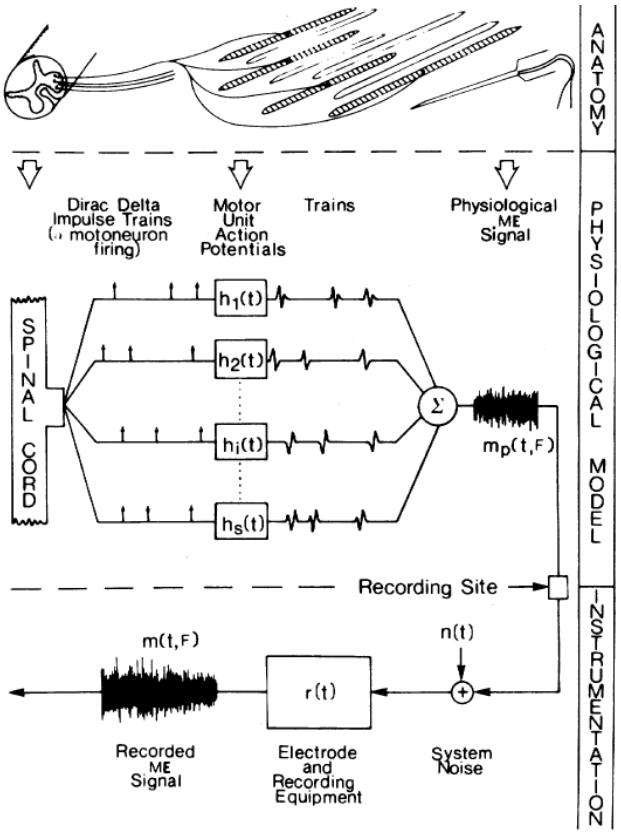

Figure 5: Complete engineering model of motor unit action potential [4]

As mentioned before, one motor unit always generates similar shape of action potential for healthy muscles, while different motor units typically produce different action potential shapes. Figure 4 shows the model of one individual motor unit. The shape of a motor unit action potential sometimes may vary due to muscle fatigue or disease. When muscle contraction level increases, several different motor units may discharge at the same time. Figure 3 shows this case as the superposition of potentials from individual fibers. When the muscle generates force, each motor unit produces successive motor unit

action potentials. This process can be modeled as: the nerve sends a series of stimuli (an impulse train) through its innervated muscle fibers (system). Then, the output can be regarded as an impulse response train. When many motor units are active at the same time, the EMG recording would be the summation of these impulse response trains. Therefore, the EMG recording looks like a random Gaussian process (i.e., the sum of many mostly-independent, rather identically shaped pulses). The total engineering model is shown as Figure 5. When EMG signal is recorded, it will include some system noise. Finally, this noisy signal may be pre-processed by some hardware filters.

1.1.3 EMG Recording

Based on the method of EMG data collection, EMG recordings can be separated as indwelling EMG and surface EMG. Traditional indwelling EMG requires a needle (or wire) to insert into muscle through skin, so the electrode location is quite close to motor units. A wireless invasive approach is under development. Indwelling needle/wire EMG is typically used to view only a few motor units of one muscle, due to the small pick-up area of these electrodes. Needles for indwelling recordings are quite small. Figure 6 shows two common needles for single channel indwelling EMG recording (Figure 6(a), Consolidated Neuro Supply, Inc.) and multiple channel indwelling EMG recording during research studies (Figure 6(b)). Since the raw EMG signal is the sum of motor unit action potentials, one obvious project for indwelling EMG is EMG decomposition which separates the composite interference pattern into its constituent motor unit action potential trains. Chapters 2–4 describe our EMG decomposition project in detail.

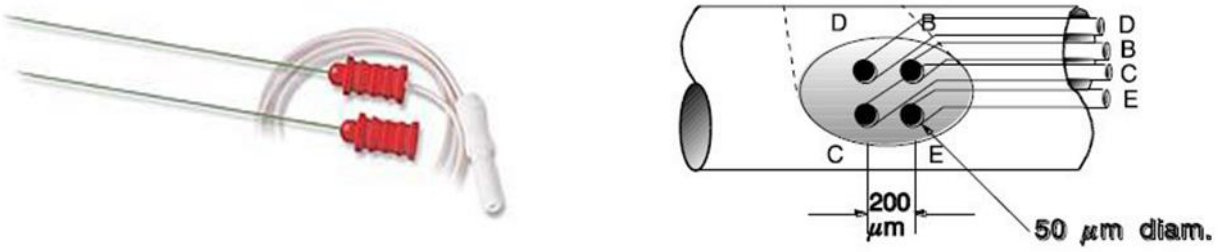

Figure 6: a) concentric (single-channel) needle; b) quadrifilar (multiple channel) needle.

However, surface EMG recording is quite different from indwelling recording. It is a non-invasive approach, in which the electrodes are secured to the skin surface. Several surface electrodes (conventional: 8mm diameter) are attached to the skin. The skin surface is often cleaned with alcohol and gelled to ensure good conductivity between the electrodes and the measured muscle. Figure 7 shows

a sample of one type of custom-made surface EMG bipolar electrodes. Chapters 5–end introduce several kinds of surface EMG projects.

Figure 8 shows one example of indwelling EMG recording (left) and surface EMG (right). From the indwelling EMG recording, each motor unit action potential is relatively easy to identify, since only a few unit motors are simultaneously viewed. The surface EMG recording looks like an amplitude-modulated random signal and cannot distinguish individual motor unit action potential spikes.

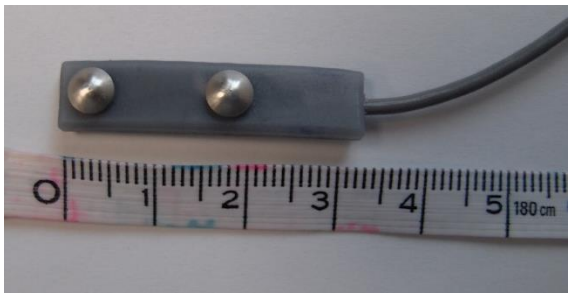

Figure 7: One pair of surface EMG electrode contacts within their plastic tab encasement.

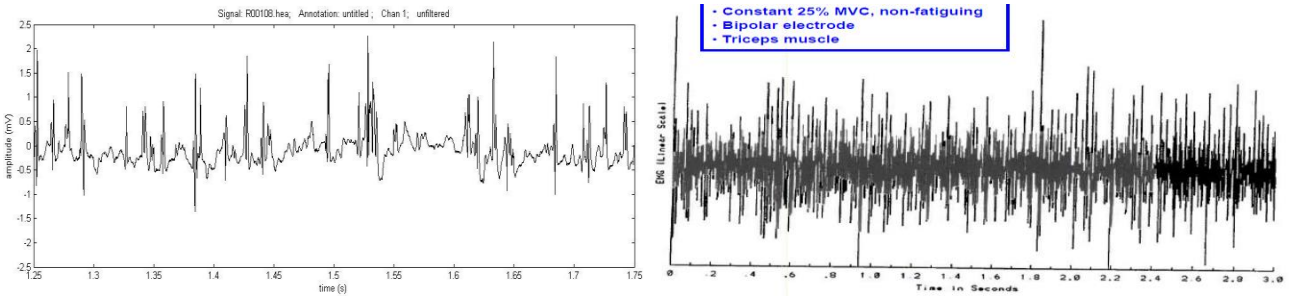

Figure 8: a) Indwelling EMG recording; b) Surface EMG recording [5]

1.1.4 Several Important EMG Signal Processing Methods

The raw EMG signal, either indwelling or surface EMG, contains a lot of noise and other interference. The signal processing methods in the remaining chapters (papers) usually only briefly describe the noise and interference. However, this thesis focuses on EMG signal processing. This small section separately introduces several important EMG signal processing methods for my EMG projects.

High-pass filter for EMG decomposition: The portion of an indwelling signal's power that exist under 1000 Hz is known to look quite similar across motor units. It is a quite adverse factor for some indwelling EMG recording projects, especially for EMG decomposition. A high-pass filter normally with 1000 Hz cut-off frequency was built, which can not only solve this issue, but also eliminate some low background noise. Filter with cut-off frequency higher than 1000 is also not recommended, since it

decreases signal to noise ratio after filter. Figure 10 shows the comparison between the unfiltered and filtered signal.

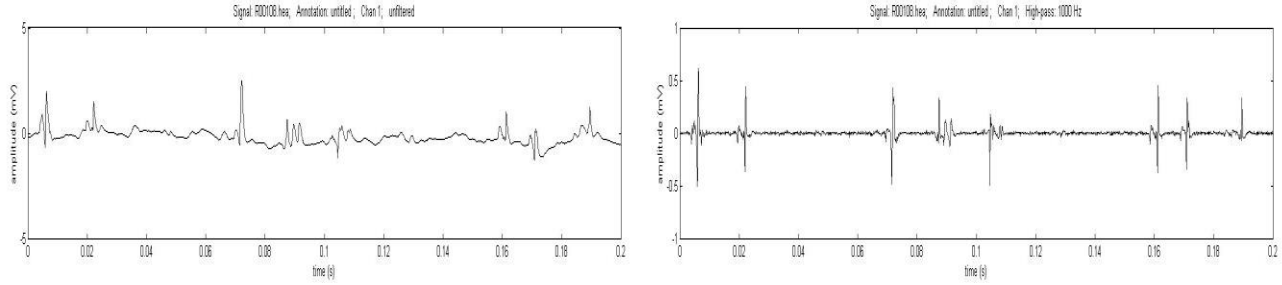

Figure 9: a) Unfiltered indwelling recording b) High-pass filtered indwelling recording

EMG amplitude estimator: As mentioned in section 1.1.3, each motor unit discharging can be regarded as an impulse response train. Therefore, when many motor units contract at the same time, the EMG signal would be the sum of lots of impulse response trains and can be regarded as an amplitude modulated, zero-mean, random Gaussian process. The math expression for this Gaussian process model is: $m[n] = s[n] \cdot v[n]$, where n is the discrete-time sample index, $m[n]$ is raw EMG signal, $s[n]$ is EMG amplitude and $v[n]$ is a random process with unit variance. One important feature which can be extracted from the EMG signal is EMG amplitude.

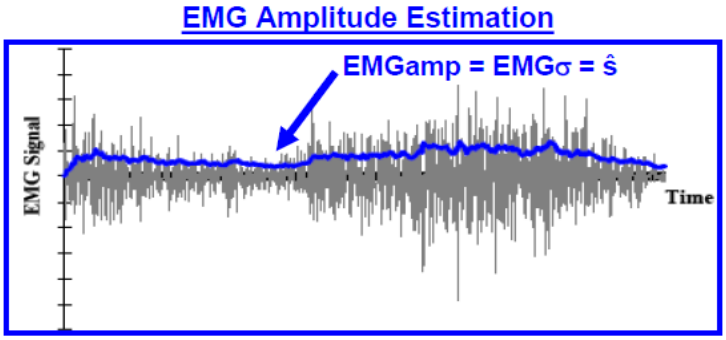

Figure 10: Diagram of EMG amplitude estimation [5]

Therefore, EMG amplitude is defined as the time-varying standard deviation of $m[n]$. A moving average filter can be used to estimate it: $\hat{s}_{MARMS}[n] = \frac{1}{L} \cdot \sum_{k=n-L+1}^{n} |m[k]|$. It performs as a low pass filter of the rectified signal. The window length, L, determines the cut-off frequency. A longer window has a low cut-off frequency, which can reduce $v[n]$ random errors and increase $s[n]$ bias errors, and vice versa [6]. The EMG amplitude estimator can be improved by removal of measurement noise, EMG signal whitening, multiple EMG channels, optimal detectors and optimal smoothing. The bandwidth of EMG amplitude is usually about 0–10 Hz and the noise often has a much broader band, so a low-pass

filter can be used for removing the noise. EMG signal whitening techniques decorrelate the data samples, allowing subsequent analysis to individually operate on each EMG sample. Multiple EMG channels means that a group of electrodes are used for detecting EMG from the same muscle; combining their information can reduce the variance. Optimal smoothing means to pick a suitable window for $\hat{s}_{MARMS}$. Usually, longer windows are picked when EMG amplitude changes slowly, while shorter windows for fast change. Since filtering causes start-up transient issue at the beginning of signal (see step 5 in figure 11), this start-up part will be discarded for data analysis.

Hence, the entire EMG amplitude estimator can be summarized as the block diagram below:

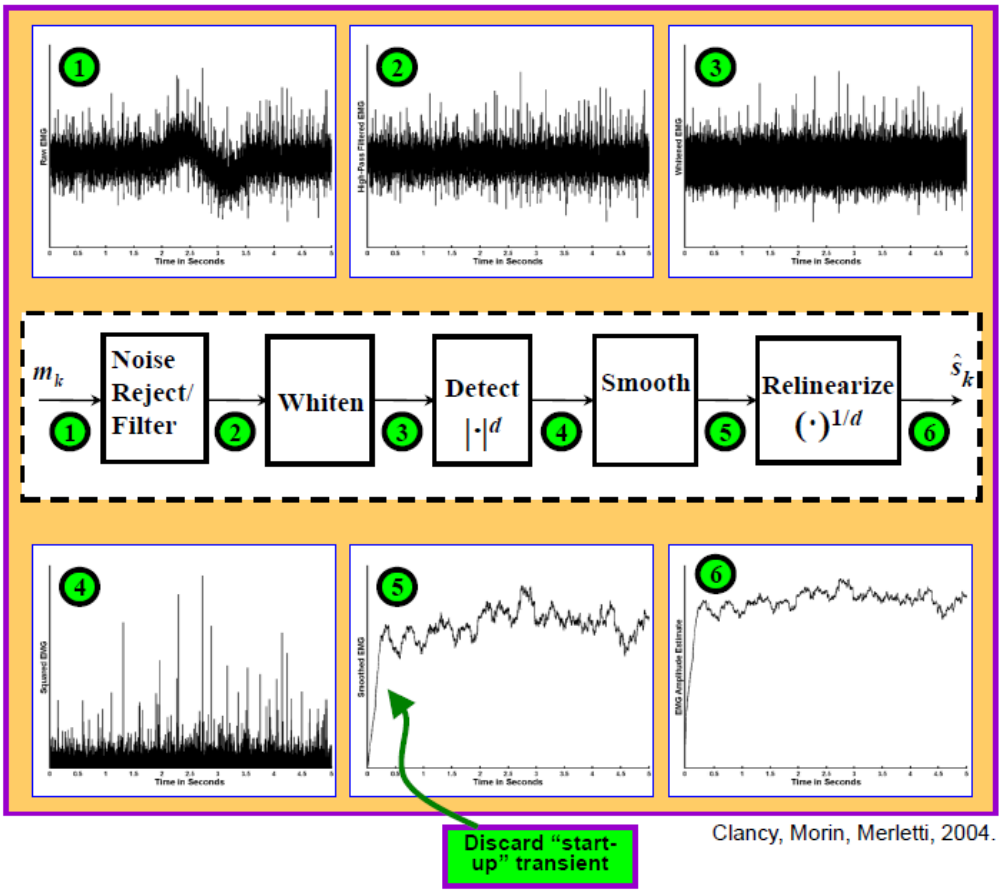

Figure 11: Detailed signal processing procedure of EMG amplitude estimation [7]

Other EMG features: Some researchers found that if more features were extracted from the raw EMG signal besides amplitude, it can improve the performance of surface EMG studies that relate surface EMG to movement classes or to force. Three common features are: waveform length, zero crossing and slope sign changes [8].

The waveform length feature describes the sum of the absolute difference between two adjacent points. The equation for waveform length is:

$$\Delta x_k = |x_{k+1} - x_k|,$$

where x_k is the k^{th} sample of EMG signal for $k = 1, \ldots, N-1$. The zero crossing feature is defined as:

$$count\ as\ 1,\ if\ x_k > 0\ and\ x_{k+1} < 0,\ or\ x_k < 0\ and\ x_{k+1} > 0,$$
$$and\ |x_k - x_{k+1}| > noise\ level.$$

Slope sign changes indicate the local peaks of the EMG signal:

$$count\ as\ 1, if\ x_k > x_{k-1} and\ x_k > x_{k+1},\ or\ x_k < x_{k-1}\ and\ x_k < x_{k+1},$$
$$and\ |x_k - x_{k+1}| > noise\ level\ or\ |x_k - x_{k-1}| > noise\ level$$

1.2 Current State of the Research Field and My Contributions

This section introduces the current state of the research field and my contributions for each of my projects. The projects in which I was the lead investigator during my Ph.D. study are EMG impedance project, dynamic elbow EMG to torque with improved methods project, dynamic wrist EMG to torque project and dynamic hand-wrist EMG to torque project. Additionally, EMG decomposition project and static wrist EMG to torque project are two team projects in which I was involved. The main analysis of EMG decomposition project was finished during my M.S. degree, and the revision work and publication were done during my Ph.D. degree. The rest of the projects were mostly finished during my Ph.D. degree. One small summary section for each project is presented in this part.

1.2.1 EMG Impedance Project

Current research field: Researchers have been studying the relationship between the surface electromyogram (EMG) and joint torque for a number of years [9-14]. However, when muscles contract, it can not only generate joint torque but also joint mechanical impedance [15]. Joint impedance exists because of the mechanical properties of soft tissues (muscles, tendons, nerves and ligaments) and is a necessary property of the musculoskeletal system because it helps stabilize our movements. Accurate measurement of joint mechanical impedance in daily activities would provide new insights on the origin of several musculoskeletal disorders [16, 17]. Previous studies found that a second order quasi-linear

model can describe joint dynamics in terms of the relationship between angle and torque for constant-effort, constant-posture contractions [18, 19]. The equation of this model is:

$$T(t) = I\,\ddot{\theta}(t) + B\,\dot{\theta}(t) + K\theta(t)$$

where T and θ are torque and angle which subtract the base mean torque and angle respectively (similar as standard deviation); t is the time index; K, B and I are the stiffness, viscosity and inertia fitting coefficients respectively. This method requires perturbation trials conducted at distinct torque levels, imparting forces on the body, disturbing the task under study; a situation quite undesirable for taking in situ measurements during applied tasks. This method means if we want to measure different torque levels, numerous time-consuming repeated trials are required.

My contribution in this field: The stiffness and viscosity increase with force/torque [18]. At the same time, the surface EMG also increases. My contribution was to relate surface EMG to joint impedance, and provide a complete second-order characterization which includes stiffness, viscosity and inertia. My work provided a new perspective which related surface EMG to estimate stiffness, viscosity and inertia. In addition, I used a single perturbation trial with slow varied torque to evaluate impedance over a complete range of nominal torques, which provided a much faster measurement than previous methods.

1.2.2 Elbow EMG to Torque with Improved Techniques Project

Current research field: For several decades, commercial myoelectric prostheses have used surface electromyogram activity from the residual biceps and triceps to control elbow joint movement [10-12]. In the early stage of research, investigators used simple proportional models between EMG and elbow torque [20-24]. This approach was functional, but with high error. From then on, numerous techniques have been used to reduce the error for this EMG-based method, including modeling both agonist and antagonist muscle activity [10, 25-27], accounting for subject-to-subject differences in the relationship [23,28], reducing EMG amplitude (EMGσ) variability by whitening the EMG signal and/or (for large muscle groups) utilizing multiple-channel EMGσ estimators [29-35], modeling EMG-torque dynamics [13, 36-38], incorporating a range of joint angles [14, 39-42], and applying robust system identification methods [11-13, 28, 38]. The various techniques are relevant in several areas in which a noninvasive EMG-torque estimate is useful, such as prosthesis control [43, 44], clinical biomechanics [45, 46] and ergonomics assessment [47, 48]. The current "best" model uses a polynomial function, multiple EMG

channels but combined into two groups (biceps EMG and triceps EMG), whitening of the EMG signal and modeling EMG-torque dynamics [12].

My contribution in this field: My contribution to this field is using three techniques to improve current models. First, I extracted three more features—waveform length, slope sign change rate and zero crossing rate—from raw EMG signals instead of EMG amplitude only (see section 1.1.4). Second, I used each EMG channel separately, rather than previous studies which combine multiple channels from biceps (and separately from triceps) into a combined processed EMG. Third, I used an exponential power law model to replace the previous polynomial model. Three new methods were individually compared with the current "best" model. Then, I examined if combining pairs of these various improvement techniques provides an additive benefit. Each of the individual improvement techniques showed a better performance ($P<0.05$ and ~10-15% error improvement) than the current "optimal" model. However, the pair combinations of these three techniques have a limited further improvement. Therefore, the three improved methods can provide more precise results for EMG to torque estimation.

1.2.3 Two-DoF Dynamic/Static Wrist EMG to Torque Using a Minimum Number of Electrodes Project

Current research field: Over 95% of traumatic upper-limb extremity amputations are transradial or more distal [49]. Commercial myoelectric hand-wrist prostheses return partial function by using surface electromyogram signals from the residual forearm muscles to control wrist extension-flexion (this DoF is still under development and will soon be a product) (Ext-Flx), radial-ulnar deviation (Rad-Uln) and pronation-supination (Pro-Sup), respectively. Most current models only control one degree of freedom (DoF) at one time. However, many basic daily tasks require simultaneous activation of more than one joint [50].

For multiple DoF control, some current studies try to realize 2-DoF control. First, Kuiken and colleagues developed targeted muscle reinnervation surgery [51, 52]. However, the high cost, invasive surgery and long recovery period likely limit its acceptability. Second, another improvement technique is based on the multifunction pattern recognition approach to select desired movements of the hand and/or wrist via EMG signals from the forearm (recently commercialized [53]). Continuous control is realized by applying pattern recognition throughout the EMG signal stream [54-58]. Multi-joint control is facilitated, but still only 1-DoF is operated at a time.

For proportional, simultaneous and independent control of multiple joints, most researchers used a large number of EMG electrodes in an array and found that the performance of algorithms is highly related to the number of EMG channels [59, 60]. They used a high density of EMG electrodes to obtain a more precise evaluation. However, such an amount of electrodes could not be used in a commercial prostheses. And some of them did not explore the influence or feasibility of reducing the quantity of EMG channels.

My contribution in this field: For the 2-DoF *static* wrist EMG to torque project, Prof. Clancy led the work. I helped him debug and analyze the experimental data.

For the 2-DoF *dynamic* wrist EMG to torque project, I led the data analysis. My task was to provide evidence for the feasibility of controlling 2-DoFs of wrist simultaneously. In addition, my study explored the minimum number of electrodes required for 2-DoFs hand control. Backward stepwise selection of EMG channels was utilized to study the minimum required number of EMG channels. This method progressively reduced the number of channels, removing the channel with the highest associated error at each step. The study results supported the use of as few as four conventional electrodes for 2-DoF of simultaneous, independent and proportional (SIP) prosthesis control at the wrist. Two-DoF EMG-force models using four electrodes had average RMS errors of 9.0–10.4 %MVC, which was similar to the one-DoF error (8.8-9.8%MVC). The results of my work showed that the existing one-DoF EMG-torque control model can be expanded to two-DoF control, and using less electrodes was feasible.

1.2.4 2-DoF Dynamic Hand-Wrist EMG to Torque Using a Minimum Number of Electrodes Project

Current research field: The current research field is similar as section 1.2.3 (Two-DoF dynamic/static wrist only EMG to torque using a minimum number of electrodes project). First, most current models only control one degree of freedom (DoF) at one time, especially control wrist or hand separately. In addition to the multiple DoF control research mentioned in section 1.2.3, other related studies have explored EMG-based control for multiple fingers [61-64]. Some of these studies used pattern recognition/ classification, which does not provide simultaneous, independent and proportional (SIP) control; there was also some limited effort to quasi-constant-force contractions, which does not model dynamic control. Second, the quantity of electrodes was highly correlated with the performance of torque estimation. Some of the prior studies did not explore the feasibility of reducing the number of electrodes.

My contribution in this field: My contribution of this field is similar as section 1.2.4 (Two-DoF dynamic/static wrist only EMG to torque using a minimum number of electrodes project). The results suggested as few as four conventional electrodes, optimally located about the forearm, could provide 2 DoFs of simultaneous, independent and proportional control with error ranging from 7.8–8.7 %MVC, which is rates similar to the 1-DoF approach (error from 8.3–9.0 %MVC) currently used for commercial prosthesis control. A prosthesis user could target 2-DoF towards control of an existing hand-wrist system. So, the above wrist work was helpful, but the more immediate opportunity is to simultaneously control both a hand and a wrist.

1.2.5 EMG Decomposition Project

Current research field: As mentioned in section 1.1.2, the raw EMG signal is the superposition of different motor unit action potentials. EMG decomposition of indwelling recording is used to separate the composite signal into its constituent motor unit action potential trains (see figure 13). EMG decomposition is widely used for clinical and scientific studies of the neuromuscular system [65-67], especially for muscle disease and fatigue. For most decomposition studies, an accurate automated algorithm is required. DeLuca and his colleagues were the pioneers of this field [68-69]. Thereafter, some other automated decomposition methods were developed [70-72]. During the early phase of this research area, manual decomposition was performed [73]. This method is quite time-consuming, and also requires experienced people. Another approach which is useful for quantifying the performance of algorithms is to utilize simulated EMG signals whose true annotations are known [74-77]. However, this method cannot mimic the experimental data completely. The third method which uses multiple channel data has been performed recently. The motor unit action potentials are detected by a group of electrodes. If the decomposition results of different electrodes have a high agreement, this gives a strong reliability of the decomposition algorithm. However, little literature has systematically discussed the strengths and weakness of previous automated methods, and very little direct or cross comparison between the different algorithms was studied.

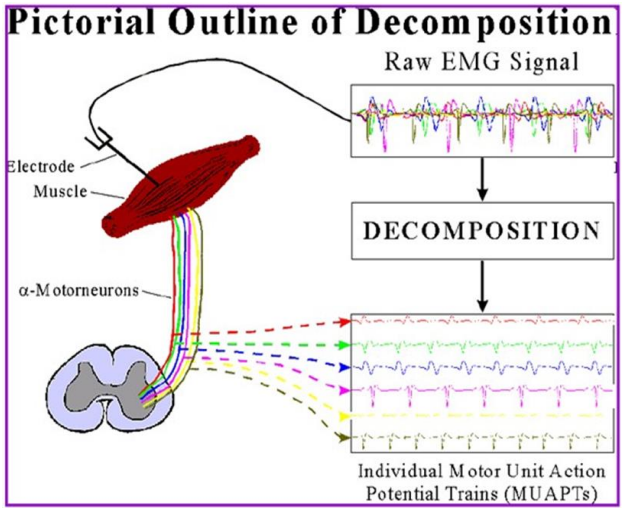

Figure 12: Diagram for EMG decomposition [78]

My contribution in this field: This project is a team project finished by Yejin Li and me. The contribution of our team project to this field was to evaluate the performance of three publicly available automated algorithms— EMGlab, Fuzzy Expert and Montreal [70-72] — using both experimental and simulated data, producing an overall evaluation of performance. My comparison information is important to the interpretation of results across studies using different analysis techniques. For the multiple channel experimental data, median agreement between the Montreal and Fuzzy Expert algorithms at 10%, 20% and 50% MVC were 95, 86 and 64%, respectively. For the single channel control and patient data, median agreement between pairs of the three algorithms was ~97% and ~92%, respectively, for each pair. Agreement across algorithms and accuracy within algorithms were strongly related to the Decomposability Index (DI). When agreement was high between algorithm pairs applied to the simulated data, so was the individual accuracy of each algorithm. My role of this team project was to generate simulated EMG data, apply three algorithms to both experimental and simulated data and cross-compare the performance of three algorithms.

1.2.6 Summary of My PhD Work and Introduction of Remaining Chapters

The remaining chapters describe all of my Ph.D. projects in detail in the form of published, accepted, submitted and in-development journal or conference manuscripts.

Chapters 2–4 are about the EMG decomposition project. First, in Chapter 2, we focus on cross-comparison of three EMG decomposition algorithms. This chapter was published as a journal paper. Second, in Chapter 3, the same three EMG decomposition algorithms were compared but based on an alternative performance measure. This chapter was published as a conference paper. Third, in Chapter 4,

only two multiple channel EMG decomposition algorithms were compared. This chapter was published as a conference paper.

Chapter 5 details the EMG impedance project. This chapter is still in preparation and going to be submitted as a journal paper.

Chapter 6 focuses on dynamic elbow EMG to torque with improved methods project. This chapter is still in preparation and going to be submitted as a journal paper, which is now under review.

Chapters 7–10 describe the two degree of freedom (DoF) hand-wrist EMG to torque project. First, in Chapter 7, we discuss the 2-DoF static wrist EMG to torque project. This chapter is still in preparation and going to be submitted as a journal paper, which is now under review. Second, in Chapter 8, we discuss the 2-DoF dynamic wrist EMG to torque project. The muscle effort discussed in this Chapter is dynamic instead of static in Chapter 7. This chapter is still in preparation and going to be submitted as a journal paper. Third, in Chapter 9, we focus on 2-DoF dynamic hand-wrist EMG to torque project. The 2-DoF effort in this chapter involved the hand-wrist. This chapter is still in preparation and going to be submitted as a journal paper. Fourth, in Chapter 10, we assessed mirrored bi-lateral training for able-bodied subjects. This chapter has been published as a conference paper.

References

[1] http://en.wikipedia.org/wiki/Muscle_fascicle

[2] http://academic.wsc.edu/faculty/jatodd1/351/ch6outline.html

[3] http://www.physicsforums.com/showthread.php?t=473984

[4] DeLuca**,** "Physiology and mathematics of myoelectric signals," *IEEE Trans Biomed Eng* 26(6): 313–325, 1979

[5] Edward A. Clancy, Stochastic Modeling of the Relationship Between the Surface Electromyogram and Muscle Torque. Ph.D. Thesis, Massachusetts Institute of Technology, January 1991.

[6] Edward A. Clancy, "Electromyogram Amplitude Estimation with Adaptive Smoothing Window Length," *IEEE Transactions on Biomedical Engineering*, Vol. 46, No. 6, pp. 717-729, 1999.

[7] Edward A. Clancy, Evelyn L. Morin and Roberto Merletti, "Sampling, Noise-Reduction and Amplitude Estimation Issues in Surface Electromyography," *Journal of Electromyography and Kinesiology*, Vol. 12, No. 1, pp. 1–16, 2002.

[8] B. Hudgins, P. Parker, and R. N. Scott, "A new strategy for multifunction myoelectric control," *IEEE Trans. Biomed. Eng.,* vol. 40, pp. 82–94, 1993.

[9] An KN, Cooney WP, Chao EY, Askew LJ, Daube JR. "Determination of forces in extensor pollicis longus and flexor pollicis longus of the thumb," *J Appl Physiol: Respirat Environ Exercise Physiol* 54:714–719, 1983.

[10] Clancy EA, Hogan N. "Relating agonist-antagonist electromyograms to joint torque during isometric, quasi-isotonic, nonfatiguing contractions," *IEEE Trans Biomed Eng* 44(10):1024–1028, 1997.

[11] Edward A. Clancy, Oljeda Bida and Denis Rancourt, "Influence of advanced electromyogram (EMG) amplitude processors on EMG-to-torque estimation during constant-posture, force-varying contractions," *Journal of Biomechanics*, Vol. 39, pp. 2690–2698, 2006.

[12] Edward A. Clancy, Lukai Liu, Pu Liu and Daniel V. Moyer, "Identification of Constant-Posture EMG-Torque Relationship About the Elbow Using Nonlinear Dynamic Models," *IEEE Transactions on Biomedical Engineering*, Vol. 59, No. 1, pp. 205–212, 2012.

[13] Hashemi J, Morin E, Mousavi P, Mountjoy K, Hashtrudi-Zaad K, "EMG-Force Modeling Using Parallel Cascade Identification," *J Electromyogr Kinesiol* 22:469–477, 2012.

[14] Hashemi J, Morin E, Mousavi P, Hashtrudi-Zaad K, "Surface EMG Force Modeling with Joint Angle Based Calibration," *J Electromyogr Kinesiol* 23:416–424, 2013.

[15] Burdet E, Osu R, Franklin DW, Milner TE, Kawato, M. "The central nervous system stabilizes unstable dynamics by learning optimal impedance," *Nature* 414:446–449, November 2001.

[16] Rancourt D, Hogan N. "Dynamics of pushing," J Motor Behavior 33(4):351–362, 2001a.

[17] Rancourt D, Hogan N. "Stability in force production tasks," *J Motor Behavior* 33(2):193–204, 2001b.

[18] Hunter IW, Kearney RE. "Dynamics of human ankle stiffness: Variation with mean ankle torque," *J Biomech* 15(1):747–752, 1982.

[19] Kearney RE, Hunter W. "System identification of human joint dynamics," *CRC Crit Reviews Biomed Eng* 18(1):55–87, 1990.

[20] J. Vredenbregt and G. Rau, "Surface electromyography in relation to force, muscle length and endurance," *New Developments Electromyogr. Clin. Neurophysiol.,* vol. 1, pp. 607–622, 1973.

[21] V. T. Inman, H. J. Ralston, J. B. Saunders, B. Feinstein, and E. W. Wright, "Relation of human electromyogram to musculuar tension," *EEG Clin. Neurophysiol.,* vol. 4, pp. 187–194, 1952.

[22] J. H. Lawrence and C. J. De Luca, "Myoelectric signal versus force relationship in different human muscles," *J. Appl. Physiol.: Respirat. Environ. Exercise Physiol.,* vol. 54, pp. 1653–1659, 1983.

[23] Z. Hasan and R. M. Enoka, "Isometric torque-angle relationship and movement-related activity of human elbow flexors: Implications for the equilibrium-point hypothesis," *Exp. Brain Res.,* vol. 59, pp. 441–450, 1985.

[24] C. W. Heckathorne and D. S. Childress, "Relationships of the surface electromyogram to the force, length, velocity, and contraction rate of the cineplastic human biceps," *Am. J. Phys. Med.,* vol. 60, pp. 1–19, 1981.

[25] R. H. Messier, J. Duffy, H. M. Litchman, P. R. Raslay, J. F. Soechting, and P. A. Stewart, "The electromyogram as a measure of tension in the human biceps and triceps muscles," *Int. J. Mech. Sci.,* vol. 13, pp. 585–598, 1971.

[26] K. N. An, W. P. Cooney, E. Y. Chao, L. J. Askew, and D. J. R., "Determination of forces in extensor pollicis longus and flexor pollicis longus of the thumb," *J Appl Physiol,* vol. 54, pp. 714–719, 1983.

[27] M. Solomonow, A. Guzzi, R. Baratta, H. Shoji, and R. D'Ambrosia, "EMG-force model of the elbows antagonistic muscle pair," *Am. J. Phys. Med.,* vol. 65, pp. 223–244, 1986.

[28] D. G. Thelen, A. B. Schultz, S. D. Fassois, and J. A. Ashton-Miller, "Identification of dynamic myoelectric signal-to-force models during isometric lumber muscle contractions," *J. Biomech.,* vol. 27, pp. 907–919, 1994.

[29] N. Hogan and R. W. Mann, "Myoelectric signal processing: Optimal estimation applied to electromyography—Part I: Derivation of the optimal myoprocessor," *IEEE Trans. Biomed. Eng.,* vol. 27, pp. 382–395, 1980.

[30] N. Hogan and R. W. Mann, "Myoelectric signal processing: Optimal estimation applied to electromyography—Part II: Experimental demonstration of optimal myoprocessor performance," *IEEE Trans. Biomed. Eng.,* vol. 27, pp. 396–410, 1980.

[31] M. I. A. Harba and P. A. Lynn, "Optimizing the acquisition and processing of surface electromyographic signals," *J. Biomech. Eng.,* vol. 3, pp. 100–106, 1981.

[32] E. A. Clancy and N. Hogan, "Single site electromyograph amplitude estimation," *IEEE Trans. Biomed. Eng.,* vol. 41, pp. 159–167, 1994.

[33] E. A. Clancy and N. Hogan, "Multiple site electromyograph amplitude estimation," *IEEE Trans. Biomed. Eng.,* vol. 42, pp. 203–211, 1995.

[34] J. R. Potvin and S. H. M. Brown, "Less is more: High pass filtering, to remove up to 99% of the surface EMG signal power, improves EMG-based biceps brachii muscle force estimates," *J. Electromyo. Kinesiol.,* vol. 14, pp. 389–399, 2004.

[35] D. Staudenmann, I. Kingma, A. Daffertshofer, D. F. Stegeman, and J. H. van Dieen, "Heterogeneity of muscle activation in relation to force direction: A multi-channel surface electromyography study on the triceps surae muscle," *J. Electromyo. Kinesiol.,* vol. 19, pp. 882–895, 2009.

[36] G. L. Gottlieb and G. C. Agarwal, "Dynamic relationship between isometric muscle tension and the electromyogram in man," *J Appl Physiol,* vol. 30, pp. 345–351, 1971.

[37] T. D. Sanger, "Bayesian filtering of myoelectric signals," *J. Neurophysiol.,* vol. 97, pp. 1839–1845, 2007.

[38] J. Hashemi, E. Morin, P. Mousavi, and K. Hashtrudi-Zaad, "Enhanced dynamic EMG-force estimation through calibration and PCI modeling," *IEEE Trans. Neural Sys. Rehabil. Eng.,* vol. 23, pp. 41–50, 2015.

[39] A. L. Hof and J. Van den Berg, "EMG to force processing I: An electrical analogue of the Hill muscle model," *J. Biomech.,* vol. 14, pp. 747–758, 1981.

[40] E. P. Doheny, M. M. Lowery, D. P. FitzPatrick, and M. J. O'Malley, "Effect of elbow joint angle on force-EMG relationships in human elbow flexor and extensor muscles," *J Electromyogr Kinesiol,* vol. 18, pp. 760–770, 2008.

[41] J. Hashemi, E. Morin, P. Mousavi, and K. Hashtrudi-Zaad, "Surface EMG force modeling with joint angle based calibration," *J Electromyogr Kinesiol,* vol. 23, pp. 416–424, 2013.

[42] P. Liu, L. Liu, and E. A. Clancy, "Influence of joint angle on EMG-torque model during constant-posture, torque-varying contractions," *IEEE Trans. Neural Sys. Rehabil. Eng.,* vol. 23, pp. 1039–1046, 2015.

[43] R. W. Mann and S. D. Reimers, "Kinesthetic sensing for the EMG controlled "Boston Arm"," *IEEE Trans. Man-Mach. Sys.,* vol. 11, pp. 110–115, 1970.

[44] P. Parker, K. Englehart, and B. Hudgins, "Myoelectric signal processing for control of powered limb prostheses," *J. Electromyo. Kinesiol.,* vol. 16, pp. 541–548, 2006.

[45] C. A. M. Doorenbosch and J. Harlaar, "A clinically applicable EMG-force model to quantify active stabilization of the knee after a lesion of the anterior cruciate ligament," *Clin. Biomech.,* vol. 18, pp. 142–149, 2003.

[46] C. Disselhorst-Klug, T. Schmitz-Rode, and G. Rau, "Surface electromyography and muscle force: Limits in sEMG-force relationship and new approaches for applications," *Clin. Biomech.,* vol. 24, pp. 225–235, 2009.

[47] S. Kumar and A. Mital, *Electromyography in Ergonomics*. Briston, PA: Taylor & Francis, 1996.

[48] G. M. Hagg, B. Melin, and R. Kadefors, "Applications in ergonomics," in *Electromyography: Physiology, Engineering, and Noninvasive Applications*, R. Merletti and P. A. Parker, Eds., ed: IEEE Press/Wiley-Interscience, 2004, pp. 343–363.

[49] T. R. Dillingham, L. E. Pezzin, and E. J. MacKenzie, "Limb Amputation and Limb Deficiency: Epidemiology and Recent Trends in the United States," *South. Med. J.,* vol. 95, pp. 875–883, 2002.

[50] D. J. Atkins, D. C. Y. Heard, and W. H. Donovan, "Epidemilogic overview of individuals with upper-limb loss and their reported research priorities," *J. Prosthet. Orthot.,* vol. 8, pp. 2–11, 1996.

[51] T. A. Kuiken, G. A. Dumanian, R. D. Lipschutz, L. A. Miller, and K. A. Stubblefield, "The use of targeted muscle reinnervation for improved myoelectric prosthesis control in a bilateral shoulder disarticulation amputee," *Prosthet. Orthot. Int.,* vol. 28, pp. 245–253, 2004.

[52] T. A. Kuiken, G. Li, B. A. Lock, R. D. Lipschutz, L. A. Miller, K. A. Stubblefield, *et al.*, "Targeted muscle reinnervation for real-time myoelectric control of multifunction artificial arms," *J. Am. Med. Assoc.,* vol. 301, pp. 619–628, 2009.

[53] Coapt, LLC. (Chicago, IL, accessed 6 June 2015). Available: http://www.coaptengineering.com.

[54] D. Graupe and W. K. Cline, "Functional separation of EMG signals via ARMA identification methods for prosthesis control purposes," *IEEE Trans. Sys. Man Cyber.,* vol. 5, pp. 252–259, 1975.

[55] B. Hudgins, P. Parker, and R. N. Scott, "A new strategy for multifunction myoelectric control," *IEEE Trans. Biomed. Eng.,* vol. 40, pp. 82–94, 1993.

[56] R. Boostani and M. H. Moradi, "Evaluation of the forearm EMG signal features for the control of a prosthetic hand," *Physiol. Meas.,* vol. 24, pp. 309–319, 2003.

[57] K. Englehart and B. Hudgins, "A robust, real-time control scheme for multifunction myoelectric control," *IEEE Trans. Biomed. Eng.,* vol. 50, pp. 848–854, 2003.

[58] M. A. Powell, R. R. Kaliki, and N. V. Thakor, "User training for pattern recognition-based myoelectric prostheses: Improving phantom limb movement consistency and distinguishability," *IEEE Trans. Neural Sys. Rehabil. Eng.,* vol. 22, pp. 522–532, 2014.

[59] S. Muceli, N. Jiang, and D. Farina, "Extracting signals robust to electrode number and shift for online simultaneous and proportional myoelectric control by factorization algorithms," *IEEE Trans. Neural Sys. Rehabil. Eng.,* vol. 22, pp. 623–633, 2014.

[60] N. Jiang, H. Rehbaum, I. Vujaklija, B. Graimann, and D. Farina, "Intuitive, online, simultaneous, and proportional myoelectric control over two degrees-of-freedom in upper limb amputees," *IEEE Trans. Neural Sys. Rehabil. Eng.,* vol. 22, pp. 501–510, 2014.

[61] H.-P. Huang and C.-Y. Chen, "Development of a myoelectric discrimination system for a multi-degree prosthetic hand," *Proc. IEEE Int. Conf. Robotics Automat.,* pp. 2392–2397, 1999.

[62] P. Liu, D. R. Brown, E. A. Clancy, F. Martel, and D. Rancourt, "EMG-force estimation for multiple fingers," *IEEE Sig. Proc. Med. Biol. Symp.,* 2013.

[63] C. Cipriani, F. Zaccone, S. Micera, and M. C. Carozza, "On the shared control of an EMG-controlled prosthetic hand: Analysis of user-prosthesis interaction," *IEEE Trans. Robotics,* vol. 24, pp. 170–184, 2008.

[64] Y. Huang, K. B. Englehart, B. Hudgins, and A. D. C. Chan, "A gaussian mixture model based classification scheme for myoelectric

[65] S. H. Nawab, R. P. Wotiz, and C. J. DeLuca, "Decomposition of indwelling EMG signals," *J. Appl. Physiol.*, vol. 105, pp. 700–710, 2008.

[66] D. Stashuk, "EMG signal decomposition: How can it be accomplished and used?," *J. Electromyogr. Kinesiol.*, vol. 11, pp. 151–173, 2001.

[67] R. C. Thornton and A. W. Michell, "Techniques and applications of EMG: Measuring motor units from structure to function," *J. Neurol.*, vol. 259, pp. 585–594, 2012.

[68] R. S. LeFever and C. J. DeLuca, "A procedure for decomposing the myoelectric signal into it constituent action potentials—Part I: Technique, theory, and implementation," *IEEE Trans. Biomed. Eng.*, vol. 29, pp. 149–157, 1982.

[69] R. S. LeFever, A. P. Xenakis, and C. J. DeLuca, "A procedure for decomposing the myoelectric signal into it constituent action potentials—Part II: Execution and test for accuracy," *IEEE Trans. Biomed. Eng.*, vol. 29, pp. 158–164, 1982.

[70] K. C. McGill, Z. C. Lateva, and H. R. Marateb, "EMGLAB: An interactive EMG decomposition program," *J. Neurosci. Meth.*, vol. 149, pp. 121–133, 2005.

[71] Z. Erim and W. Lin, "Decomposition of intramuscular EMG signals using a heuristic fuzzy expert system," *IEEE Trans. Biomed. Eng.*, vol. 55, pp. 2180–2189, 2008.

[72] J. R. Florestal, P. A. Mathieu, and K. C. McGill, "Automatic decomposition of multichannel intramuscular EMG signals," *J. Electromyogr. Kinesiol.*, vol. 19, pp. 1–9, 2009.

[73] J. Fang, G. C. Agarwal, and B. T. Shahani, "Decomposition of multiunit electromyographic signals," *IEEE Trans. Biomed. Eng.*, vol. 46, pp. 685–697, 1999.

[74] D. Ge, E. Le Carpentier, Farina D, "Unsupervised Bayesian decomposition of multiunit EMG recordings using tabu search," *IEEE Trans. Biomed. Eng.*, vol. 57, pp. 561–571, 2010.

[75] R. Gut and G. S. Moschytz, "High-precision EMG signal decomposition using communications techniques," *IEEE Trans. Sig. Proc.*, vol. 48, pp. 2487–2494, 2000.

[76] D. Zennaro, P. Wellig, V. M. Koch, G. S. Moschytz, and T. Laubli, "A software package for the decomposition of long-term multichannel EMG signals using wavelet coefficients," *IEEE Trans. Biomed. Eng.*, vol. 50, pp. 58–69, 2003.

[77] J. R. Florestal, P. A. Mathieu, and A. Malanda, "Automated decomposition of intramuscular electromyographic signals," *IEEE Trans. Biomed. Eng.*, vol. 53, pp. 832–839, 2006.

[78] http://nmrc.bu.edu/tutorials/motor_units/decomp.html

Chapter 2: Cross-Comparison of Three Electromyogram Decomposition Algorithms Assessed with Experimental and Simulated Data

This chapter has been published as: Chenyun Dai, Yejin Li, Anita Christie, Paolo Bonato, Kevin C. McGill and Edward A. Clancy, "*Cross-Comparison of Three Electromyogram Decomposition Algorithms Assessed with Experimental and Simulated Data*," *IEEE Transactions on Neural Systems and Rehabilitation Engineering*, Vol. 23, No. 1, pp.32–40, 2015. Color versions of one or more of the figures in this paper are available online at http://ieeexplore.ieee.org/stamp/stamp.jsp?tp=&arnumber=6819816.

***Abstract*— The reliability of clinical and scientific information provided by algorithms that automatically decompose the electromyogram (EMG) depends on the algorithms' accuracies. We used experimental and simulated data to assess the agreement and accuracy of three publicly available decomposition algorithms—EMGlab [1] (single channel data only), Fuzzy Expert [2] and Montreal [3]. Data consisted of quadrifilar needle EMGs from the tibialis anterior of 12 subjects at 10%, 20% and 50% maximum voluntary contraction (MVC); single channel needle EMGs from the biceps brachii of 10 controls and 10 patients during contractions just above threshold; and matched simulated data. Performance was assessed via *agreement* between pairs of algorithms for experimental data and *accuracy* with respect to the known decomposition for simulated data. For the quadrifilar experimental data, median agreements between the Montreal and Fuzzy Expert algorithms at 10%, 20% and 50% MVC were 95%, 86% and 64%, respectively. For the single channel control and patient data, median agreements between the three algorithm pairs were statistically similar at ~97% and ~92%, respectively. Accuracy on the simulated data exceeded this performance. Agreement/accuracy was strongly related to the Decomposability Index [3]. When agreement was high between algorithm pairs applied to simulated data, so was accuracy.**

Index Terms—**Electromyogram (EMG), motor units, decomposition, intramuscular EMG, biomedical signal analysis.**

2.1 Introduction

Decomposition of indwelling recordings of the electromyogram (EMG) is the process of separating the composite interference pattern into its constituent motor unit action potential trains (MUAPTs), permitting the evaluation and study of individual motor unit (MU) firing patterns and action potential shapes. Decomposition is useful in a wide range of clinical and scientific studies of the neuromuscular system (for reviews, see [4]–[6]). For most decomposition-based studies, an automated algorithm is utilized to perform most of the decomposition, with expert manual editing often completed thereafter. Methods for automated decomposition were pioneered by DeLuca and colleagues [7], [8]. Since that time, a number of other significant approaches and variations have been developed and refined [2], [4], [9]–[17].

The performance of automated decomposition algorithms has primarily been evaluated in a few manners [18]. First, "reference" or "true" annotations have been achieved via manual expert editing of experimental data [2], [4], [12], [13], [17]. This technique can be extremely time consuming (e.g., one hour per second of data [2]) and the accuracy of the reference annotations can be difficult to assess. Nonetheless, assessment on experimental data guarantees signal conditions representative of actual use. Second, EMGs have been simulated [8], [9], [11]–[13], [15], [17]. In this case, the true annotations are known to be correct. However, even highly detailed simulated data cannot guarantee all of the complexities of an actual signal. Third, a few studies have recorded EMGs from multiple indwelling needles, each of which is decomposed [4], [19]–[21]. Some of the motor unit action potentials (MUAPs) are detected by more than one electrode. Agreement in their firing times is strong evidence of correct detection and classification of those firings. Recent studies have also compared decomposition results between EMGs that have been simultaneously acquired from indwelling electrodes and surface EMG arrays [22]–[24]. Most commonly, a combination of evidence—from experimental and simulated data—is used to evaluate an algorithm, as each evaluation technique has its own strengths and weaknesses.

To date, very little direct comparison has been made between the performance of various automated algorithms [25]. Since algorithm performance depends on the characteristics of the signal being analyzed, the same set of signals should be used when comparing different algorithms. For example, relative decomposition accuracy is known to decrease when: more spikes occur per second,

MUAPs from distinct trains exhibit more similar shapes, the signal-to-noise ratio (SNR) lowers, MUAP shapes change over time and/or firing times are irregular [4]. Moreover, when multiple algorithms are able to agree on the annotation of a particular signal, it increases confidence that the annotation is correct. Three of the major decomposition algorithms are now publicly available within the MATLAB software environment [1]–[3]. In addition, a versatile simulator of indwelling EMGs is also publicly available [26]. Hence, we cross-compared the performance of these three algorithms utilizing a variety of experimental and simulated needle EMG data.

2.2 Methods

2.2.1 Experimental Data

Portions of experimental data from two prior studies were reanalyzed, and simulated data were generated. No new subject data were collected. The data reanalysis was approved by the WPI Institutional Review Committee. The experimental data spanned a range of MVC levels and included both controls and patients, to provide data with a range of challenges to decomposition algorithms.

Three-channel quadrifilar needle EMGs had been acquired from the dominant leg of seven young (three male, four female; aged 18–30 years) and five elderly (two male, three female; aged 65 years or older) healthy subjects at the University of Massachusetts. Subjects were seated, the upper leg of their preferred limb restrained and the ipsilateral foot secured to a stiff transducer that measured ankle dorsiflexion force. The skin over the tibialis anterior (TA) muscle was cleaned with rubbing alcohol and a 27-gauge four-wire quadrifilar needle electrode was inserted into the belly of the TA muscle, avoiding the innervation zone. The needle was maneuvered into a position from which activity from several MUs could be obtained. Four 50-μm diameter platinum-iridium wires terminating at a side port 7.5 mm from the tip of the electrode comprised the recording surfaces [27]. The four wires in this electrode were arranged in a square array with approximately 200 μm on each side. The signals detected with this needle were connected to three differential amplifiers (10^{12} Ω input resistance; 25 pA bias current), bandpass filtered from 1,000– 10,000 Hz, sampled at 25,600 Hz (16-bit resolution), upsampled by a factor of two to a sampling rate of 51,200 Hz, and stored at this higher rate for off-line processing. Prior to electrode insertion, maximum voluntary contraction (MVC) dorsiflexion force was measured as the average of 3–5 maximum contractions of 5 s duration each. Following electrode insertion, subjects performed constant-force contractions at 10%, 20% and 50% MVC, with target force levels displayed

on a video monitor. Subjects slowly increased their force to the target level, and then maintained the force while a 30 s recording was made. A rest period of three minutes was provided between each contraction to prevent fatigue. One, 5 s segment during the constant-force portion of each recording was analyzed. Thus, 36 recordings of 5 s duration each were used (12 subjects x 3 levels of contraction). EMGs detected during higher levels of contraction are usually more challenging to decompose [4].

Single channel needle EMGs were reanalyzed from ten control subjects (6 males, 4 females; aged 21–37 years) and ten patients [5 diagnosed with ALS (3 males, 2 females; aged 56– 65 years); 5 diagnosed with myopathy (4 males, 1 female; aged 26–44 years)] in the publicly-available "N2001" database of Nikolic [28]. Of the available recordings within the database, recordings exhibiting a low background noise level (assessed visually) were selected. Recordings were acquired from the biceps brachii muscles during low level (just above threshold), constant-force contractions using a concentric needle electrode in accordance with standard clinical recording procedures. The signals were bandpass filtered between 2–10,000 Hz and sampled at 23,437.5 Hz with 16 bit resolution. Twenty 5 s recordings (20 subjects x one recording/subject) were used for analysis. Patient data are considered more challenging than that of healthy controls for decomposition algorithms [4]. For each signal, a "Spike Rate" measure was computed, expressing the number of MUAP firings per second. Within the analyzed 5 s segment of each recording, the number of pulses exceeding the background noise was manually counted. Spikes of duration greater than 3 ms, representing superimpositions, were counted as two pulses. Those with duration greater than 6 ms were counted as three pulses, etc. This approach accentuates the influence of longer duration spikes (which are, presumably, more complex to decompose) and causes the Spike Rate to be larger than the rate that would be derived by using the number of events found by the detection stage of a classical decomposition algorithm. For multiple-channel data, all three channels were simultaneously viewed and a pulse was counted if it was discernible from the background in any channel. The Spike Rate measure was expressed in pulses per second (pps). Spike Rate measures from the experimental data were used to guide generation of the simulated data.

2.2.2 Simulated Data

Constant-force, quadrifilar and single channel data were simulated using the publicly-available needle EMG simulator of Hamilton-Wright and Stashuk [26]. The resulting signals closely resembled those acquired experimentally from healthy subjects. The simulator parameters were selected to model

the physical layout of the TA muscle, MU firing patterns, action potential propagation and type of EMG electrode. To emulate quadrifilar recordings, four noise-free monopolar tip electrodes (50 μm diameter) were simultaneously simulated in a square array configuration at 200 μm distances. This configuration mimics a quadrifilar needle. The three differential voltages were then computed offline in MATLAB and white Gaussian noise was added to give a SNR of 20 dB. For each experimental contraction level to be simulated, trial and error was used to determine the contraction level parameter input value of the simulator software such that the average Spike Rate of the simulated data matched the average Spike Rate of the corresponding experimental data. Five-second constant-force recording segments were created at force levels representing 10%, 20% and 50% MVC. Each simulated condition was iterated 12 times, providing 12 realizations, to give the same number of trials as with the quadrifilar experimental data. The true time instances and identities of each MUAP firing (i.e., MUAP annotations), which are fully known in simulated data, were recorded along with the simulated signals (sampled at 31,250 Hz, 16-bit resolution). To emulate healthy (control) single channel recordings, one 10 mm concentric electrode was simulated and white Gaussian noise was added to give a SNR of 20 dB. The Spike Rate of these simulated data was matched to the average Spike Rate of the single channel needle (N2001) data of the control subjects, again via selection of the contraction level parameter input value of the simulator software. Ten recordings, each of 5 s duration, were created at a sampling rate of 31,250 Hz with 16-bit resolution, along with the true MUAP annotations.

2.2.3 Automated Decomposition Algorithms

Three publicly-available decomposition algorithms were compared. Each is implemented in MATLAB, which was used for all computation. Each algorithm was used *without* manual editing, although such editing is the norm in scientific studies. Prior to automated decomposition, the quadrifilar experimental data were digitally highpass filtered at 100 Hz. Although the signal had been analog highpass filtered at 1,000 Hz, this digital filter removed any offsets due to subsequent analog filter stages, including the analog to digital converter. The single channel experimental data were digitally highpass filtered at 500 Hz. This cut-off frequency was selected after visual review of a subset of the data, so as to reduce background noise and best accentuate spikes. All simulated data were digitally highpass filtered at 1,000 Hz, this cut-off frequency also being selected after visual review of a data subset. In all cases, a first-order Butterworth filter was designed, and then applied in the forward and reverse time directions to achieve zero phase shift.

All three algorithms detected voltage spikes within the EMG (each spike is a candidate MUAP, typically with a registration time corresponding to its peak magnitude), classified spikes with similar shapes and resolved superimpositions. The first automated decomposition algorithm was the default algorithm implemented in the publicly-available "EMGlab" software [1]. This algorithm can only analyze single channel EMGs and thus was only used for our single channel data. The second algorithm was the "Montreal" algorithm [3]. This algorithm has no adjustable parameters. The third algorithm was the "Fuzzy Expert" algorithm [2]. With the Fuzzy Expert algorithm, we utilized ten algorithm passes and limited resolution of superimpositions to three MUs on the first two passes, five MUs on the third pass and six MUs thereafter.

2.2.4 Methods of Analysis

After highpass filtering (described above), all experimental and simulated quadrifilar data were automatically decomposed by the Fuzzy Expert and Montreal algorithms. The single channel experimental (from the controls and the patients) and simulated data were decomposed by all three automated algorithms. Decompositions of *experimental* signals were compared pair-wise between algorithms for each signal. Each MUAP annotation was said to match if both algorithms found a MUAP from the same train within a ±0.5 ms match window, after determining a timing offset that accounts for the difference in MUAPT registration locations between the different algorithms [18], [24]. "Agreement" was measured as the number of matched annotations, divided by the sum of: (1) matched annotations and (2) unmatched annotations from either algorithm. Agreement results were expressed in percent. For the experimental quadrifilar data, results are only presented for those MUAPTs that exhibited a minimum of 20 matches between the Fuzzy Expert and Montreal algorithms (average of 4 matches per second over a 5 s recording duration). For the experimental single channel data, results are only presented for those MUAPTs that exhibited a minimum of 20 matches for each pairing between the three algorithms (i.e., those MUAPTs "found" by all three algorithms). For simulated data, the minimum number of required matches was one (i.e., every MUAPT that was extracted was analyzed). In addition to agreement results, decompositions of *simulated* signals were also compared directly to the true annotations (all MUAPTs included), this result being denoted "Accuracy," since the true annotations were known.

For each identified MUAPT for single channel data, the Decomposability Index (DI) [3] was computed as the minimum RMS difference between that MUAP template and each other MUAP

template (or the baseline), divided by the RMS value of the entire channel. For quadrifilar data, this value was computed from each channel and the norm of the three values reported as the DI. The DI is non-dimensional. For experimental and simulated signals, DI was computed multiple times, using the annotations from each respective decomposition algorithm. For simulated signals, the measures were also computed using the true annotations. Cross-plots of DI vs. agreement (or accuracy) were created for each contraction level for each data set. The data from each plot were then least squares fit to the exponential model: $Agreement = 100a \cdot e^{-b \cdot SNR_{MU}}$ where a and b are the fit parameters. Except where indicated otherwise, performance differences were tested statistically using ANOVAs (two- or one-way), with *post hoc* pair-wise comparisons (when significant) conducted using Tukey's honest significant difference (HSD) test.

2.3 Results

Table I lists the number of MUAPTs detected and analyzed in the various data sets, the total number of excluded MUAPTs (due to fewer than 20 matches) for the experiments, as well as the actual (true) number of MUAPTs generated for the simulated data. MUAPTs were only analyzed if they were detected by all algorithms and contained 20 or more matches. Thus, the number of analyzed MUAPTs must be less than or equal to the minimum number of MUAPTs detected from the individual algorithms. For all experiments, the number of excluded MUAPTs averaged 1–2 per recording, and was primarily comprised of small amplitude MUAPs. A smaller number of exclusions were due to individual MUAPTs that were erroneously decomposed into two distinct MUAPTs, either (or both) of which was comprised of less than 20 MUAPs. For all simulated data, the number of MUAPTs analyzed was always less than the number of true MUAPTs, since some algorithms failed to detect some MUAPTs. For the simulated quadrifilar data, the proportion of detected units (out of the total number of units actually simulated) decreased as the MVC level increased.

Spike Rate values for the quadrifilar experimental data at 10%, 20% and 50% MVC were 100.1±49.8, 119.3±46.4 and 211.8±54.6 pps, respectively. An ANOVA showed a significant difference in Spike Rate between MVC levels [$F(2,33)=16.9$, $p<10^{-5}$], with pair-wise *post hoc* Tukey comparisons showing that Spike Rate was significantly higher at 50% MVC compared to the other two contraction levels ($p<0.01$). Depending on the subject, spikes with a duration between 3–6 ms (counted as two spikes in the Spike Rate) occurred at a rate of 3–10/s at 10% MVC, 5–15/s at 20% MVC and 30–40/s at 50% MVC. Spike durations longer than 6 ms were rare (< 2/s) in the 10% and 20% MVC data. In the

50% MVC data, spikes of duration 6–9 ms occurred at a rate of ~15/s and spikes of duration 9–12 ms occurred at a rate of ~5/s. Spike Rate values for the corresponding simulated quadrifilar signals at 10%, 20% and 50% MVC were 99.2±21.3, 120.7±25.5 and 215.9±59.4 pps, respectively. Spike Rate values for the single channel experimental control and patient data were 61.8±19.8 pps and 48.8±27.0 pps, respectively. These values for the control and patient data did not differ statistically (p=0.16, t-test). The corresponding values for the simulated single channel signals were 62.6±12.3 pps. Hence, the average experimental control trial and simulated trial Spike Rate values were quite well matched, as designed. Spike durations between 3–6 ms were rare in the patient ALS data and occurred at a rate of 3-10/s in the control and patient myopathy data. Spike durations longer than 6 ms were rare in all single channel data.

General statistical comparisons of agreement and accuracy are shown in Table II. For quadrifilar experimental results, one-way ANOVAs assessed differences across the three MVC levels. Agreement decreased with increasing MVC level. The higher contraction data exhibited a substantial number of superimpositions (particularly at 50% MVC). Additionally, the higher-level contractions contained substantial smaller-amplitude "background" MUAPs that were not detected and, thus, contributed to an increased noise floor. For experimental single channel results, a two-way ANOVA (algorithm as one factor and control/patient as the other) found a mild difference between controls and patients (p=0.044), but no differences (p>0.07) on any of the three *post hoc* Tukey tests (one per algorithm pair, comparing controls to patients). Hence, no statistical differences between experimental single channel results are labeled in Table II. For simulated quadrifilar data results, one-way ANOVAs assessed differences across the three MVC levels, separately for both algorithms. For these results only, paired t-tests examined statistical differences between the Montreal and Fuzzy Expert algorithms, at each MVC level. The Montreal algorithm was significantly more accurate than the Fuzzy Expert algorithm at 10% and 20% MVC, although both algorithms performed quite well. Note that several of these results list both a median and 75th percentile value of 100%. In these cases, more than half of the result values equaled 100%. For simulated single channel results, a one-way ANOVA assessed differences among algorithms.

The Fuzzy Expert algorithm performed poorer than the other two with these data.

TABLE I
NUMBER OF MOTOR UNIT ACTION POTENTIAL TRAINS (MUAPTS) DETECTED AND ANALYZED. EXCLUDED MUAPTS REFER TO THOSE WITH LESS THAN 20 MATCHES

Experimental signals	MUAPTs per signal	Total MUAPTs detected: Mont-real	Fuzzy	EMG-lab	MUAPTs ana-lyzed	Total MUAPTs excluded
Quadrifilar						
10% MVC	3–10	118	91	—	78	12
20% MVC	3–11	124	98	—	90	7
50% MVC	4– 9	162	93	—	81	21
Single channel						
Controls	3–10	70	62	72	46	6–11
Patients	3–10	56	66	65	34	9–20

Simulated signals						True total MUAPTs
Quadrifilar						
10% MVC	7–12	104	109	—	103	110
20% MVC	7–16	116	115	—	110	127
50% MVC	7–18	132	133	—	120	166
Single channel	6– 9	68	68	73	68	73

TABLE II
SUMMARY *AGREEMENT* RESULTS FOR EXPERIMENTAL DATA AND *ACCURACY* RESULTS FOR SIMULATED DATA. EACH ENTRY LISTS MEDIAN [25TH PERCENTILE, 75TH PERCENTILE]. SIGNIFICANT DIFFERENCES INDICATED BY * ($P < 0.05$) OR ** ($P < 0.01$). SEE TEXT FOR STATISTICAL TEST RESULTS BETWEEN SINGLE CHANNEL EXPERIMENTAL CONTROLS AND PATIENTS.

Experimental signals	*Agreement* between algorithms (%): Montreal v Fuzzy	Montreal v EMGlab	Fuzzy v EMGlab
Quadrifilar			
10% MVC	* 95 [81, 100]	—	—
20% MVC	86 [70, 97]	** —	—
50% MVC	** 64 [34, 83]	—	—
Single channel			
Controls	97 [87, 100]	97 [89, 98]	96 [91, 98]
Patients	91 [84, 98]	93 [81, 98]	91 [82, 97]

Simulated signals	*Accuracy* of algorithm (%): Montreal	Fuzzy	EMGlab
Quadrifilar			
10% MVC	100 [98, 100]	*** 100 [92, 100]	—
20% MVC	** 100 [98, 100]	** 100 [89, 100]	—
50% MVC	99 [93, 100]	97 [86, 100]	—
Single channel	100 [98, 100]	*** 96 [84, 100]	*** 100 [96, 100]

Fig. 1 shows *agreement* results (Montreal vs. Fuzzy Expert) vs. DI for the experimental quadrifilar data. Figs. 2 and 3 show *accuracy* vs. DI for the simulated quadrifilar data, both as a function of MVC level and combined across levels. Similarly, agreement and accuracy results for experimental (control and, separately, patient) and simulated single channel data are shown vs. DI in Fig. 4. Each plot in Figs. 1–4 also shows the best-fit exponential model. Quantitatively, it is anticipated that agreement/accuracy is associated with DI. Here, that relation is expressed by the goodness-of-fit of the exponential model, also listed in the plots. In general, agreement/accuracy increased with DI.

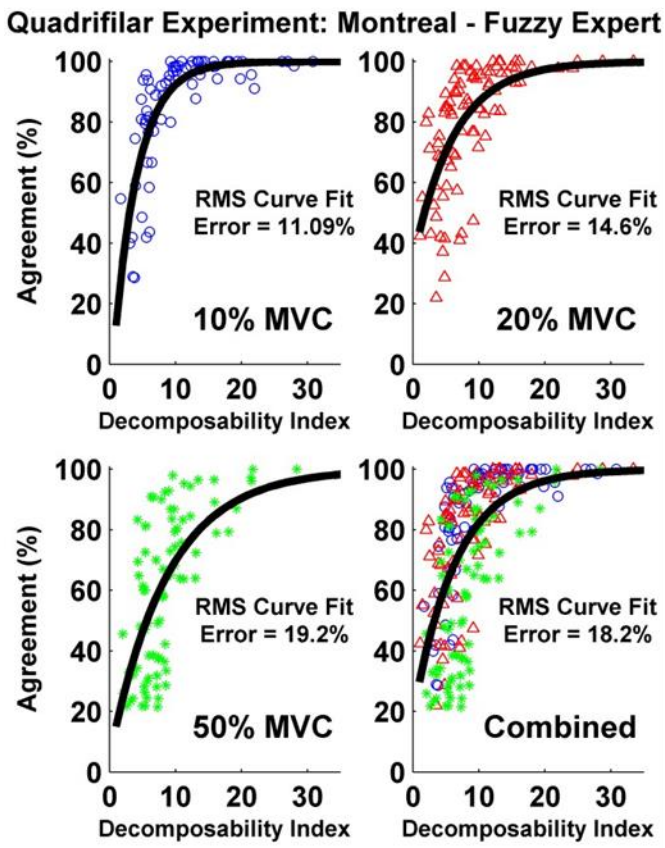

Fig. 1. *Agreement* between the Fuzzy Expert and Montreal algorithms as a function of DI for the quadrifilar experimental data. Each point represents one MUAPT. Results shown separately for each MVC level, and for all levels combined. Best fit exponential model shown in each plot, along with the RMS fit error.

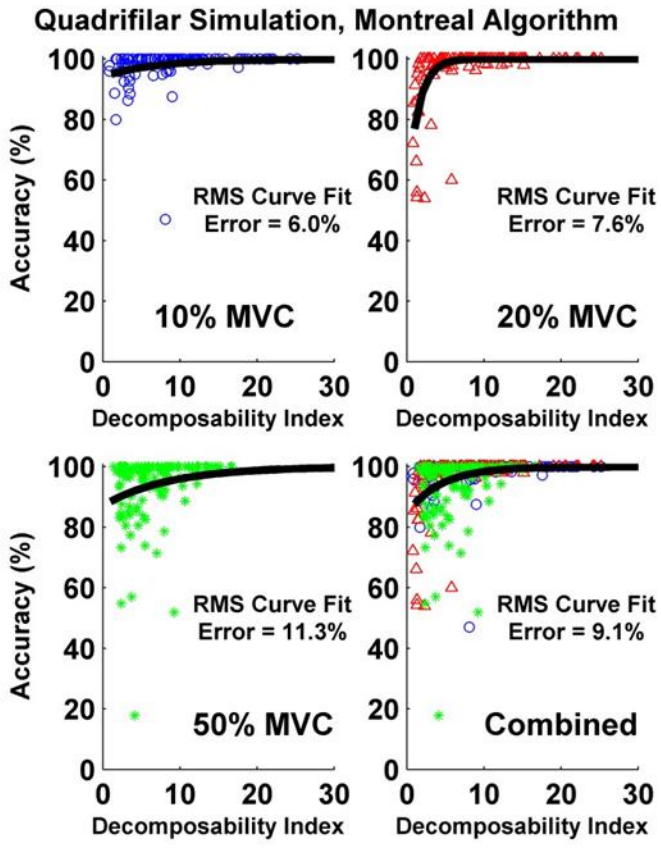

Fig. 2. *Accuracy* with respect to the true decomposition for the simulated quadrifilar data as a function of DI for the Montreal algorithm. Each point represents one MUAPT. Results shown separately for each MVC level, and for all levels combined. Best fit exponential model shown in each plot, along with the RMS fit error.

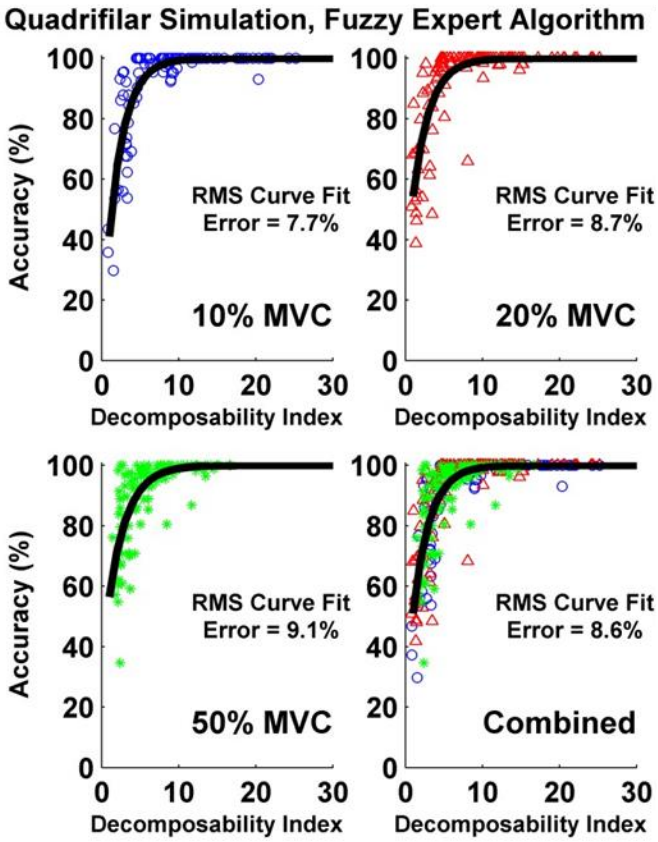

Fig. 3. *Accuracy* with respect to the true decomposition for the simulated quadrifilar data as a function of DI for the Fuzzy Expert algorithm. Each point represents one MUAPT. Results shown separately for each MVC level, and for all levels combined. Best fit exponential model shown in each plot, along with the RMS fit error.

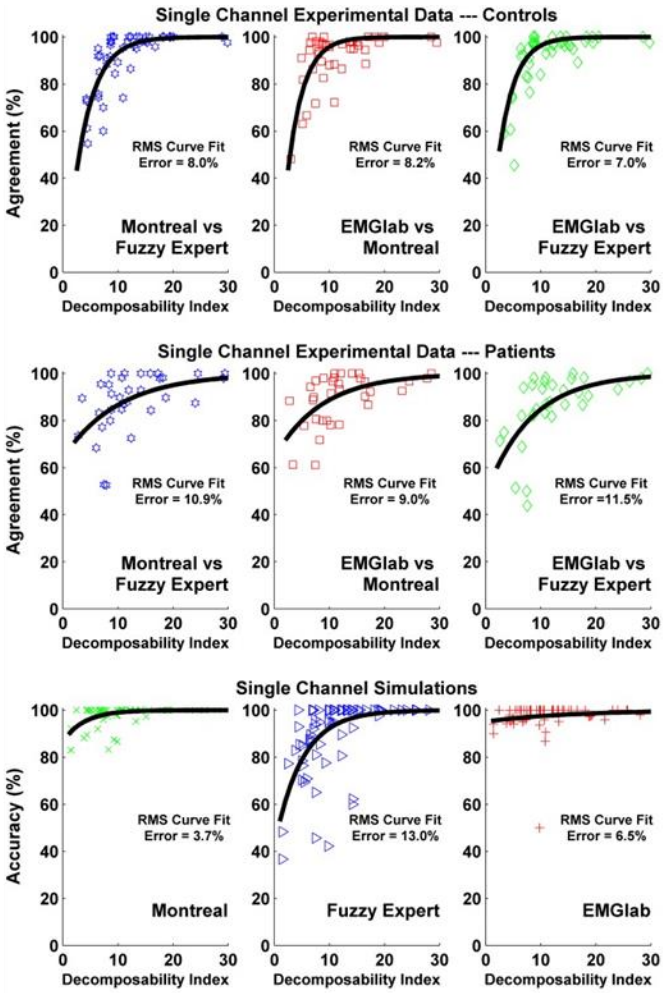

Fig. 4. *Agreement* (top) between algorithm pairs (as labeled) as a function of DI for the single channel experimental *control* data. *Agreement* (middle) between algorithm pairs as a function of DI for the single channel experimental patient data. *Accuracy* (bottom) with respect to the true decomposition for the simulated single channel data as a function of DI. Best fit exponential model shown in each plot, along with the RMS fit error. Each point in a plot represents one MUAPT.

Fig. 5 shows agreement between algorithm pairs and their individual accuracies for the simulated quadrifilar data and, separately, for the simulated single channel data. Each paired agreement value (paired between decomposition algorithms) is plotted twice, once corresponding to each individual accuracy value. The vast majority of accuracy values are higher than their corresponding agreement values. Note that most of the plotted values are difficult to visualize because they are clustered in the upper right corner of each plot, with multiple values over-plotted. The "tails" extending towards the origin primarily depict the limited number of low accuracy/agreement values. Thus, the combined data from each plot are presented in the corresponding surface density plots of Fig. 6. The density (z-axis) value at each node in the x-y rectangle (resolution of 1%) of these plots is the sum of all cross-plot

points within a radius of ten percentage points (with corrections made at the edges, since the radius extends outside of the *x*-*y* rectangle, distorting density calculation). A smoothed estimate of the density at each *x*-*y* node is produced. The preponderance of high agreement-accuracy values is now evident, although the accuracy distinctions between the algorithms cannot be represented.

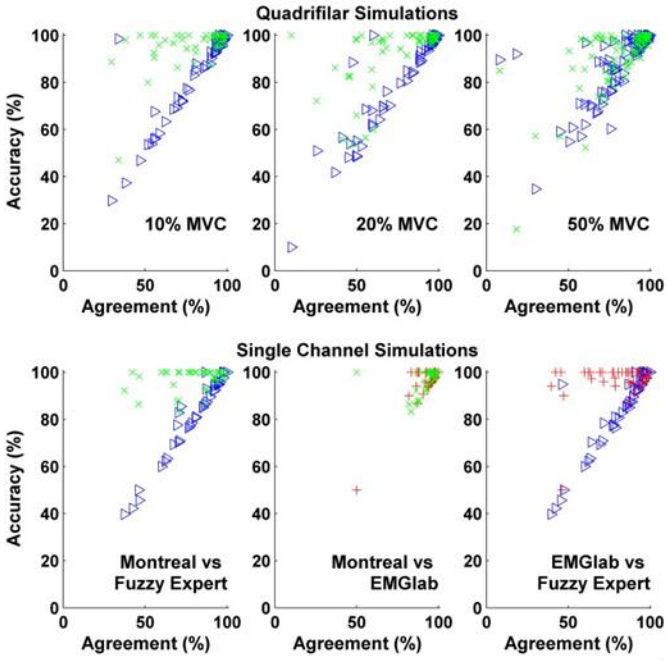

Fig. 5. (Top) Agreement between Montreal and Fuzzy Expert algorithms vs. their individual accuracies for the simulated quadrifilar data, separated by MVC level. Each *x*-axis agreement value corresponds to two *y*-axis accuracy values. Each such pair of points represents one MUAPT. (Bottom) Agreement between algorithm pairs vs. their individual accuracies for the simulated single channel data. For all plots, red plus=EMGlab, green "X"=Montreal, blue triangle=Fuzzy Expert. Note that many plot values in the upper right corner of each plot fall on top of each other, exaggerating the poorer performing trials.

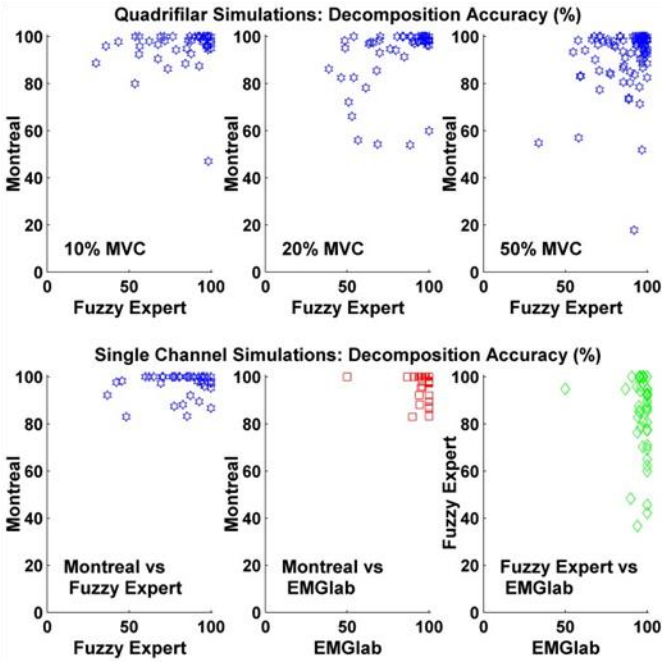

Fig. 6. Combined data points from each plot within Fig. 5 are shown here using surface density plots. (Top) Agreement between Montreal and Fuzzy Expert algorithms vs. their accuracies for the simulated quadrifilar data, separated by MVC level. (Bottom) Agreement between algorithm pairs vs. their accuracies for the simulated single channel data. Note the preponderance of high agreement-accuracy values in each plot.

Finally, Fig. 7 (cross-plots) and Fig. 8 (surface density plots) directly compare accuracy performance on the simulated data between algorithm pairs. Again, the cross-plots in Fig. 7 best visualize performance at the tails of the distribution, while the surface plots in Fig. 8 best display the overall trend of high accuracies.

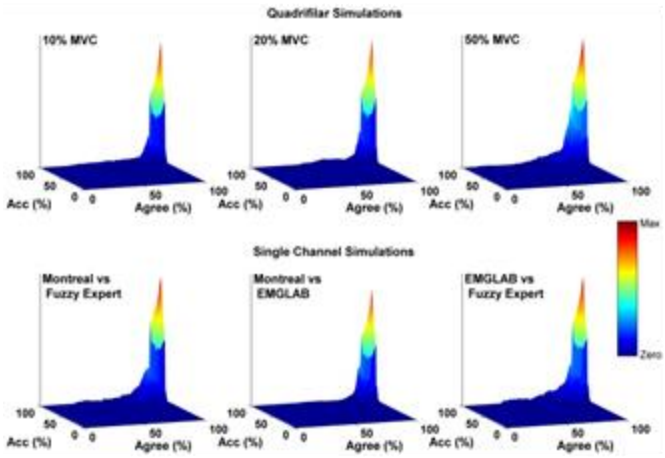

Fig. 7. (Top) Cross-plot comparisons of accuracy between Montreal and Fuzzy Expert algorithms for the simulated quadrifilar data, separated by MVC level. Each point represents one MUAPT. (Bottom) Cross-plot comparisons of accuracy for the simulated single channel data, separated by algorithm pair. All plot axes in units of percent accuracy. Note that many plot values in the upper right corner of each plot fall on top of each other, exaggerating the poorer performing trials.

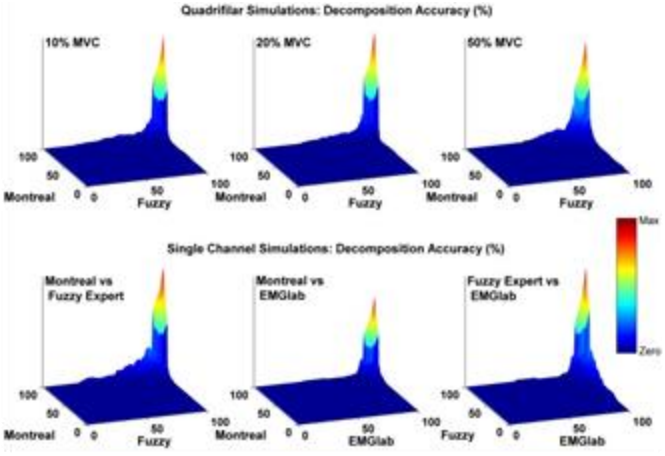

Fig. 8. Data points from each plot within Fig. 7 are shown here using surface density plots. (Top) Accuracies of Montreal and Fuzzy Expert algorithms for the simulated quadrifilar data, separated by MVC level. (Bottom) Accuracies of algorithms for the simulated single channel data. All x- and y-axis units are percent accuracy. Note the preponderance of high accuracy-accuracy values in each plot.

2.4 Discussion

This study evaluated the *agreement* between pairs of automated decomposition algorithms when applied to experimental data, as well as the *accuracy* of these algorithms when applied to simulated data. A large subject pool and wide range of contraction levels (10%, 20% and 50% MVC) was considered, as well as quadrifilar and single channel (control and patient) electrode recordings. Only the automated portion of the algorithms was evaluated—algorithm parameters, when available, were not varied. In research practice, algorithm parameters may be tuned as a function of the data set and decomposition results may be manually edited. As such, it is likely that the agreements/accuracies listed herein represent a lower bound on those that might be found in practice [23]. In particular, cursory examination of the results showed that one common source of errors occurred when one algorithm created two or more distinct (often non-overlapping) MUAPTs that really corresponded to the same MU. In our analyses, the partial MUAPT with the larger number of firings would tend to be correctly paired, but the MUAPT with the smaller number of firings would produce an error at each of its firings. Manual editing tends to find and correct this issue; a single "merging" of MUAPTs would correct a large number of agreement/accuracy errors. Automated merging/splitting of MUAPTs during the decomposition process has also been shown to improve decomposition performance [29]. In addition,

the lower agreement of the experimental quadrifilar data might be enhanced with manual editing, as it is likely that many missed detections and unclassified spikes could be resolved.

For the multiple channel data, there was a clear performance decrement as contraction level increased (Table II). This result is expected, as MU recruitment and firing rates rise with contraction level, producing more overlapping discharges and increasing the likelihood of MUAP shape similarity. Both of these issues are known challenges to decomposition algorithms [3], [4], [8]. Additionally, median *accuracy* on the simulated data exceeded experimental *agreement*, particularly at higher MVC levels. Of course, *agreement* between two algorithms counts an error whenever either algorithm errs, whereas *accuracy* with respect to the known firings of simulated data only counts an error when the test algorithm produces a mistaken firing. Additionally, the decomposition difficulty may have differed between the experimental and simulated data. Even though their Spike Rate values were matched, this one measure may not adequately capture all factors that affect decomposition difficulty. Note that most experimental validation studies are based on data from relatively low contraction levels. Thus, the 95% median agreement for the 10% MVC quadrifilar experimental data, as well as the near-perfect median accuracies for the simulated quadrifilar data results are consistent with prior performance assessments of these and other mature decomposition algorithms [1]–[4]. Anecdotally, it was noted that the Montreal algorithm more frequently produced decompositions with very high accuracy (e.g., median accuracy ≥99%), but occasionally (~3% of the simulated MUs) failed to detect MUAPTs with high DI.

The experimental single channel *control* data led to excellent median agreement results between all three pairs of algorithms. Agreement was not statistically different between any algorithm pair. These data were recorded at much lower contraction levels (just above threshold), thus were likely less challenging. For the simulated single channel data, the Montreal and EMGlab algorithms out-performed the Fuzzy Expert algorithm, although all three algorithms exhibited median accuracies ≥ 96%.

In a more challenging data set, the experimental single channel *patient* data exhibited a lower average Spike Rate than that of the controls (albeit not statistically different with this small sample size) and a lower number of MUAPTs analyzed, both of which might be expected from diagnosed ALS and myopathy patients. Although only marginally significant, the overall agreement results were lower for the patient data. Variation in MUAP shape is more prevalent with neuromuscular disease, which is consistent with making decomposition more challenging.

Figs. 1–4 show a rather clear relationship between DI and agreement/accuracy, suggesting that high accuracy is most probably achieved whenever the DI is high. Nonetheless, these figures also show that the RMS errors from the best fit exponential model between agreement/accuracy and DI were in the range of 3.7–19.2%, depending on MVC level and electrode recording type. This RMS error seems moderately high, indicating that DI does not account for all of the factors that affect decomposition accuracy. For example, the definition of the DI measure does not account for the frequency of superimpositions, even though superimpositions are known to decrease the accuracy of decomposition algorithms. In Figs. 1– 4, the exponential model relates decomposition accuracy to DI by fitting *across* all available MUAPTs from many recordings, providing a population-derived measure. In contrast, McGill and Marateb [30] developed a quality measure based on the properties of an individual recording.

Figs. 5 and 6 compared agreement vs. accuracy for the simulated data. Fig. 5 clearly segregates results between algorithms. However, many plot values in the upper right corner of each plot fall on top of each other, exaggerating the poorer performing trials. In contrast, Fig. 6 clarifies the density of points in the upper right corners of each plot, but does not segregate results between algorithms. Taken together, the pair of figures provides a fuller explanation of the data. In these plots, accuracy nearly always exceeded agreement, perhaps again reflecting that accuracy performance is only influenced by errors in the test algorithm while agreement is influenced by errors in both algorithms. Most important, whenever agreement was high (e.g., above 90–95%), accuracy was similarly high—suggesting that each algorithm was correctly detecting the same MU discharges and properly classifying them. Fig. 5 also seems to indicate that agreement is largely determined by the algorithm with the weaker performance. The weaker algorithm has many values along the diagonal (line of agreement). Figs. 7 and 8 provide additional information, comparing accuracy performance directly between the algorithms with the simulated data. In general, all algorithms performed quite well on the simulated data, even where statistical differences were found.

The evidence found herein did not support universal selection of one algorithm over the other. In fact, the high agreement/accuracy at lower contraction levels suggests that each of the three algorithms is virtually identical in classifying the commonly detected MU discharges. This result is supportive that all algorithms are performing well on these data. Further, Figs. 5 and 6 strongly suggest that when two algorithms are in strong *agreement*, then they are each likely to also be highly *accurate*. One strategy,

therefore, might be to decompose experimental EMG data with more than one of these algorithms, and then retain only those MUAPTs that exhibit high *agreement* among algorithms. It is common to only post-process a subset of the identified MUAPTs, typically those exhibiting a large SNR or DI (as these trains presumably have been accurately decomposed). Our evidence suggests that such individual measures are useful, but not definitive. Perhaps decomposition agreement between these distinct algorithms could provide another useful selection measure.

Reliable assessment of EMG decomposition algorithms is an important, yet difficult, challenge with many inherent limitations. In studies of simulated data, known true decompositions exist, but the simulator cannot fully capture the character of real EMGs. In experimental studies, the true decomposition is not known. Thus, it is common to study decomposition algorithm performance with both real and simulated data. Some algorithms focus on decomposition of only those spikes exhibiting a large SNR. Algorithms that decompose all detected spikes—even those corresponding to low SNR MUAPs—might be penalized with a lower *average* accuracy/agreement performance, even though they perform as well on those MUAPs with high SNR. Anecdotally, this type of detection error was observed from the Fuzzy Expert algorithm, whose default settings tended to detect more low-SNR MUAPs compared to the other algorithms. False positive noise spike detections seemed more prevalent in these low-SNR MUAPs. In this study, we indirectly limited the number of low-SNR MUAPs by excluding MUAPTs from analysis if less than 20 matches were available. Relaxing this condition would likely have reduced the accuracy/agreement of all algorithms. And, of course, distinct algorithms should be compared using the same data, since algorithm performance is influenced by the characteristics of the signal recordings. Accordingly, some algorithms may perform better on certain signals as compared to other algorithms, and vice versa.

2.5 Conclusion

This study provides a systematic comparison of agreement/accuracy performance between three publicly available algorithms which perform decomposition on indwelling EMGs. Our comparison information is important to the interpretation of results across studies using different analysis techniques. For the quadrifilar experimental data, median agreement between the Montreal and Fuzzy Expert algorithms at 10%, 20% and 50% MVC were 95, 86 and 64%, respectively. For the single channel control and patient data, median agreement between pairs of the three algorithms was ~97% and ~92%, respectively, for each pair. Agreement across algorithms and accuracy within algorithms were strongly

related to the DI. When agreement was high between algorithm pairs applied to the simulated data, so was the individual accuracy of each algorithm. These results, therefore, provide confidence that the algorithms perform reliably on experimental quadrifilar and single channel indwelling EMGs.

References

[1] K. C. McGill, Z. C. Lateva, and H. R. Marateb, "EMGLAB: An interactive EMG decomposition program," *J. Neurosci. Meth.*, vol. 149, pp. 121–133, 2005.

[2] Z. Erim and W. Lin, "Decomposition of intramuscular EMG signals using a heuristic fuzzy expert system," *IEEE Trans. Biomed. Eng.*, vol. 55, pp. 2180–2189, 2008.

[3] J. R. Florestal, P. A. Mathieu, and K. C. McGill, "Automatic decomposition of multichannel intramuscular EMG signals," *J. Electromyogr. Kinesiol.*, vol. 19, pp. 1–9, 2009.

[4] S. H. Nawab, R. P. Wotiz, and C. J. DeLuca, "Decomposition of indwelling EMG signals," *J. Appl. Physiol.*, vol. 105, pp. 700–710, 2008.

[5] D. Stashuk, "EMG signal decomposition: How can it be accomplished and used?," *J. Electromyogr. Kinesiol.*, vol. 11, pp. 151–173, 2001.

[6] R. C. Thornton and A. W. Michell, "Techniques and applications of EMG: Measuring motor units from structure to function," *J. Neurol.*, vol. 259, pp. 585–594, 2012.

[7] R. S. LeFever and C. J. DeLuca, "A procedure for decomposing the myoelectric signal into it constituent action potentials—Part I: Technique, theory, and implementation," *IEEE Trans. Biomed. Eng.*, vol. 29, pp. 149–157, 1982.

[8] R. S. LeFever, A. P. Xenakis, and C. J. DeLuca, "A procedure for decomposing the myoelectric signal into it constituent action potentials—Part II: Execution and test for accuracy," *IEEE Trans. Biomed. Eng.*, vol. 29, pp. 158–164, 1982.

[9] E. Chauvet, O. Fokapu, J. Y. Hogrel, D. Gamet, and J. Duchene, "Automatic identification of motor unit action potential trains from electromyographic signals using fuzzy techniques," *Med. Biol. Eng. Comput.,*, vol. 41, pp. 646–653, 2003.

[10] C. I. Christodoulou and C. S. Pattichis, "Unsupervised pattern recognition for the classification of EMG signals," *IEEE Trans. Biomed. Eng.*, vol. 46, pp. 169–178, 1999.

[11] J. Fang, G. C. Agarwal, and B. T. Shahani, "Decomposition of multiunit electromyographic signals," *IEEE Trans. Biomed. Eng.*, vol. 46, pp. 685– 697, 1999.

[12] D. Ge, E. Le Carpentier, Farina D, "Unsupervised Bayesian decomposition of multiunit EMG recordings using tabu search," *IEEE Trans. Biomed. Eng.*, vol. 57, pp. 561–571, 2010.

[13] R. Gut and G. S. Moschytz, "High-precision EMG signal decomposition using communications techniques," *IEEE Trans. Sig. Proc.*, vol. 48, pp. 2487–2494, 2000.

[14] H. Parsaei, D. W. Stashuk, S. Rasheed, C. Farkas, and A. Hamilton-Wright, "Intramuscular EMG signal decomposition," *Crit. Rev. Biomed. Eng.*, vol. 38, pp. 435–465, 2010.

[15] D. Zennaro, P. Wellig, V. M. Koch, G. S. Moschytz, and T. Laubli, "A software package for the decomposition of long-term multichannel EMG signals using wavelet coefficients," *IEEE Trans. Biomed. Eng.*, vol. 50, pp. 58–69, 2003.

[16] K. C. McGill, K. L. Cummins, and L. J. Dorfman, "Automatic decomposition of the clinical electromyogram," *IEEE Trans. Biomed. Eng.*, vol. 32, pp. 470–477, 1985.

[17] J. R. Florestal, P. A. Mathieu, and A. Malanda, "Automated decomposition of intramuscular electromyographic signals," *IEEE Trans. Biomed. Eng.*, vol. 53, pp. 832–839, 2006.

[18] D. Farina, R. Colombo, R. Merletti, and H. B. Olsen, "Evaluation of intra-muscular EMG signal decomposition algorithms," *J. Electromyogr. Kinesiol.*, vol. 11, pp. 175–187, 2001.

[19] C. J. DeLuca, "Reflections on EMG signal decomposition," in *Computer-Aided Electromyography and Expert Systems,* J. E. Desmedt, Ed. Elsevier, 1989, pp. 33–37.

[20] B. Mambrito and C. J. DeLuca, "A technique for the detection, decomposition and analysis of the EMG signal," *EEG Clin. Neurophysiol.*, vol. 58, pp. 175–188, 1984.

[21] K. C. McGill, Z. C. Lateva, and M. E. Johanson, "Validation of a computer-aided EMG decomposition method," in *IEEE Eng. Med. Biol. Conf.,* 2004, pp. 4744–4747.

[22] C. J. DeLuca, A. Adam, R. Wotiz, L. D. Gilmore and S. H. Nawab, "Decomposition of surface EMG signals," *J. Neurophysiol.*, vol. 96, pp. 1646–1657, 2006.

[23] A. Holobar, M. A. Minetto, A. Botter, F. Negro, and D. Farina, "Experimental analysis of accuracy in the identification of motor unit spike trains from high-density surface EMG," *IEEE Trans. Neural. Sys. Rehab. Eng.*, vol. 18, pp. 221–229, 2010.

[24] H. R. Marateb, K. C. McGill, A. Holobar, Z. C. Lateva, M. Mansourian, and R. Merletti, "Accuracy assessment of CKC high-density surface EMG decomposition in biceps femoris muscle," *J. Neural. Eng.*, vol. 8, 066002, 2011.

[25] K. C. McGill, "A comparison of three quantitative motor unit analysis algorithms," *Suppl. Clin. Neurophysiol.*, vol. 60, 273–278, 2009.

[26] A. Hamilton-Wright and D. W. Stashuk, "Physiologically based simulation of clinical EMG signals," *IEEE Trans. Biomed. Eng.*, vol. 52, 171–183, 2005.

[27] A. Christie and G. Kamen, "Doublet discharges in motoneurons of young and older adults," *J. Neurophysiol.*, vol. 95, 2787–2795, 2006.

[28] M. Nikolic, "Detailed Analysis of Clinical Electromyography Signals EMG Decomposition, Findings and Firing Pattern Analysis in Controls and Patients with Myopathy and Amytrophic Lateral Sclerosis," Ph.D. thesis, Faculty of Health Science, University of Copenhagen, 2001.

[29] H. Parsaei and D. W. Stashuk, "EMG signal decomposition using motor unit potential train validity," *IEEE Trans. Neural Sys. Rehabil. Eng.*, vol. 21, pp. 265–274, 2013.
[30] K. C. McGill and H. R. Marateb, "Rigorous *a posteriori* assessment of accuracy in EMG decomposition," *IEEE Trans. Neural Sys. Rehabil. Eng.*, vol. 19, pp. 54–63, 2011.

Chapter 3: Performance of Three Electromyogram Decomposition Algorithms as a Function of Signal to Noise Ratio: Assessment with Experimental and Simulated Data

This chapter has been published as: Chenyun Dai, Yejin Li, Edward A. Clancy, Anita Christie, Paolo Bonato and Kevin C. McGill. "*Performance of Three Electromyogram Decomposition Algorithms as a Function of Signal to Noise Ratio: Assessment with Experimental and Simulated Data*," *2014 IEEE Signal Processing in Medicine and Biology Symposium (SPMB)*, Temple University, Philadelphia, PA, 13 December 2014. Color versions of one or more of the figures in this paper are available online at http://ieeexplore.ieee.org/stamp/stamp.jsp?tp=&arnumber=7002963.

***Abstract*— We have previously published a full report [25] comparing the performance of three automated electromyogram (EMG) decomposition algorithms. In our prior report, the primary measure of decomposition difficulty/challenge for each data record was the "Decomposability Index" of Florestal et al. [3]. This conference paper is intended to augment our prior work by providing companion results when the measure of difficulty is the motor unit signal-to-noise ratio (SNR_{MU}) — a measure that is commonly used in the literature. Thus, we analyzed experimental and simulated data to assess the agreement and accuracy, as a function of SNR_{MU}, of three publicly available decomposition algorithms—EMGlab [1] (single channel data only), Fuzzy Expert [2] and Montreal [3]. Data consisted of quadrifilar needle EMGs from the tibialis anterior of 12 subjects at 10%, 20% and 50% maximum voluntary contraction (MVC); single channel needle EMGs from the biceps brachii of 10 control subjects during contractions just above threshold; and matched simulated data. Performance vs. SNR_{MU} was assessed via *agreement* between pairs of algorithms for experimental data and *accuracy* with respect to the known decomposition for simulated data. For experimental data, RMS errors between the achieved *agreement* and those predicted by an exponential model as a function of SNR_{MU} ranged from 8.4% to 19.2%. For the simulations, RMS errors between achieved *accuracy* and those predicted by the SNR_{MU} exponential model ranged from 3.7% to 14.7%. Agreement/accuracy was strongly related to SNR_{MU}.**

Keywords— Electromyogram (EMG), motor units, decomposition, intramuscular EMG, biomedical signal analysis.

3.1 Introduction

Indwelling electromyogram (EMG) recordings are decomposed by separating the interference pattern into its constituent motor unit action potential trains (MUAPTs). Doing so permits the evaluation and study of individual motor unit (MU) firing patterns and action potential shapes, which is useful in a wide range of clinical and scientific studies (for reviews, see [4]–[6]). In most decomposition schemes, an automated algorithm detects and clusters each MUAP firing, typically with expert manual editing performed thereafter. Signal processing methods for automated decomposition were pioneered by DeLuca and colleagues [7], [8]; with numerous variations and alternative approaches proposed and studied thereafter [2], [4], [9]–[17].

Quantitative performance evaluation of automated decomposition algorithms has been conducted in a few manners [18]. First, reference annotations have been produced via manual expert editing of experimental data [2], [4], [12], [13], [17]. This technique is extremely time consuming (e.g., one hour per second of data [2]) and its true accuracy can be difficult to assess. Yet, the use of experimental data guarantees signal conditions representative of actual use. Second, EMGs can be simulated [8], [9], [11]–[13], [15], [17]. In this case, the true annotations are known. But, even highly detailed simulators produce data that cannot replicate all of the complexities of an experimental signal. Third, a few studies have recorded EMGs from multiple indwelling needles, comparing the decompositions of MUs detected by more than one electrode [4], [19]–[21]. Agreement in their firing times is strong evidence of accurate detection and classification. Recently, studies have compared decomposition results between EMG simultaneously acquired from indwelling electrodes and surface EMG arrays [22]–[24]. Overall, a combination of evidence from experimental and simulated data is typically used to evaluate an algorithm, as each evaluation technique exhibits strengths and weaknesses.

For all automated algorithms, it is well established that performance depends on the characteristics of the signal being analyzed. Relative decomposition accuracy is known to decrease when: more spikes occur per second, MUAPs from distinct trains exhibit similar shapes, the signal-to-noise ratio (SNR) lowers, MUAP shapes change over time and/or firing times are irregular [4]. Florestal et al. [3] attempted to capture these signal characteristics in their Decomposability Index (DI), defined as the

minimum RMS difference between the given MUAP template and each other MUAP template (or the baseline), divided by the RMS value of the entire channel. This measure takes into account both the size and the distinguishability of the MUAPs.

In our prior full report [25], we contrasted the performance of three automated algorithms [1]–[3] that are publicly available for use in the MATLAB environment, with DI as our primary measure of the difficulty/challenge expected from each recording. Since algorithm performance varies depending on the data set analyzed, the same data were presented to each algorithm. We augmented the experimental data with data created by a publicly available EMG simulator [26], providing a more comprehensive evaluation.

In this conference publication, we augment our prior work by presenting complimentary results when the measure of data set difficulty/challenge is the SNR of a MU (SNR_{MU}). Distinct from the DI, the SNR_{MU} is sensitive only to the amplitude of a MUAP, relative to the noise floor. This difficulty measure is more traditional than the DI and arguably simpler to understand. Thus, we present a companion cross-comparison of the performance of the three decomposition algorithms, as a function of the SNR_{MU}. Readers are advised to review our prior full report [25], which contains complete project methods, etc.

3.2 Methods

3.2.1 Experimental Data

Portions of experimental data from two prior studies were reanalyzed, and simulated data were generated. No new subject data were collected. The data reanalysis was approved by the WPI Institutional Review Board. The experimental data spanned a range of MVC levels as well as laboratory and clinical data collection settings, to provide data with a range of challenges to decomposition algorithms.

Three-channel quadrifilar needle EMGs had been acquired from the dominant leg of seven young (three male, four female; aged 18–30 years) and five elderly (two male, three female; aged 65 years or older) healthy subjects at the University of Massachusetts [25]. Briefly, the skin over the tibialis anterior (TA) muscle was cleaned with rubbing alcohol and a 27-gauge four-wire quadrifilar needle electrode was inserted into the belly of the TA muscle, avoiding the innervation zone. Four 50-μm diameter platinum-iridium wires terminating at a side port 7.5 mm from the tip of the electrode comprised the

recording surfaces [27]. The four wires in this electrode were arranged in a square array with approximately 200 μm on each side. The signals detected with this needle were connected to three differential amplifiers (10^{12} Ω input resistance; 25 pA bias current), bandpass filtered from 1,000–10,000 Hz, and sampled at an effective rate of 51,200 Hz (16-bit resolution). Following electrode insertion, subjects performed 30s duration constant-force contractions at 10%, 20% and 50% MVC, with target force levels displayed on a video monitor. A rest period of three minutes was provided between contractions to prevent fatigue. One, 5 s segment during the constant-force portion of each recording was analyzed. Thus, 36 recordings of 5 s duration each were used (12 subjects x 3 levels of contraction).

Single channel needle EMGs were reanalyzed from ten control subjects (6 males, 4 females; aged 21–37 years) in the publicly-available "N2001" database of Nikolic [28]. Of the available recordings within the database, recordings exhibiting a low background noise level (assessed visually) were selected. Recordings were acquired from the biceps brachii muscles during low level (just above threshold), constantforce contractions using a concentric needle electrode in accordance with standard clinical recording procedures. The signals were bandpass filtered between 2–10,000 Hz and sampled at 23,437.5 Hz with 16 bit resolution. Ten 5 s recordings (10 subjects x one recording/subject) were used for analysis.

For each signal, a "Spike Rate" measure was computed, expressing the number of MUAP firings per second. Within the analyzed 5 s segment of each recording, the number of pulses exceeding the background noise was manually counted. Spikes of duration greater than 3 ms, representing superimpositions, were counted as two pulses. Those with duration greater than 6 ms were counted as three pulses, etc. This approach accentuates the influence of longer duration spikes (which are, presumably, more difficult to decompose) and causes the Spike Rate to be larger than the rate that would be derived by using the number of events found by the detection stage of a classical decomposition algorithm. For multiple-channel data, all three channels were simultaneously viewed and a pulse was counted if it was discernible from the background in any channel. The Spike Rate measure was expressed in pulses per second (pps). Spike Rate measures from the experimental data were used to guide generation of the simulated data.

3.2.2 Simulated Data

Constant-force, quadrifilar and single channel data were simulated using the publicly-available needle EMG simulator of Hamilton-Wright and Stashuk [26]. The resulting signals closely resembled

those acquired experimentally. The simulator parameters were selected to model the physical layout of the TA muscle, MU firing patterns, action potential propagation and type of EMG electrode. To emulate quadrifilar recordings, four noise-free monopolar tip electrodes (50 μm diameter) were simultaneously simulated in a square array configuration at 200 μm distances. This configuration mimics a quadrifilar needle. The three differential voltages were then computed offline in MATLAB and white Gaussian noise was added to give a SNR of 20 dB. For each experimental contraction level to be simulated, trial and error was used to determine the contraction level parameter input value of the simulator software such that the average Spike Rate of the simulated data matched the average Spike Rate of the corresponding experimental data. Fivesecond constant-force recording segments were created at force levels representing 10%, 20% and 50% MVC. Each simulated condition was iterated 12 times, providing 12 realizations, to give the same number of trials as with the quadrifilar experimental data. The true time instances and identities of each MUAP firing (i.e., MUAP annotations), which are fully known in simulated data, were recorded along with the simulated signals (sampled at 31,250 Hz, 16-bit resolution). To emulate healthy (control) single channel recordings, one 10 mm concentric electrode was simulated and white Gaussian noise was added to give a SNR of 20 dB. The Spike Rate of these simulated data was matched to the average Spike Rate of the single channel needle (N2001) data of the control subjects, again via selection of the contraction level parameter input value of the simulator software. Ten recordings, each of 5 s duration, were created at a sampling rate of 31,250 Hz with 16-bit resolution, along with the true MUAP annotations.

3.2.3 Automated Decomposition Algorithms

Three publicly-available decomposition algorithms were compared. Each is implemented in MATLAB, which was used for all computation. Each algorithm was used *without* manual editing, although such editing is the norm in scientific studies. Prior to automated decomposition, the quadrifilar experimental data were digitally highpass filtered at 100 Hz. Although the signal had been analog highpass filtered at 1,000 Hz, this digital filter removed any offsets due to subsequent analog filter stages, including the analog to digital converter. The single channel experimental data were digitally highpass filtered at 500 Hz. This cut-off frequency was selected after visual review of a subset of the data, so as to reduce background noise and best accentuate spikes. All simulated data were digitally highpass filtered at 1,000 Hz, this cut-off frequency also being selected after visual review of a data

subset. In all cases, a first-order Butterworth filter was designed, and then applied in the forward and reverse time directions to achieve zero phase shift.

All three algorithms detected voltage spikes within the EMG (each spike is a candidate MUAP, typically with a registration time corresponding to its peak magnitude), classified spikes with similar shapes and resolved superimpositions. The first automated decomposition algorithm was the default algorithm implemented in the publicly-available "EMGlab" software [1]. This algorithm can only analyze single channel EMGs and thus was only used for our single channel data. The second algorithm was the "Montreal" algorithm [3]. This algorithm has no adjustable parameters. The third algorithm was the "Fuzzy Expert" algorithm [2]. With the Fuzzy Expert algorithm, we utilized ten algorithm passes and limited resolution of superimpositions to three MUs on the first two passes, five MUs on the third pass and six MUs thereafter.

3.2.4 Methods of Analysis

After highpass filtering (described above), all experimental and simulated quadrifilar data were automatically decomposed by the Fuzzy Expert and Montreal algorithms. The single channel experimental and simulated data were decomposed by all three automated algorithms. Decompositions of *experimental* signals were compared pair-wise between algorithms for each signal. Each MUAP annotation was said to match if both algorithms found a MUAP from the same train within a ±1 ms match window[1], after determining a timing offset that accounts for the difference in MUAPT registration locations between the different algorithms [18], [24]. "Agreement" was measured as the number of matched annotations, divided by the sum of: (1) matched annotations and (2) unmatched annotations from either algorithm. Agreement results were expressed in percent. For the experimental quadrifilar data, results are only presented for those MUAPTs that exhibited a minimum of 20 matches between the Fuzzy Expert and Montreal algorithms (average of 4 matches per second over a 5 s recording duration). For the experimental single channel data, results are only presented for those MUAPTs that exhibited a minimum of 20 matches for each pairing between the three algorithms (i.e., those MUAPTs "found" by all three algorithms). For simulated data, the minimum number of required matches was one (i.e., every MUAPT that was extracted was analyzed). In addition to agreement results, decompositions of *simulated* signals were also compared directly to the true annotations (all MUAPTs included), this result being denoted "Accuracy," since the true annotations were known.

[1] Note that a different match window of ±0.5 ms was used in [25].

For each identified MUAPT for single channel data, a MU SNR (SNR_{MU}) was computed as the peak-to-peak height of the MU divided by the RMS value of the entire channel [21]. A ten-bin histogram of all (negative/positive) peak values from all firings of a MUAPT was computed. A peak value was estimated as the average height of all values contributing to the histogram mode bin. This selection helps to reject peak values that might be unrepresentative due to MUAP superimpositions. For multiple-channel data, the SNR_{MU} was computed separately for each channel and then averaged. The SNR_{MU} is non-dimensional. For experimental signals, SNR_{MU} was computed multiple times, using the annotations from each respective decomposition algorithm. For simulated signals, the measures were also computed using the truth annotations. Cross-plots of SNR_{MU} vs. agreement (or accuracy) were created for each contraction level for each data set. The data from each plot were then least squares fit to the exponential model: $Agreement = 100a \cdot e^{-b \cdot SNR_{MU}}$ where a and b are the fit parameters. Except where indicated otherwise, performance differences were tested statistically using ANOVAs (two- or one-way), with *post hoc* pair-wise comparisons (when significant) conducted using Tukey's honest significant difference (HSD) test.

3.3 Results

Table I in the companion work [25] lists and discusses the number of MUAPTs detected and analyzed in the various data sets, the total number of excluded MUAPTs (due to fewer than 20 matches) for the experiments, as well as the actual (true) number of MUAPTs generated for the simulated data. The companion work also details the Spike Rate values for each data set. Spike Rate increased with MVC level. The average experimental control trial and simulated trial Spike Rate values were quite well matched, as designed.

TABLE II
SUMMARY *AGREEMENT* RESULTS FOR EXPERIMENTAL DATA AND *ACCURACY* RESULTS FOR SIMULATED DATA. EACH ENTRY LISTS MEDIAN [25TH PERCENTILE, 75TH PERCENTILE]. SIGNIFICANT DIFFERENCES INDICATED BY * ($P < 0.05$) OR ** ($P < 0.01$).

Experimental signals	*Agreement* between algorithms (%) Montreal v Fuzzy	Montreal v EMGlab	Fuzzy v EMGlab
Quadrifilar			
10% MVC	96 [81, 100]	—	—
20% MVC	86 [72, 97]	—	—
50% MVC	65 [35, 84]	—	—
Single channel Controls	97 [87, 100]	97 [89, 98]	96 [91, 98]

Simulated signals	*Accuracy* of algorithm (%) Montreal	Fuzzy	EMGlab
Quadrifilar			
10% MVC	100 [98, 100]	100 [92, 100]	—
20% MVC	100 [98, 100]	100 [89, 100]	—
50% MVC	99 [93, 100]	97 [86, 100]	—
Single channel	100 [100, 100]	96 [84, 100]	100 [98, 100]

General statistical comparisons of agreement and accuracy are shown in Table II. Table II also indicates statistically significant differences in results from one-way ANOVA comparisons and post hoc Tukey tests. For the quadrifilar simulation results only, paired t-tests examined statistical differences between the Montreal and Fuzzy Expert algorithms, at each MVC level. Agreement generally decreased with MVC level for the multiple-channel experimental data. The higher contraction data exhibited a substantial number of superimpositions (particularly at 50% MVC), which is not reflected in the SMR_{MU} measure. Additionally, the higher-level contractions contained substantial smaller-amplitude "background" MUs that were not detected and, thus, contributed to an increased noise floor. For the quadrifilar simulation, Table II further shows that the Montreal algorithm was significantly more accurate than the Fuzzy Expert algorithm at 10% and 20% MVC, although both algorithms performed quite well.

Fig. 1 shows agreement results (Montreal vs. Fuzzy Expert) vs. SMR_{MU} for the experimental quadrifilar data. Figs. 2 and 3 show accuracy vs. SMR_{MU} for the simulated quadrifilar data, both as a function of MVC level and combined across levels. Similarly, agreement and accuracy results for experimental and simulated single channel data are shown vs. SMR_{MU} in Fig. 4.

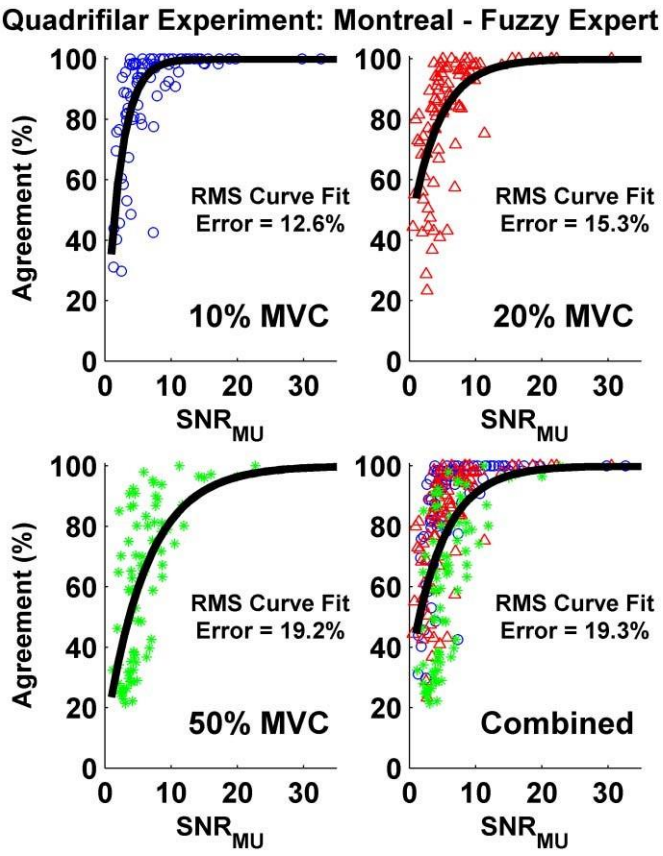

Fig. 1. *Agreement* between the Fuzzy Expert and Montreal algorithms as a function of SMR_{MU} for the quadrifilar experimental data. Each point represents one MUAPT. Results shown separately for each MVC level, and for all levels combined. Best fit exponential model shown in each plot, along with the RMS fit error.

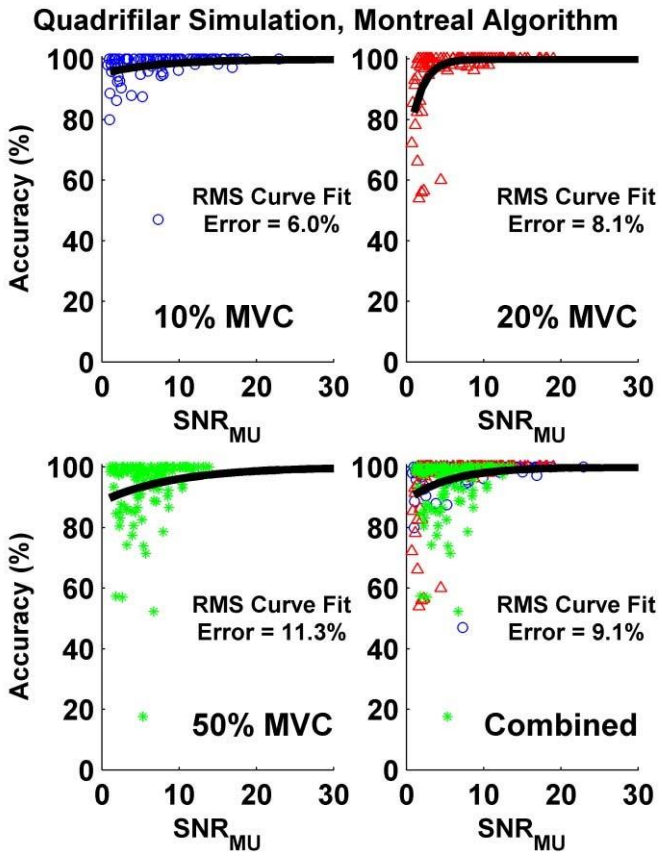

Fig. 2. *Accuracy* with respect to the true decomposition for the simulated quadrifilar data as a function of SNR_{MU} for the Montreal algorithm. Each point represents one MUAPT. Results shown separately for each MVC level, and for all levels combined. Best fit exponential model shown in each plot, along with the RMS fit error.

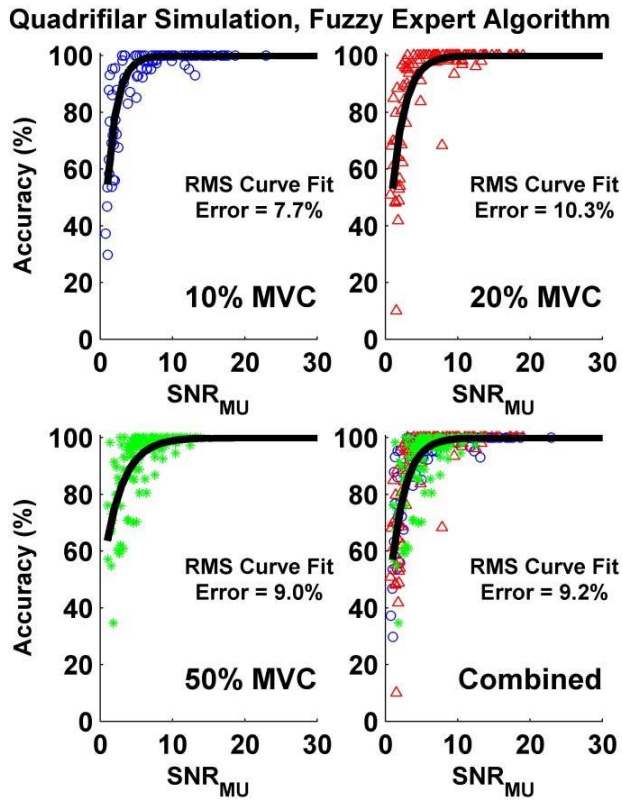

Fig. 3. *Accuracy* with respect to the true decomposition for the simulated quadrifilar data as a function of SNR_{MU} for the Fuzzy Expert algorithm. Each point represents one MUAPT. Results shown separately for each MVC level, and for all levels combined. Best fit exponential model shown in each plot, along with the RMS fit error.

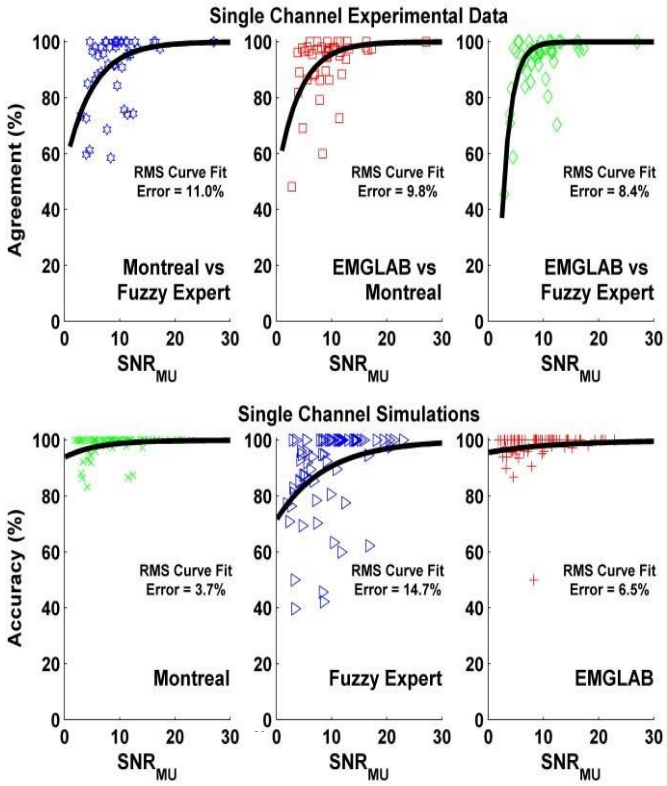

Fig. 4. Agreement (top) between algorithm pairs (as labeled) as a function of SNRMU for the single channel experimental control data. Accuracy (bottom) with respect to the true decomposition for the simulated single channel data as a function of SNRMU. Best fit exponential model shown in each plot, along with the RMS fit error. Each point in a plot represents one MUAPT.

Each plot in Figs. 1–4 also shows the best-fit exponential model. Quantitatively, it is anticipated that agreement/accuracy is associated with SNR_{MU}. Here, that relation is expressed by the goodness-of-fit of the exponential model, also listed in the plots. In general, agreement/accuracy increased with SNR_{MU}.

3.4 Discussion

This study evaluated the *agreement* between pairs of automated decomposition algorithms when applied to experimental data, as well as the *accuracy* of these algorithms when applied to simulated data, each as a function of SNR_{MU}. This study provides companion results to a prior full report that appeared in [25], using the DI. As such, we will concentrate our discussion on comparison of the SNR_{MU}based results in the present paper to the equivalent results based on the DI. Note that our prior full report utilized a shorter duration match window for MU comparisons (±0.5 ms), analyzed additional

data not discussed herein and provided additional analysis not directly related to the SNR_{MU} and DI measures.

Figs. 1–4 in the present paper (SNR_{MU}-based analysis) show a strong relationship between SNR_{MU} and agreement/ accuracy, suggesting that high accuracy is most probably achieved whenever the SNR_{MU} is high. Yet, these figures also show that the RMS errors from the best fit exponential model between agreement/accuracy and SNR_{MU} were in the range of 3.7–19.3%, depending on MVC level and electrode recording type. This RMS error seems moderately high, indicating that SNR_{MU} does not account for all of the factors that affect decomposition accuracy.

Comparison of the SNR_{MU}-based results in Figs. 1–4 to the DI-based results shown in the prior full report (see corresponding Figs. 1–4, respectively, in [25]) shows that nearly identical trends are found. It is, in fact, difficult to note performance differences between the SNR_{MU}-based and DIbased models. Thus, the simpler SNR_{MU} measure seems to predict achieved agreement/accuracy equally as well as the more complex DI measure. Future research might examine whether the combined use of these (and other) measures might provide better estimation of achieved agreement/accuracy.

3.5 Conclusion

In summary, this companion study provides a systematic comparison of agreement/accuracy performance between three publicly available algorithms which perform decomposition on indwelling EMGs, as a function of SNR_{MU}. For experimental data, RMS errors between the achieved *agreement* and those predicted by an exponential model as a function of SNR_{MU} ranged from 8.4% to 19.2%. For the simulations, RMS errors between achieved *accuracy* and those predicted by the SNR_{MU} exponential model ranged from 3.7% to 14.7%.

Agreement/accuracy was strongly related to SNR_{MU}. Prediction of agreement/accuracy based on SNR_{MU} was essentially equivalent in performance to prediction based on DI.

References

[1] K. C. McGill, Z. C. Lateva, and H. R. Marateb, "EMGLAB: An interactive EMG decomposition program," *J. Neurosci. Meth.*, vol. 149, pp. 121–133, 2005.

[2] Z. Erim and W. Lin, "Decomposition of intramuscular EMG signals using a heuristic fuzzy expert system," *IEEE Trans. Biomed. Eng.*, vol. 55, pp. 2180–2189, 2008.

[3] J. R. Florestal, P. A. Mathieu, and K. C. McGill, "Automatic decomposition of multichannel intramuscular EMG signals," *J. Electromyogr. Kinesiol.*, vol. 19, pp. 1–9, 2009.

[4] S. H. Nawab, R. P. Wotiz, and C. J. DeLuca, "Decomposition of indwelling EMG signals," *J. Appl. Physiol.*, vol. 105, pp. 700–710, 2008.

[5] D. Stashuk, "EMG signal decomposition: How can it be accomplished and used?," *J. Electromyogr. Kinesiol.*, vol. 11, pp. 151–173, 2001.

[6] R. C. Thornton and A. W. Michell, "Techniques and applications of EMG: Measuring motor units from structure to function," *J. Neurol.*, vol. 259, pp. 585–594, 2012.

[7] R. S. LeFever and C. J. DeLuca, "A procedure for decomposing the myoelectric signal into it constituent action potentials—Part I: Technique, theory, and implementation," *IEEE Trans. Biomed. Eng.*, vol. 29, pp. 149–157, 1982.

[8] R. S. LeFever, A. P. Xenakis, and C. J. DeLuca, "A procedure for decomposing the myoelectric signal into it constituent action potentials—Part II: Execution and test for accuracy," *IEEE Trans. Biomed. Eng.*, vol. 29, pp. 158–164, 1982.

[9] E. Chauvet, O. Fokapu, J. Y. Hogrel, D. Gamet, and J. Duchene, "Automatic identification of motor unit action potential trains from electromyographic signals using fuzzy techniques," *Med. Biol. Eng. Comput.,*, vol. 41, pp. 646–653, 2003.

[10] C. I. Christodoulou and C. S. Pattichis, "Unsupervised pattern recognition for the classification of EMG signals," *IEEE Trans. Biomed. Eng.*, vol. 46, pp. 169–178, 1999.

[11] J. Fang, G. C. Agarwal, and B. T. Shahani, "Decomposition of multiunit electromyographic signals," *IEEE Trans. Biomed. Eng.*, vol. 46, pp. 685–697, 1999.

[12] D. Ge, E. Le Carpentier, Farina D, "Unsupervised Bayesian decomposition of multiunit EMG recordings using tabu search," *IEEE Trans. Biomed. Eng.*, vol. 57, pp. 561–571, 2010.

[13] R. Gut and G. S. Moschytz, "High-precision EMG signal decomposition using communications techniques," *IEEE Trans. Sig. Proc.*, vol. 48, pp. 2487–2494, 2000.

[14] H. Parsaei, D. W. Stashuk, S. Rasheed, C. Farkas, and A. HamiltonWright, "Intramuscular EMG signal decomposition," *Crit. Rev. Biomed. Eng.*, vol. 38, pp. 435–465, 2010.

[15] D. Zennaro, P. Wellig, V. M. Koch, G. S. Moschytz, and T. Laubli, "A software package for the decomposition of long-term multichannel EMG signals using wavelet coefficients," *IEEE Trans. Biomed. Eng.*, vol. 50, pp. 58–69, 2003.

[16] K. C. McGill, K. L. Cummins, and L. J. Dorfman, "Automatic decomposition of the clinical electromyogram," *IEEE Trans. Biomed. Eng.*, vol. 32, pp. 470–477, 1985.

[17] J. R. Florestal, P. A. Mathieu, and A. Malanda, "Automated decomposition of intramuscular electromyographic signals," *IEEE Trans. Biomed. Eng.*, vol. 53, pp. 832–839, 2006.

[18] D. Farina, R. Colombo, R. Merletti, and H. B. Olsen, "Evaluation of intra-muscular EMG signal decomposition algorithms," *J. Electromyogr. Kinesiol.*, vol. 11, pp. 175–187, 2001.

[19] C. J. DeLuca, "Reflections on EMG signal decomposition," in *Computer-Aided Electromyography and Expert Systems,* J. E. Desmedt, Ed. Elsevier, 1989, pp. 33–37.

[20] B. Mambrito and C. J. DeLuca, "A technique for the detection, decomposition and analysis of the EMG signal," *EEG Clin. Neurophysiol.*, vol. 58, pp. 175–188, 1984.

[21] K. C. McGill, Z. C. Lateva, and M. E. Johanson, "Validation of a computer-aided EMG decomposition method," in *IEEE Eng. Med. Biol. Conf.,* 2004, pp. 4744–4747.

[22] C. J. DeLuca, A. Adam, R. Wotiz, L. D. Gilmore and S. H. Nawab, "Decomposition of surface EMG signals," *J. Neurophysiol.*, vol. 96, pp. 1646–1657, 2006.

[23] A. Holobar, M. A. Minetto, A. Botter, F. Negro, and D. Farina, "Experimental analysis of accuracy in the identification of motor unit spike trains from high-density surface EMG," *IEEE Trans. Neural. Sys. Rehab. Eng.*, vol. 18, pp. 221–229, 2010.

[24] H. R. Marateb, K. C. McGill, A. Holobar, Z. C. Lateva, M. Mansourian, and R. Merletti, "Accuracy assessment of CKC high-density surface EMG decomposition in biceps femoris muscle," *J. Neural. Eng.*, vol. 8, 066002, 2011.

[25] C. Dai, Y. Li, A. Christie, P. Bonato, K. C. McGill and E. A. Clancy, "Cross-comparison of three electromyogram decomposition algorithms assessed with experimental and simulated data," *IEEE Trans. Neural Sys. Rehabil. Eng.*, in press. Available: http://dx.doi.org/10.1109/TNSRE.2014.2322586.

[26] A. Hamilton-Wright and D. W. Stashuk, "Physiologically based simulation of clinical EMG signals," *IEEE Trans. Biomed. Eng.*, vol. 52, 171–183, 2005.

[27] A. Christie and G. Kamen, "Doublet discharges in motoneurons of young and older adults," *J. Neurophysiol.*, vol. 95, 2787–2795, 2006.

[28] M. Nikolic, "Detailed Analysis of Clinical Electromyography Signals EMG Decomposition, Findings and Firing Pattern Analysis in Controls and Patients with Myopathy and Amytrophic Lateral Sclerosis," Ph.D. thesis, Faculty of Health Science, University of Copenhagen, 2001.

Chapter 4: Cross-Comparison Between Two Multi-Channel EMG Decomposition Algorithms Assessed with Experimental and Simulated data

This chapter has been published as: Yejin Li, Chenyun Dai, Edward A. Clancy, Anita Christie, Paolo Bonato and Kevin C. McGill. "*Cross-Comparison Between Two Multi-Channel EMG Decomposition Algorithms Assessed with Experimental and Simulated Data*," *2013 IEEE 39th Annual Northeast Bioengineering Conference,* Syracuse University, 191–192, 5–7 April, 2013. Color versions of one or more of the figures in this paper are available online at http://ieeexplore.ieee.org/stamp/stamp.jsp?arnumber=6574423.

***Abstract*—The reliability of automated electromyogram (EMG) decomposition algorithms is important in clinical and scientific studies. In this paper, we analyzed the performance of two multi-channel decomposition algorithms—Montreal [1] and Fuzzy Expert [2] using both experimental and simulated data. Comparison data consisted of quadrifiler needle EMG from the tibialis anterior muscle of 12 subjects (young and elderly) at three contraction levels (10, 20 and 50% MVC), and matched simulation data. Performance was assessed via agreement between the two algorithms for experimental data and accuracy with respect to the known decomposition for simulated data. For the experimental data, median agreement between the Montreal and Fuzzy Expert algorithms at 10, 20 and 50% MVC was 95.7, 86.4 and 64.8%, respectively. For the simulation data, median accuracy was 99.8%, 100% and 95.9% for Montreal, and 100%, 98% and 93.5% for Fuzzy Expert at the different contraction levels.**

Keywords—EMG; Motor unit potential; Decomposition; SNR; Composite Decomposability Index (CDI); Cross-comparison.

4.1 Introduction

Decomposition of EMG signals separates the composite signal into its constituent motor unit (MU) firing times and action potential shapes. Decomposition is used in many clinical and research studies of the neuromuscular system [3]. In most cases, an automatic algorithm and expert manual editing are combined to produce a more reliable result [4].

Evaluating the performance between multiple automated algorithms is crucial, since EMG recordings can be extremely difficult to decompose under conditions of low signal to noise ratio (SNR) and/or high similarity of MU shapes. Hence, if high agreement is achieved between algorithms, more confidence is gained in each decomposition.

Two major multi-channel decomposition algorithms are now publically available within the MATLAB software environment [1], [2]. In addition, a detailed indwelling EMG simulator is also publically available [5]. Hence, we cross-compared the performance of these two algorithms, utilizing a variety of experimental and simulated data at different contraction levels.

4.2 Methods

4.2.1 Experimental and Simulated Data

The data used in this paper consisted of two parts: the experimental data were recorded at the University of Massachusetts and simulated data were generated. The data reanalysis was approved and supervised by the WPI Institutional Review Board.

Three-channel quadrifiler needle EMG signals were acquired from the tibialis anterior muscle of the dominant leg of seven young (three male, four female) and five elderly (two male, three female), healthy subjects during isometric contractions of 10%, 20% and 50% MVC. Four 50-μm diameter wires with 200 μm distance between electrode pairs comprised the recording surfaces. The signals were bandpass filtered from 1,000–10,000 Hz and sampled at 51,200 Hz at 16-bit resolution. One 5s segment of each signal was analyzed. Thus, 36 recordings of 5 s duration each were used (12 subjects x 3 levels of contraction).

Quadrifiler data were simulated using the EMG needle simulator of Hamilton-Wright [5]. The resulting signals resembled those acquired experimentally as closely as possible including electrode configuration and shape, recording duration, contraction levels and background noise.

4.2.2 Automated Decomposition Algorithms

Before decomposition, each recording was highpass filtered. For the experimental data, the acquisition hardware already provided some filtering. Thus, a 1st-order zero-phase Butterworth high-pass filter with 100 Hz cut off frequency was applied digitally. For the simulated data, the same process was implemented, except that the cut off frequency was 500 Hz.

Both algorithms detected EMG spikes, classified spikes with similar shapes and patterns, and resolved superimpositions. The first algorithm was the "Montreal" algorithm [1]. This algorithm has no adjustable parameters. The second algorithm was the "Fuzzy Expert" algorithm [2]. We utilized ten passes and limited resolution of superimpositions to three MUs on the first two passes, five MUs on the third pass and six MUs thereafter.

4.2.2 Methods of Analysis

The experimental data were analyzed separately from the simulated data. After highpass filtering, all experimental and simulated quadrifiler data were automatically decomposed by the Fuzzy Expert and Montreal algorithms.

For each MU in the experimental signals that was identified by both algorithms, the agreement rate was calculated as the percentage of the MU firings on which the two algorithms agreed to within ± 1 ms [6]. For each MU in the simulated signals, the accuracy of each algorithm was calculated as the percentage of firings which the algorithm correctly identified to within ± 1 ms. The "decomposability index" [1] of each MU was calculated as the minimum RMS difference between that MU and any other MU or the baseline, divided by the RMS value of the entire signal. The index was computed from each channel and the norm of the individual indexes reported.

4.3 Results

Average performance results vs. contraction level are listed in the Abstract. Fig. 1 shows the relationship between agreement rate and decomposability index for the experimental data at each contraction level. For 10% MVC, the number of matched MUs ranged from 7–10 per subject (total of 103 MUs). For 20% MVC, the number ranged from 7–13 (total 110). For 50% MVC, the number ranged from 7–12 (total 120). Fig. 2 shows the accuracy vs. decomposability index for the simulated data at 20% MVC. The number of matched MUs identified by Fuzzy Expert for each subject ranged from 7–13 (total of 117 MUs) and from 7–15 by Montreal (total of 114 MUs).

The data from each plot were then fit to the exponential model: $Agreement = 100 - a \cdot e^{-b \cdot x}$, where x is the Decomposability index of each motor unit.

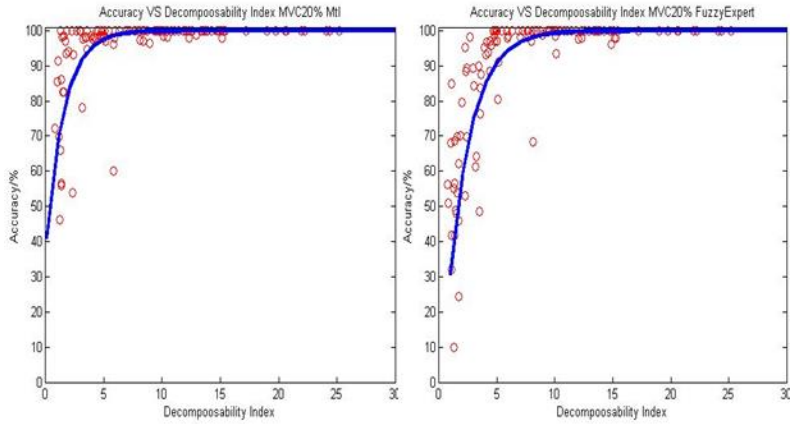

Figure 1. The relationship between Decomposability Index and agreement at MVC 10%, 20% and 50% (Montreal vs. Fuzzy Expert).

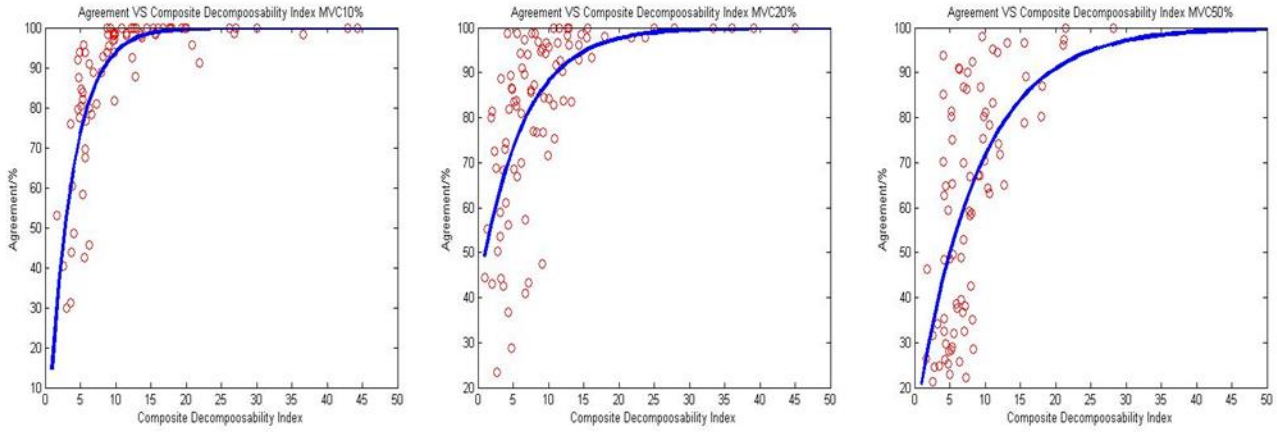

Figure 2. The relationship between Decomposability Index and accuracy at MVC 20% (Montreal vs. Fuzzy Expert).

4.4 Discussion/Conclusion

This study evaluated two automated decomposition algorithms when applied to experimental and simulated data. The results show good accuracy and substantial agreement between the algorithms, especially for MUs with a larger decomposability index at lower levels of contraction. These results provide a measure of confidence that the algorithms perform reliably on real EMG signals.

Performance was poorer for MUs with lower decomposability indices and in signals from higher levels of contraction (Figs. 1 and 2). This result is expected, as MU recruitment and firing rates rise with contraction level, producing more overlapping discharges and increasing the likelihood of MU shape similarity.

References

[1] Florestal JR, Mathieu PA, Malanda A. Automated decomposition of intramuscular electromyographic signals. IEEE Trans Biomed Eng. 2006;53:832–839.

[2] Erim Z, Lin W. Decomposition of intramuscular EMG signals using a heuristic fuzzy expert system. IEEE Trans Biomed Eng. 2008; 55:2180–2189.

[3] Stashuk D. EMG signal decomposition: How can it be accomplished and used? J Electromyogr Kinesiol. 2001;11:151–173.

[4] Nawab SH, Wotiz RP, DeLuca CJ. Decomposition of indwelling EMG signals. J Appl Physiol 2008;105:700–710.

[5] Hamilton-Wright A, Stashuk DW. Physiologically based simulation of clinical EMG signals. IEEE Trans Biomed Eng 2005;52:171–183. [Software available at http://emglab.net.]

[6] McGill KC, Lateva ZC, Johanson ME. Validation of a computer-aided EMG decomposition method. IEEE Eng Med Biol Conf 2004;4744–4747.

Chapter 5: Single-Trial Estimation of Quasi-Static EMG-to-Joint-Mechanical-Impedance Relationship Over a Range of Joint Torques

***Abstract*—Researchers have been studying the relationship between the surface electromyogram (EMG) and joint impedance for a number of years, as a means of non-invasively estimating musculoskeletal loads and joint/musculoskeletal dynamics. For constant-posture tasks, point-to-point motion tasks and other limited dynamic tasks, mechanical impedance has been measured by a second order differential equation between the resulting change in position/angle and joint torque. However, joint impedance increases as the force level, and this method can only measure the joint impedance at one fixed force level. My work provided a complete second-order EMG-based impedance characterization of stiffness, viscosity and inertia over a complete range of nominal torques, from a single perturbation trial with slowly varied torque. A single perturbation trial provides a more convenient method for impedance evaluation. The RMS errors of EMG based method were 20.01% for stiffness and 7.05% for viscosity, compared with the traditional mechanical measurement.**

***Keywords*—Joint impedance, Joint torque, Electromyogram, Biological system modeling, EMG signal processing, Myoelectric control, Prosthesis, Prosthesis control**

5.1 Introduction

Researchers have been studying the relationship between the surface electromyogram (EMG) and joint torque for a number of years, as a means of non-invasively estimating musculoskeletal loads and joint/musculoskeletal dynamics [e.g., (An et al., 1983; Clancy et al., 2006; Clancy and Hogan, 1997; Clancy et al., 2012; Doheny et al., 2008; Gottlieb and Agarwal, 1971; Hashemi et al., 2013; 2015; Hashemi et al., 2012; Liu et al., 2015; Staudenmann et al., 2010; Thelen et al., 1994; Vredenbregt and Rau, 1973)]. Measurement and understanding of these dynamics is important in several areas, including: ergonomic assessment (Hagg and Melin, 2004), prosthetic control (Parker et al., 2006), clinical biomechanics (Disselhorst-Klug et al., 2009; Doorenbosch and Harlaar, 2003) and basic motor control research. A distinct aspect of musculoskeletal loading, but of equal importance, is the joint

mechanical impedance. A joint exhibits non-zero mechanical impedance since it produces a reaction torque if it is subjected to a generalized displacement (or vice versa.). Joint impedance exists because of the mechanical properties of tissues (muscles, tendons, ligaments, bones) and is a necessary property of the musculoskeletal system because it helps stabilize force interactive tasks such as tool usage [c.f., (Burdet et al., 2001)]. Joint mechanical impedance can be modulated by co-contracting agonist-antagonist muscles about the joint. For example, a worker using a power tool (e.g., a hand drill) will purposely co-contract their muscles to increase hand mechanical impedance up to *at least* the minimum required to stabilize the task (Rancourt and Hogan, 2001a; b)—often without producing any externally measurable torques/forces. Impedance formally characterizes the torque-angle relationship state of the joint, and does so using an absolute physical scale (e.g., the stiffness component of linear impedance models is expressed in units of Newton-meters per degree) as opposed to the non-dimensional measures that are common based on EMG co-activation levels (Andison, 2011; Ford et al., 2008; Rosa et al., 2014). Accurate measurement of joint mechanical impedance in daily activities may provide new insights into the origin of several musculoskeletal disorders.

For constant-posture tasks, point-to-point motion tasks and other limited dynamic tasks, mechanical impedance has been measured by imparting forces on the body and measuring the resulting change in position/angle (or vice versa) (Bennett et al., 1992; Burdet, Osu, 2001; Cannon and Zahalak, 1982; Gomi and Osu, 1998; Hunter and Kearney, 1982; Kearney and Hunter, 1990; Kearney et al., 1997; McIntyre et al., 1996; Zhang and Rymer, 1997). These methods have performed well for their intended scientific studies, but have some important limitations for broader application. First, numerous measurements are typically required to fully characterize impedance over a range of operating conditions. For example, if perturbations are imparted about a nominal joint angle at a nominal torque level, then the impedance relationship is well characterized via the *stiffness, viscosity and inertia* of a second-order linear system (Kearney and Hunter, 1990; Zhang and Rymer, 1997). Perturbation trials conducted at distinct torque levels can characterize the system over that range of torques—but numerous repeated trials are required. Second, such measurements require imparting forces on the body, disturbing the task under study, a situation quite undesirable for taking in situ measurements during applied tasks.

Considering existing technologies, surface electromyography (EMG) may be an excellent solution to simultaneously estimate torque and impedance during applied motor tasks as it provides a non-invasive approach (once calibrated). Previous work has successfully related EMG to joint *quasi-*

stiffness—which does not seek to account for short-range stiffness (Rack and Westbury, 1974; Rouse et al., 2013). Osu et al. (Osu and Gomi, 1999) assumed a baseline stiffness representing passive joint properties and a second additive quasi-stiffness component proportional to muscular activity of both agonist and antagonist muscles of the joint. Others have successfully related EMG to joint *quasi-stiffness* in various tasks by differentiating the EMG-torque relationship as a function of joint angle (Kawase et al., 2012; Pfeifer et al., 2012; Shin et al., 2009). These methods are attractive in that only simpler torque measurements are required in order to calibrate the model. But, the model identification process utilizes multiple trials which are cumbersome for applied studies, the model form is limited by the EMG-torque model and no viscosity term is estimated. Of course, the inertial properties of a classic second-order characterization do not vary with the level of joint torque.

Our work described herein seeks to advance the above work in a few manners. First, we propose a simple EMG-impedance model which includes stiffness, viscosity and inertia, that can be estimated using calibration perturbations along with EMG recordings. A complete second-order characterization is provided. Second, the form of the EMG-impedance model is parametric and can be selected to include a nonlinear shape. Third, we demonstrate the use of perturbation contractions in which the nominal ("background") torque level is slowly varied, such that a single perturbation trial can be used to calibrate a model over a complete range of nominal torques. Our experimental evaluation was completed on human subjects producing torques about their elbow joint.

5.2 Methods

5.2.1 Experimental Methods

The original experimental protocol was approved by the Institutional Review Board (IRB) of Laval University (Québec, Canada) and all subjects provided written informed consent. The analysis described herein was approved by the Worcester Polytechnic Institute IRB. Seven subjects (7 females, 10 males; aged 21–43 years) each participated in one experimental session. The skin above the investigated muscles was cleaned with alcohol and four bipolar EMG electrode-amplifiers placed transversely across each of the biceps and triceps muscles, midway between the elbow and the midpoint of the upper arm, centered on the muscle midline. The two contacts (5 mm diameter, stainless steel, separated 10 mm edge-to-edge) of each electrode-amplifier were oriented along the muscle's long axis. Adjacent electrodes were spaced ~1.75 cm apart. A reference electrode was applied over the acromion process.

Each electrode-amplifier had a common mode rejection ratio greater than 90 dB at 60 Hz. Signals were highpass filtered at 15 Hz (eighth-order Butterworth) and then lowpass filtered at 1800 Hz (fourth-order Butterworth). As shown in Fig. 1, a subject was seated in front of a two degree of freedom planar joystick manipulandum that can produce 15 Nm of torque about each axis (about 50 N at the tip) with a frequency response up to 15 Hz. The vertical axis of the joystick was locked to allow horizontal (medial-lateral) motion only. Subject's held their right arm in the plane parallel to the floor, with the shoulder abducted 90°, the forearm oriented in the sagittal plane, the wrist fully supinated and the elbow flexed 90°. The wrist was rigidly attached to the manipulandum load cell via a cuff covering the distal forearm. The EMG signals were sampled at 4096 Hz and the load cell signal at 400 Hz (time synchronized), each using 16 bits.

Subjects initially performed two, 2 s maximum voluntary contractions (MVCs) in each of flexion and extension, the maximum of which was used as the subject's MVC. Next, they performed a 0% MVC (rest contraction) and separate flexion and extension 50% MVCs for 5 s, utilizing force feedback on a computer screen. These contractions were used to calibrate the advanced EMG processors (Clancy and Farry, 2000; Prakash et al., 2005). Pseudo-random perturbations (manipulandum set in angle control, 0¬–6 Hz frequency range, Gaussian distributed with zero mean and std. dev. of xxo) were then performed twice for 20 s on the manipulandum alone to identify its inertia. The same process was performed with the subject's arm secured in the cuff while the subject remained relaxed to measure the total inertia of the combined arm-manipulandum system.

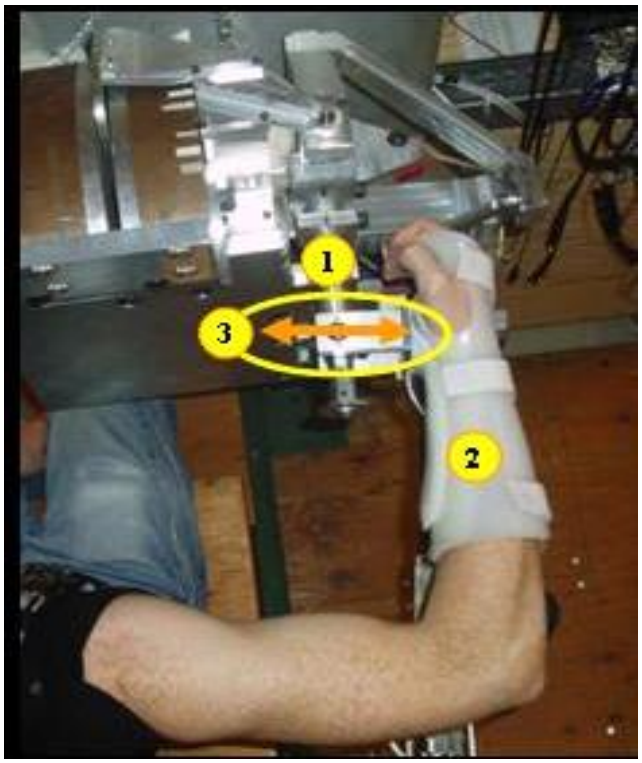

Fig. 1. Top view of subject seated in the impedance measurement apparatus. Label 1 shows the location of the actuated joy stick and load cell. Label 2 identifies the cuff restraint. Label 3 shows the medial-lateral orientation of the applied force perturbations.

Subjects then performed two sequences of perturbation tasks at eight distinct, fixed nominal effort levels, 30 s each in duration (Fig. 2). The eight effort levels were 10%, 20%, 30% and 40% MVC extension and flexion. During each trial, the angle of the manipulandum was feedback to the subject on a computer screen. The subject was instructed to maintain their average joint angle at 90° throughout the trial. The manipulandum exerted constant flexion/extension torque for 5 s, after which an additional 0–15 Hz bandwidth pseudo-random torque perturbation was applied during the 5–25 s period. The order of the trials was randomly selected. The subject's forearm was removed from the wrist cuff between all trials for 2–3 min of rest to avoid fatigue.

A second set of trials was conducted in which subjects maintained their elbow joint angle at 90° while a ramp force, combined with the force perturbations, was exerted by the manipulandum over 50 s (Fig. 3). As shown in Fig. 3, each trial was segmented as: during the first 20 s, the nominal torque started at 40% MVC extension and linearly ramped to 0% MVC; during the next 10 s, the nominal torque was 0% MVC; and during the last 20 s, the nominal torque linearly ramped from 0% MVC to 40% MVC

flexion. Three such trials were performed. The pause at 0% MVC was added after initial evaluation found it difficult for subjects to follow the nominal torque trajectory across zero. Finally, three other perturbation trials were performed with the ramping reversed, i. e. with nominal torque linearly ramping from 40% MVC flexion to 0% MVC (20 s), 10 s of 0% MVC nominal torque, and 20 s of nominal torque linearly ramping from 0% MVC to 40% MVC extension.

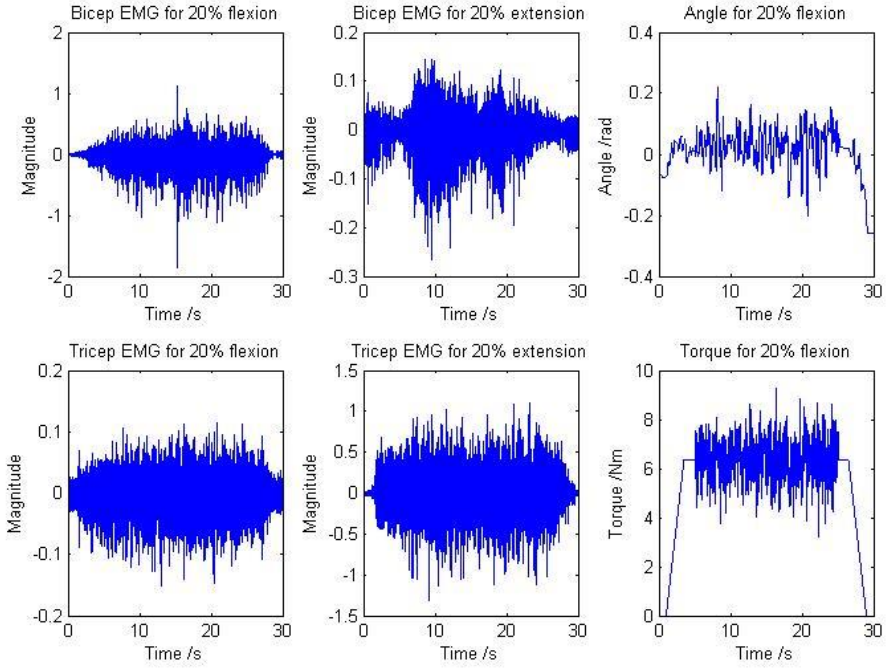

Fig. 2. Sample time-series data from a constant-torque trial. Show sample biceps EMG, triceps EMG, angle and torque.

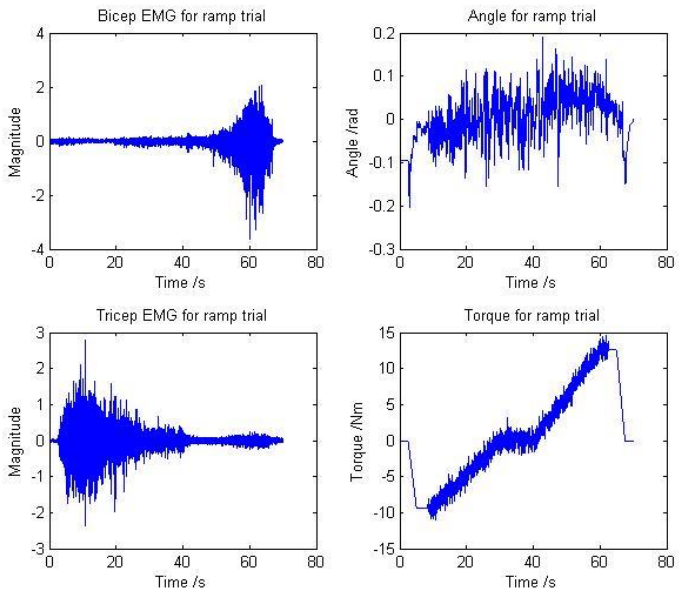

Fig. 3. Sample time-series data from a ramp torque trial. Show sample biceps EMG, triceps EMG, angle and torque.

5.2.2 Methods of Analysis

Signal preprocessing: Analysis was performed offline in MATLAB. All filter specifications reported herein refer to the designed filters—these filters were applied in the forward, then reverse, time directions to achieve zero phase (and the square of the designed magnitude response). EMG signals were highpass filtered (15 Hz cutoff, 5th-order Butterworth). Then, two distinct EMG amplitude (EMGσ) estimates were computed for each of extension and flexion—a single-channel, unwhitened estimate (using a centrally-located electrode) and a four-channel, whitened estimate using adaptive whitening (Clancy and Farry, 2000; Prakash, Salini, 2005). Each used a first-order demodulator (rectifier), followed by lowpass filtering at 1 Hz (4th-order Butterworth) and then resampling to 100 Hz. This lower rate is appropriate for system identification (Clancy, Bida, 2006; Ljung, 1999, pp. 491–519).

The general second-order linear mechanical joint impedance model at a particular operating point is (Kearney and Hunter, 1990):

$$\Delta T[m] = I\,\ddot{\theta}[m] + B\,\dot{\theta}[m] + K\,\Delta\theta[m], \qquad (1)$$

where m is the resampled rate, ΔT is the change in joint torque, $\Delta\theta$ is the change in joint angle; and I (inertia), B (viscosity) and K (stiffness) are the fit parameters. Since torque and angle *change* are required, each of these recorded signals was highpass filtered at 0.25 Hz using a 2nd-order Butterworth

filter. This approach was applicable to both constant-torque and ramp-torque trials. For the first derivative of angle, a central difference was computed, followed by 5th-order lowpass filtering with a Butterworth filter with cutoff frequency at 15 Hz. For the second derivative of angle, two successive central differences were computed, followed by the same lowpass filter. These filter selections were determined via preliminary analysis. All mechanical signals were lowpass filtered at 40 Hz and then resampled to 100 Hz.

System Identification: Initially for each subject, the rest trial was used to estimate the rest impedance parameters of the arm-manipulandum system. These I_o, B_o and K_o values were estimated via least squares. All least squares used the pseudo-inverse technique in which singular values of the design matrix were removed if their ratio to that of the largest singular value was less than a tolerance value. Through preliminary analysis, a tolerance value of 0.005 was selected (Clancy, Liu, 2012). In all subsequent analysis, the torque ΔT_o estimated via these parameters (according to equation 1) was subtracted from the overall ΔT, leaving only the torque change due to muscle activation, ΔT_{EMG}. In addition, the inertia was fixed and not further estimated, as it does not change with muscular activation level.

Next, viscosity and stiffness parameters were least squares estimated from the constant-torque trials, *without* the use of EMG. The middle 20 s of data, avoiding the recording portion that did not include perturbations, was used. Parameter values were estimated separately for the eight contraction levels and two sets, with the results from the two trials per condition averaged. These parameter values served as the "true" parameter values, in that they were estimated via the established method.

Then, EMG signals were used to estimate viscosity and stiffness from the constant-torque trials. EMGσ was incorporated into the joint mechanical impedance model of equation 1 in a linear fashion by setting:

$$B[m] = B_e\,\sigma_e[m] + B_f\,\sigma_f[m] \quad \text{and} \quad K = K_e\,\sigma_e[m] + K_f\,\sigma_f[m], \tag{2}$$

where σ_e and σ_f are the EMGσ values for extension and flexion, respectively; and the B_i and K_i are the viscosity and stiffness fit parameters, respectively. Again, the middle 20 s data segment was used. A full set of eight trials (one per contraction level) was combined as training data, so that EMG would be related to impedance parameters across the range of effort levels. The parameters were then fixed and the second set of eight trials used for testing. The values of *B[m]* and *K[m]* (equation 2) from the 20 s

middle segment of a test trial was averaged and then compared to the truth parameters estimated strictly from the mechanical measures. Error was taken as 100% times the absolute difference between the truth and test measures, divided by the truth measure. Both single-channel unwhitened and four-channel whitened EMG performance was compared.

Next, EMG signals were used to estimate viscosity and stiffness from the ramp-torque trials. The model of equation 2 was again used, except that only one ramp trial was used for training. A second trial was used for testing. [How to measure error? Probably need to evaluate error only at the eight locations at which a mechanical measure was made.]

Finally, some researchers would benefit from single-trial estimation of impedance parameters over a range of effort levels without the use of EMG. We utilized our ramp-torque trials to investigate doing so. Modeling a linear relationship between mean torque level and viscosity/stiffness (Hunter and Kearney, 1982; Kearney and Hunter, 1990) was incorporated into equation 1 by setting:

$$B[m] = c_B \bar{T}[m] \quad \text{and} \quad K = c_K \bar{T}[m], \tag{3}$$

where c_B and c_B are fit parameters and $\bar{T}[m]$ is the quasi-static (background) torque level. One model fit was made using the 20-s portion of the ramp perturbation contraction that was extension-dominant and a second fit was made using the 20-s portion of the ramp perturbation contraction that was flexion-dominant. In this manner, the slope of the viscosity/slope vs. mean torque could differ in extension from that of flexion.

5.3 Results

Fig. 2 shows sample time-series data from a constant-torque trial, while Fig. 3 does so for a ramp trial. Fig. 4 shows test trial viscosity and stiffness estimates for a single subject. For the ramp contractions, impedance parameter estimates are available continuously throughout the contraction, as shown in the figure. The figure also shows the specific ramp-calibrated estimates at the eight constant-torque contraction levels. Error was assessed at these locations.

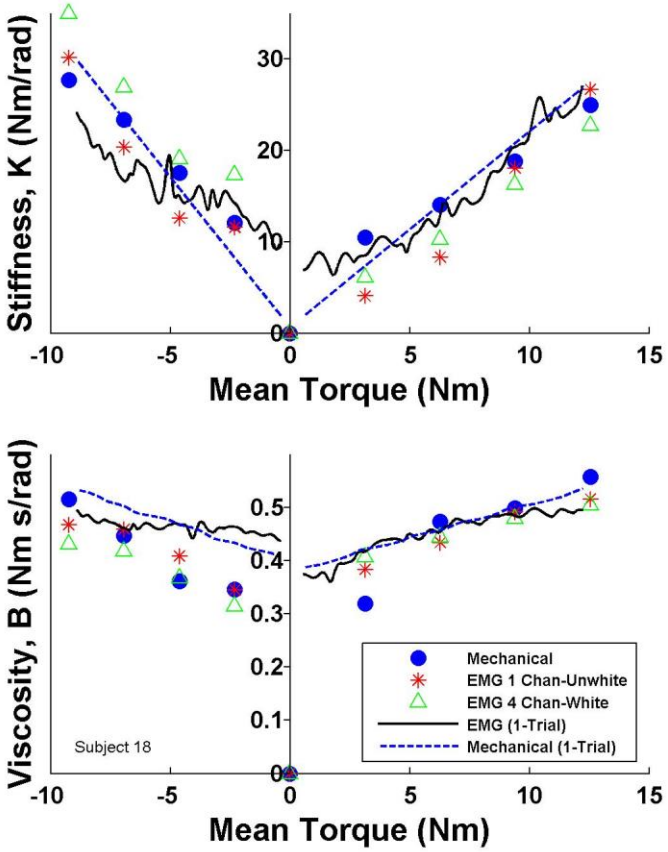

Fig. 4. Viscosity and stiffness estimates for one of the seven subjects.

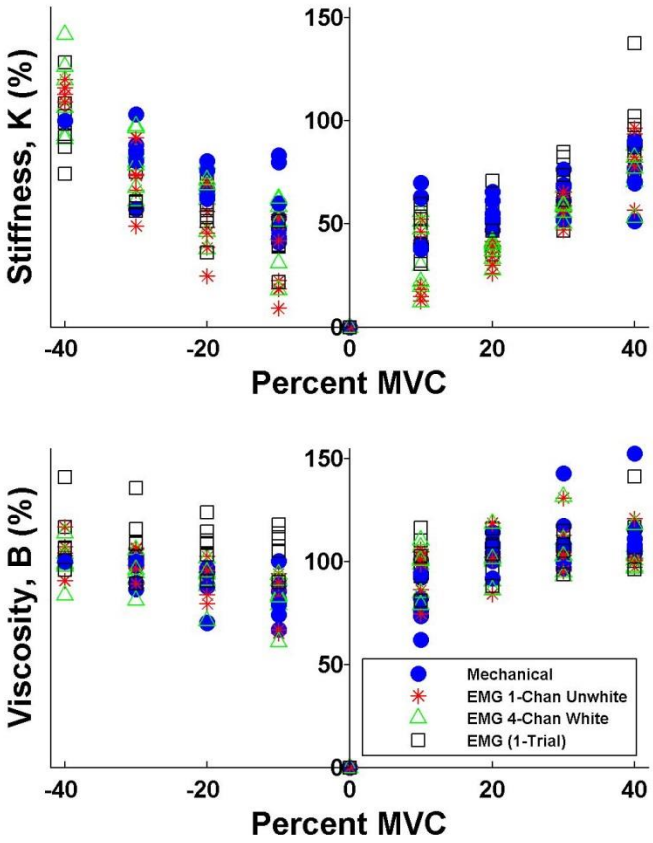

Fig. 5. Viscosity and stiffness estimates from all seven subjects, normalized to each subject's mechanically-estimated value at 40% extension.

5.4 References

An KN, P CW, Chao EY, Askew LJ, R DJ. Determination of forces in extensor pollicis longus and flexor pollicis longus of the thumb. J Appl Physiol. 1983;54:714–9.

Andison C. EMG-based assessment of active muscle stiffness and co-contraction in muscles with primary and secondary actions at the wrist during piano playing. Ottawa, Ontario, Canada: Carleton University; 2011.

Bennett DJ, Hollerbach JM, Xu Y, Hunter IW. Time-varying stiffness of human elbow joint during cyclic voluntary movement. Exp Brain Res. 1992;88:433–42.

Burdet E, Osu R, Franklin DW, Milner TE, Kawato M. The central nervous system stabilizes unstable dynamics by learning optimal impedance. Nature. 2001;414:446–9.

Cannon SC, Zahalak GI. The mechanical behavior of active human skeletal muscle in small oscillations. J Biomech. 1982;15:111–21.

Clancy EA, Bida O, Rancourt D. Influence of advanced electromyogram (EMG) amplitude processors on EMG-to-torque estimation during constant-posture, force-varying contractions. J Biomech. 2006;39:2690–8.

Clancy EA, Farry KA. Adaptive whitening of the electromyogram to improve amplitude estimation. IEEE Trans Biomed Eng. 2000;47:709–19.

Clancy EA, Hogan N. Relating agonist-antagonist electromyograms to joint torque during isometric, quasi-isotonic, non-fatiguing contractions. IEEE Trans Biomed Eng. 1997;44:1024–8.

Clancy EA, Liu L, Liu P, Moyer DV. Identification of constant-posture EMG-torque relationship about the elbow using nonlinear dynamic models. IEEE Trans Biomed Eng. 2012;59:205–12.

Disselhorst-Klug C, Schmitz-Rode T, Rau G. Surface electromyography and muscle force: Limits in sEMG-force relationship and new approaches for applications. Clin Biomech. 2009;24:225–35.

Doheny EP, Lowery MM, FitzPatrick DP, O'Malley MJ. Effect of elbow joint angle on force-EMG relationships in human elbow flexor and extensor muscles. J Electromyogr Kinesiol. 2008;18:760–70.

Doorenbosch CAM, Harlaar J. A clinically applicable EMG-force model to quantify active stabilization of the knee after a lesion of the anterior cruciate ligament. Clin Biomech. 2003;18:142–9.

Ford KR, van den Bogert J, Myer GD, Shapiro R, Hewett TE. The effects of age and skill level on knee musculature co-contraction during functional activities: A systematic review. Br J Sports Med. 2008;42:561–6.

Gomi H, Osu R. Task-dependent viscoelasticity of human multijoint arm and its spatial characteristics for interaction with environments. J Neurosci. 1998;18:8965–78.

Gottlieb GL, Agarwal GC. Dynamic relationship between isometric muscle tension and the electromyogram in man. J Appl Physiol. 1971;30:345–51.

Hagg GM, Melin B. Applications in ergonomics. In: Merletti R, Parker PA, editors. Electromyography: Physiology, Engineering, and Noninvasive Applications: IEEE Press/Wiley-Interscience; 2004. p. 343–63.

Hashemi J, Morin E, Mousavi P, Hashtrudi-Zaad K. Surface EMG force modeling with joint angle based calibration. J Electromyogr Kinesiol. 2013;23:416–24.

Hashemi J, Morin E, Mousavi P, Hashtrudi-Zaad K. Enhanced dynamic EMG-force estimation through calibration and PCI modeling. IEEE Trans Neural Sys Rehabil Eng. 2015;23:41–50.

Hashemi J, Morin E, Mousavi P, Mountjoy K, Hashtrudi-Zaad K. EMG-force modeling using parallel cascade identification. J Electromyogr Kinesiol. 2012;22:469–77.

Hunter IW, Kearney RE. Dynamics of human ankle stiffness: Variation with mean ankle torque. J Biomech. 1982;15:747–52.

Kawase T, Kambara H, Koike Y. A power assist device based on joint equilibrium point estimation from EMG signals. J Robot Mechatron. 2012;24:205–18.

Kearney R, E., Hunter IW. System identification of human joint dynamics. CRC Crit Reviews Biomed Eng. 1990;18:55–87.

Kearney R, E., Stein RB, Parameswaran L. Indentification of intrinsic and reflex contributions to human ankle stiffness dynamics. IEEE Trans Biomed Eng. 1997;44:493–504.

Liu P, Liu L, Clancy EA. Influence of joint angle on EMG-torque model during constant-posture, torque-varying contractions. IEEE Trans Neural Sys Rehabil Eng. 2015;23:1039–46.

Ljung L. System Identification: Theory for the User. Upper Saddle River, NJ: Prentice-Hall; 1999, pp. 491–519.

McIntyre J, Mussa-Ivaldi FA, Bizzi E. The control of stable postures in the multijoint arm. Exp Brain Res. 1996;110:248–64.

Osu R, Gomi H. Multijoint muscle regulation mechanisms examined by measured human arm stiffness and EMG signals. J Neurophysiol. 1999;81:1458–68.

Parker P, Englehart K, Hudgins B. Myoelectric signal processing for control of powered limb prostheses. J Electromyo Kinesiol. 2006;16:541–8.

Pfeifer S, Vallery H, Hardegger M, Riener R, Perreault EJ. Model-based estimation of knee stiffness. IEEE Trans Biomed Eng. 2012;59:2604–12.

Prakash P, Salini CA, Tranquilli JA, Brown DR, Clancy EA. Adaptive whitening in electromyogram amplitude estimation for epoch-based applications. IEEE Trans Biomed Eng. 2005;52:331–4.

Rack PMH, Westbury DR. The short range stiffness of active mammalian muscle and its effect on mechanical properties. J Physiol. 1974;240:331–50.

Rancourt D, Hogan N. Dynamics of pushing. J Motor Behavior. 2001a;33:351–62.

Rancourt D, Hogan N. Stability in force-production tasks. J Motor Behavior. 2001b;33:193–204.

Rosa MCN, Marques A, Demain S, Metcalf CD, Rodrigues J. Methodologies to assess muscle co-contraction during gait in people with neurological impairment—A systematic literature review. J Electromyo Kinesiol. 2014;24:179–91.

Rouse EJ, Gregg RD, Hargrove LJ, Sensinger JW. The difference between stiffness and quasi-stiffness in the context of biomechanical modeling. IEEE Trans Biomed Eng. 2013;60:562–8.

Shin D, Kim J, Koike Y. A myokinetic arm model for estimating joint torque and stiffness from EMG signals during maintained posture. J Neurophysiol. 2009;101:387–401.

Staudenmann D, Roeleveld K, Stegeman DF, van Dieen JH. Methodological aspects of EMG recordings for force estimation—A tutorial and review. J Electromyogr Kinesiol. 2010;20:375–87.

Thelen DG, Schultz AB, Fassois SD, Ashton-Miller JA. Identification of dynamic myoelectric signal-to-force models during isometric lumber muscle contractions. J Biomech. 1994;27:907–19.

Vredenbregt J, Rau G. Surface electromyography in relation to force, muscle length and endurance. New Developments Electromyogr Clin Neurophysiol. 1973;1:607–22.

Zhang L-Q, Rymer WZ. Simultaneous and nonlinear identification of mechanical and reflex properties of human elbow joint muscles. IEEE Trans Biomed Eng. 1997;44:1192–209.

Chapter 6: Comparison of Constant-Posture Force-Varying EMG-Force Dynamic Models About the Elbow

This chapter has been accepted as: Chenyun Dai, Berj Bardizbanian, and Edward A. Clancy, "*Comparison of Constant-Posture Force-Varying EMG-Force Dynamic Models About the Elbow*," *IEEE Transactions on Neural Systems and Rehabilitation Engineering*, in press. Color versions of one or more of the figures in this paper are available online at http://ieeexplore.ieee.org/stamp/stamp.jsp?arnumber=7782853.

***Abstract*—Numerous techniques have been used to minimize error in relating the surface electromyogram (EMG) to elbow joint torque. We compare the use of three techniques to further reduce error. First, most EMG-torque models only use estimates of EMG standard deviation as inputs. We studied the additional features of average waveform length, slope sign change rate and zero crossing rate. Second, multiple channels of EMG from the biceps, and separately from the triceps, have been combined to produce two low-variance model inputs. We contrasted this channel combination with using each EMG separately. Third, we previously modeled nonlinearity in the EMG-torque relationship via a polynomial. We contrasted our model vs. that of the classic exponential power law of Vredenbregt and Rau [1]. Results from 65 subjects performing constant-posture, force-varying contraction gave a "baseline" comparison error (i.e., error with none of the new techniques) of 5.5 ± 2.3% maximum flexion voluntary contraction (%MVC_F). Combining the techniques of multiple features with individual channels reduced error to 4.8 ± 2.2 %MVC_F, while combining individual channels with the power-law model reduced error to 4.7 ± 2.0 %MVC_F. The new techniques further reduced error from that of the baseline by ≈15%.**

***Index Terms*—Biological system modeling, electromyogram, EMG-force, multiple-channel EMG**

6.1 Introduction

Since at least the work of Inman *et al.* in 1952 [2], the surface electromyogram (EMG) has been investigated as an estimator of muscle force/joint torque. Much of the early work studied the linearity of the relation using agonist muscle EMG during constant-posture, quasi-constant force contractions ("quasi-static") [1-5]. During the intervening years, numerous studies (see review in [6]) have expanded the experimental conditions and reduced the error in the EMG-torque relationship through various improvements, including: modeling both agonist and antagonist muscle activity [7-10], accounting for subject-to-subject differences in the relationship [4, 11], reducing variability in the estimate of EMG standard deviation (EMGσ) by whitening the EMG signal and/or (for large muscle groups) utilizing multiple-channel EMGσ–torque estimators [12-21], modeling EMG-torque dynamics [19, 22-24], incorporating a range of joint angles [25-29], and applying robust system identification methods [11, 19, 24, 30, 31]. The various techniques are relevant in several areas in which a noninvasive EMG-torque estimate is useful, such as prosthesis control [32, 33], clinical biomechanics [34, 35] and ergonomics assessment [36, 37].

In a related problem in EMG-based prosthetics control, multiple EMG features have been used as inputs to the task of classifying distinct movement classes. In particular, Hudgins *et al.* [38] (see [39] for a review) added to EMGσ the features of slope sign change rate (SSC), zero crossing rate (ZC) and average waveform length (WL). Only recently has the success of these "additional" features in the EMG classification problem led to their investigation as model inputs in the EMG-torque problem [40-45].

In this study, we report on three techniques for continuing performance improvement in the EMG-torque relationship. First, most past studies using dynamic models of EMG-torque have exclusively utilized EMGσ as the input EMG feature. Thus, we look at the applicability of adding the additional features of Hudgins *et al.*, comparing models with and without their inclusion. Second, for large muscles, EMGσ variability has been reduced by combining the information from multiple electrodes into one EMGσ estimate [12-14, 16]. This method of channel combination is optimal assuming that the underlying muscle contains the same information across its multiple electrode locations, varying only due to the stochastic nature of motor unit firing times. However, there is evidence that large muscles—this research studies the biceps and triceps muscles—contain some degree of control based on neuromuscular compartments [46-48]. As such, combining EMG sites to produce a feature estimate would no longer be justified. Thus, we contrast combining EMG sites to estimate a feature vs. extracting features from each individual electrode. Third, our own dynamic EMG-torque models have incorporated

the static power-law nonlinearity described by Vredenbregt and Rau [1] via the use of a polynomial relation [29, 31]. This method simplifies the mathematics, allowing the use of *linear* least squares estimation, but can require many parameters—which can have its own detrimental effects [49]. Other authors have captured a nonlinear relationship with other model forms, e.g., parallel-cascade models [24] and neural networks [40, 42, 44, 45, 50]. Therefore, we directly compared use of the power-law nonlinearity of [1] (requiring parameter estimation via *nonlinear* least squares) to that of the polynomial model. Finally, we examined if combining pairs of these various improvement techniques provides an additive benefit. We also varied the dynamic model order (i.e., number of time lags) and the tolerance value associated with the Moore-Penrose inverse method used to linear least squares fit model parameters. These parameters influence EMG-force errors [31] and thus should be optimized within each of the three primary techniques studied in this work.

6.2 Methods

6.2.1 Experimental Subjects, Apparatus and Methods

Experimental data from 54 subjects acquired during three prior experiments [29, 51, 52] were combined with the data from 11 new subjects to form a pool of 65 total subjects. The new data collection and all analysis was approved and supervised by the WPI Institutional Review Board. Each of the 65 subjects provided written informed consent for their respective experiment. For the new data collection (similar methods were used in the prior experiments), subjects were seated and strapped via three belts into the custom-built straight-back chair shown in Fig. 1, with their right shoulder abducted 90°, the angle between their upper arm and forearm 90°, their forearm oriented in a parasaggital plane, and their supinated right wrist (palm perpendicular to the floor) tightly cuffed to a load cell (Vishay Tedea-Huntleigh Model 1042, 75 kg full scale). Skin above the biceps and triceps muscles was vigorously scrubbed with an alcohol wipe and a bead of electrode gel was massaged into the overlying skin. Four custom-built bipolar EMG electrode-amplifiers were applied in a transverse row across each of the biceps and triceps muscle groups, midway between the elbow and the midpoint of the upper arm (to avoid the innervation zone proximally and the tendon distally), centered along the muscle mid-line. Each electrode-amplifier had a pair of 8 mm diameter, stainless steel, hemispherical contacts separated 1 cm edge-to-edge, oriented along the muscle's long axis. The distance between adjacent electrode-amplifiers was ~1.75 cm. A reference electrode was gelled and secured to the lateral aspect of the upper arm,

between the flexion and extension electrodes. All electrodes were secured in place on the right arm with elastic bandages. Custom electronics amplified and filtered each EMG signal (CMRR > 90 dB at 60 Hz; 8th-order Butterworth highpass at 15 Hz; 4th-order Butterworth lowpass at 1800 Hz) before being sampled at 4096 Hz with 16-bit resolution. The RMS EMG signal level at rest (representing equipment noise plus ambient physiological activity) was on average 5.0 ± 7.3% of the RMS EMG at 50% maximum voluntary contraction (MVC) for these 11 new subjects. The load cell (torque) signal was synchronously sampled at 4096 Hz with 16-bit resolution.

All contractions were constant-posture. Subjects were provided a warm-up period. Separate extension and flexion MVCs were then measured in which subjects took 2–3 seconds to slowly ramp up to MVC and maintained that force for two seconds. The average load cell value during the contraction plateau was taken as the MVC. Five second duration, constant-force contractions at 50% MVC extension, 50% MVC flexion and at rest (arm removed from the wrist cuff) were next recorded. These contractions were used to calibrate whitening filters and to gain-normalize the EMG and force data [52, 53], as further described below. Then, three tracking trials of 30 s duration were recorded during which the subjects used the load cell as a feedback signal to track a computer-generated torque target. The target moved on the screen in the pattern of a bandlimited (1 Hz) uniform random process, spanning 50% MVC extension to 50% MVC flexion. Three minutes of rest were provided between trials to avoid cumulative fatigue.

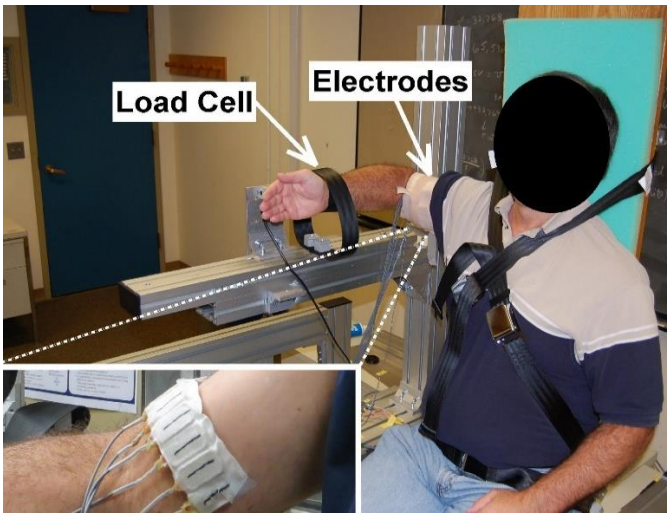

Fig. 1. Subject seated in the experimental apparatus with right arm cuffed at the wrist to the load cell and electrodes applied over the biceps and triceps muscles. Inset shows six electrodes positioned transversely across the biceps muscles (with securing bandage removed for visualization). Middle four electrodes used for the analysis reported herein. Triceps electrodes were arranged similarly.

6.2.2 Methods of Analysis

Analysis was performed offline in MATLAB. All EMG filters were designed as specified below, then applied in the forward and reverse time directions to achieve zero phase and the square of the magnitude response. Each EMG channel was powerline notch filtered (2nd-order IIR notch filter at the fundamental and each harmonic, bandwidth $\leq$ 1.5 Hz), since whitening at high frequencies is particularly susceptible to powerline interference. These filters attenuate powerline noise with limited reduction in signal statistical bandwidth [54]. Each EMG channel was then highpass filtered to reject motion artifacts (5th-order Butterworth, 15 Hz cutoff) and whitened using the adaptive whitening algorithm of [52] and [53]. Features were next extracted from each of the eight whitened EMG signals. EMGσ[n] was formed by rectifying each signal and WL[n] was computed as the absolute difference between adjacent samples [38, 39, 55], where n was the discrete-time sample index at the sampling rate of 4096 Hz. ZC[n] and SSC[n] [38, 39, 55] were formed by assigning a value of one to each sample corresponding to a thresholded zero crossing/slope sign change, and a value of zero otherwise. For each electrode, the noise threshold used for ZC and SSC was 3% of the RMS of a rest contraction. Two different EMG channel selection options were studied: (1) features from the four biceps and, separately, triceps channels were each ensemble averaged to form four-channel feature estimates (for EMGσ and WL, the channels were gain normalized prior to doing so [16]), or (2) features from each of the eight individual EMGs were retained separately. EMG features and the torque measurement were next lowpass filtered at 16 Hz, then downsampled to 40.96 Hz. This rate is fast enough to capture the system dynamics while also eliminating high-frequency noise outside of the torque signal band that can confound the ensuing system identification [30, 49]. Note that the lowpass filter stage prevents aliasing when downsampling, while simultaneously smoothing (/averaging) the EMG features. Further smoothing is inherently customized to each subject, provided by the dynamic models (described in the next paragraph). Hence, the dynamic models optimize the final lowpass cutoff frequency (and shape) in order to minimize EMG-torque error [56].

The decimated extension and flexion EMG features from each subject (inputs) were related to their respective elbow torque (output) via one of two dynamic models. The first "quadratic" model incorporated a second degree polynomial (based on prior optimization of a subset of these data [31], and consistent with the nonlinearity in the EMG-force curve at the elbow [1]):

$$T[m] = \sum_{q=0}^{Q} \sum_{f=1}^{F} \sum_{e=1}^{E} \left\{ c_{1,q,f,e} V_{f,e}[m-q] + c_{2,q,f,e} V_{f,e}^2[m-q] \right\}, \quad (1)$$

where m was the decimated discrete-time sample index, $T[m]$ the measured torque, Q the number of time lags in the model (to provide dynamics), F the number of EMG features included (EMGσ was always included; optionally either one or all of the remaining three features was included), E the number of EMG channels (E=2 was used when the four biceps and four triceps channels were combined into two channels; E=8 was used when eight individual channels were retained), c_i were the fit coefficients, and $V[\cdot]$ were the EMG feature values. The fit coefficients were estimated using regularized (Moore-Penrose inverse) linear least squares, in which singular values of the design matrix were discarded if their ratio to the largest singular value was less than a selected tolerance value (Tol) [31, 57]. Thus, the EMG features, and their squared values, were least squares fit to torque.

The second "power-law" model was:

$$T[m] = \sum_{q=0}^{Q} \sum_{f=1}^{F} \sum_{e=1}^{E} c_{q,f,e} V_{f,e}^{r_{f,e}}[m-q], \quad (2)$$

where r was also a fit parameter equal to a continuous-valued exponent applied to the feature value. This exponent directly implemented the EMG-force nonlinearity of Vredenbregt and Rau [1]. The fit coefficients (c_i, r_i) were fit using nonlinear least squares. Anecdotally, initial solution guesses for r of 0.5, 1 and 2 were evaluated, with the c_i coefficients then initialized via linear least squares (using a pseudo-inverse tolerance of 0.005). Only the r = 1 value converged rapidly for most subjects. When each of these three r values led to convergence, they arrived at the same minimum soution. Thus, r = 1 was used as the initial guess value. This initial guess value happens to be the optimal linear solution.

Of the three available tracking trials, two were used for training and one for testing. Since the nonlinear minimizations were time-intensive and the sample size was already quite large for an EMG-torque study (65 subjects), cross-validation was not used. Error is reported as the test set RMS error between the actual and EMG-estimated torque, normalized to maximum flexion torque for each subject. The first and last 2 s of data were excluded to account for filter startup and tail transients[2]. We investigated combinations of: model orders between Q=5 to 40, five distinct EMG feature selections (EMGσ only, EMGσ paired with each of the other three features and all four features), two EMG

[2] In real-time applications, all processing would be conducted using causal filters, eliminating the need to exclude any tail transients. (They would not exist.) The startup transient would occur at device power-up and thus not interfere with regular device operation.

channel selections (a four-channel biceps EMGσ with a four-channel triceps EMGσ, or retaining all eight individual electrodes), two models (quadratic and power-law), and various pseudo-inverse linear least squares tolerance values (starting at *Tol*=0.1 and decrementing by 0.002 to 10^{-3}, and 10^{-4} and 10^{-5}). Note that we did not investigate every combination of model order and pseudo-inverse tolerance vs. the other parameters, since doing so would have been prohibitively time-consuming and the influence of model order and tolerance has already been characterized in prior work [31]. Rather, tolerance was fixed at *Tol*=0.005 while model order was varied; and model order was fixed at *Q*=15 while tolerance was varied.

Finally, for comparison to conventional EMG-torque models, we also investigated cascade of a fixed, second-order Butterworth filter (cut-off frequency of 1.5 Hz , as optimized for a subset of these data in prior work [56]) after each of the extension and flexion EMGσ signals, as derived from single-channel unwhitened EMG (selecting one of the central electrodes on each muscle). The gains of both filters (i.e., the fit coefficients for the Butterworth model) were calibrated from the test data using linear least squares (*Tol* = 0.005, two training trials, one test trial).

Statistical evaluation used multivariate ANOVA (significance level of $p = 0.05$), with *post hoc* pair-wise comparisons conducted using Tukey's honestly significant difference test (which adjusts for multiple comparisons).

6.3 Results

Our strategy was to individually compare the three study techniques of EMG features, EMG channel combination and model vs. our "baseline" best prior technique [31] comprised of the EMGσ feature only, four-channel EMG processors and the quadratic polynomial model. As appropriate, we also assessed performance as a function of dynamic model order (*Q*) and pseudo-inverse tolerance (*Tol*). Then, we assessed improvement (beyond that found due to one study technique) when pairs of study techniques were combined. We do not report results from all three study techniques combined, since the nonlinear minimization frequency failed to converge—presumably due to the large number of features encountered when using all (five) features and eight individual EMG channels. Note that for several analyses, model order was fixed at *Q*=15 and the pseudo-inverse tolerance was fixed at *Tol*=0.005. These fixed values were determined based on prior analysis of a portion of these data [31] (and are consistent with our results reported herein). Example time-series EMG-torque estimates are shown in

Fig. 2. For comparison, the conventional Butterworth model had average ± std. dev. RMS error of 8.9 ± 3.0 %MVC$_F$.

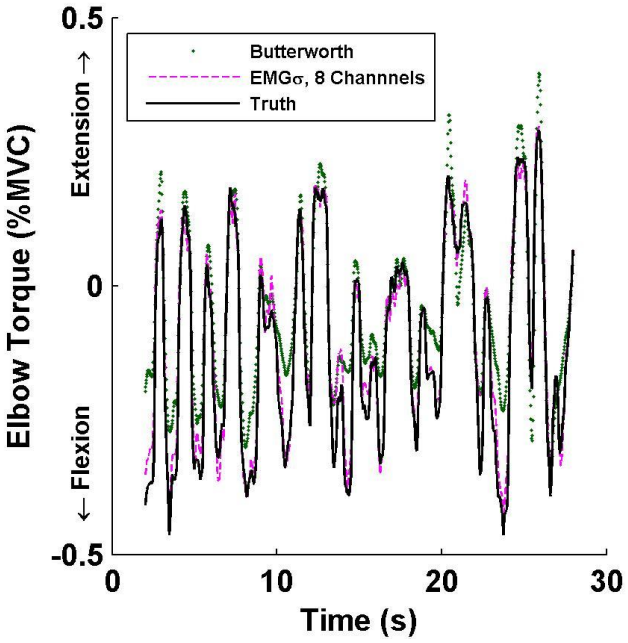

Fig. 2. Example EMGσ-torque estimation results for selected models. Butterworth model (2 Hz lowpass filter cut-off) exhibited an RMS error of 10.2 %MVC. Eight-channel EMGσ model (Q = 15 order, pseudo-inverse tolerance of Tol = 0.005) exhibited an RMS error of 4.5 %MVC. "Truth" refers to the recorded load cell values. Subject LA04, trial 45.

6.3.1 Baseline Technique vs. One Improvement Technique

EMG Feature Set: We began by comparing the results between the baseline technique (EMGσ only, four-channel EMG and quadratic model) vs. EMG feature set. Fig. 3, top, shows average error results vs. dynamic model order (Q) with pseudo-inverse tolerance fixed at Tol=0.005. Error reduced rapidly as model order initially increased and the full feature set showed the lowest error. A two-way ANOVA (Factors: model order, feature set) was significant for both main effects [F(35, 140)=17, p=10^{-4} for model order; F(4, 140)=4.9, p=10^{-3} for feature set], without interaction. *Post hoc* Tukey evaluation of model order found that lower orders exhibited higher errors than the highest orders for orders Q=5 through 8. Results for model orders 9–40 did not differ. *Post hoc* Tukey differences were also found as a function of the feature set: EMGσ had higher error than either EMGσ+WL or the full set. At Q=15, the baseline technique error (mean ± std.) was 5.5 ± 2.3 %MVC$_F$. Fig. 3, bottom, shows results vs. pseudo-inverse tolerance (Tol) with model order fixed at Q=15. Error reduced rapidly as tolerance decreased,

and the full feature set showed the lowest error. To avoid the interactions at the larger tolerance values, a two-way ANOVA (Factors: tolerance, feature set [3]) omitted tolerance values above 0.011. This comparison was only significant for the main effect of feature set [$F(4, 40)=3.1$, $p=0.01$], without interaction. *Post hoc* Tukey comparisons only found differences between the EMGσ-only feature vs. the full feature set. Overall, the full feature set generally produced lower errors.

EMG Channel Selection: Next, we compared results between the baseline technique vs. individual EMG channels. Fig. 4, top, shows results vs. model order Q (*Tol* fixed at 0.005). Error reduced as model order initially increased and the individual EMG channels had lower error. A two-way ANOVA (Factors: model order, EMG channel selection) was significant for both main effects [$F(35, 35)=7.4$, $p=10^{-6}$ for model order; $F(1, 35)=96$, $p=10^{-6}$ for channel selection], without interaction. *Post hoc* Tukey evaluation of model order found that lower orders had higher errors than the highest orders for orders Q=5 through 7. Results for model orders 8–40 did not differ. *Post hoc* Tukey evaluation of EMG channel selection found individual EMG channels to have lower error. Fig. 4, bottom, shows results vs. tolerance (Q fixed at 15). For consistency, a two-way ANOVA (Factors: tolerance, EMG channel selection) omitted tolerance values above 0.011. This comparison was only significant for the main effect of EMG channel selection [$F(1, 10)=34$, $p=10^{-6}$; no interaction], with *post hoc* Tukey evaluation finding individual EMG channels to have lower error. Overall, using eight separate channels—as opposed to extension/flexion four-channel processors—consistently led to lower error.

Power-Law Model: Then, we compared results between the baseline technique and the power-law model. Fig. 5 shows these results vs. model order (Q), with *Tol*=0.005 selected for the quadratic model. Tolerance was not examined as a separate factor, as it is not varied with the power-law model. Error using the power-law model was consistently lower than that of the baseline model. A two-way ANOVA (Factors: model order, model type) was significant for both main effects [$F(35, 35)=9.4$, $p=10^{-6}$ for model order; $F(1, 35)=33$, $p=10^{-6}$ for model type], without interaction. *Post hoc* Tukey evaluation of model order found that lower orders exhibited higher errors than the highest orders for orders Q=5 through 7. Results for model orders 8–40 did not differ. *Post hoc* Tukey evaluation of model form found lower errors with the power-law model. Overall, the power-law model produced lower errors.

[3] Note that a three-way ANOVA with factors model order, tolerance and feature set was not pursued since results from all combinations of model order and tolerance were not computed (see Methods). Instead, model order and tolerance were analyzed in separate two-way ANOVAs (here and also below).

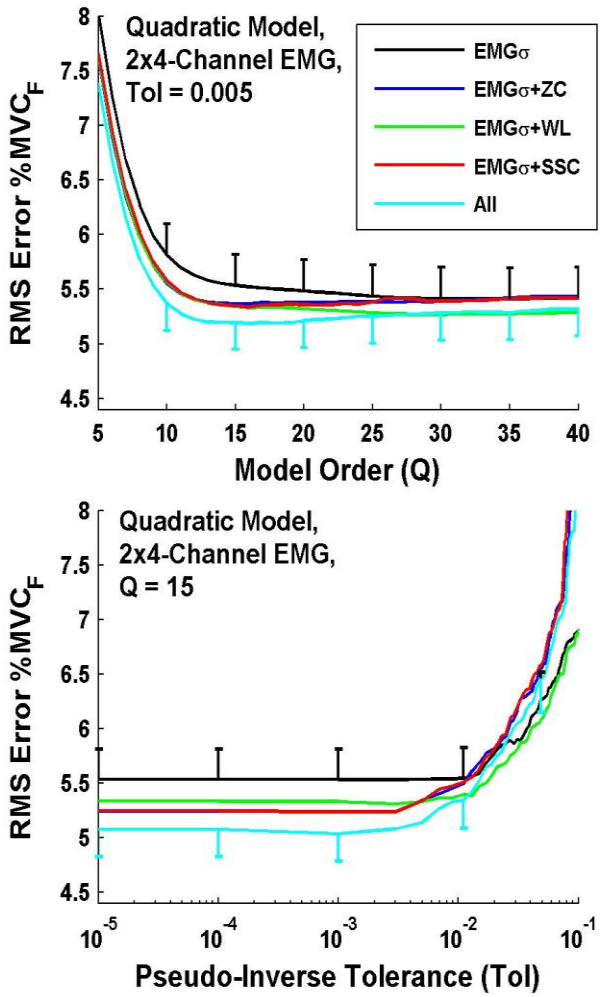

Fig. 3. Baseline Model vs. Feature Set: Average RMS errors from 65 subjects, four-channel EMG. Legend refers to both plots. Single-sided standard error bars shown for two of five feature sets (standard errors were similar for the other three feature sets) for selected Q values. Top: Results vs. quadratic model order (Q), using pseudo-inverse tolerance of Tol=0.005. Bottom: Results vs. pseudo-inverse tolerance, with quadratic model order Q=15.

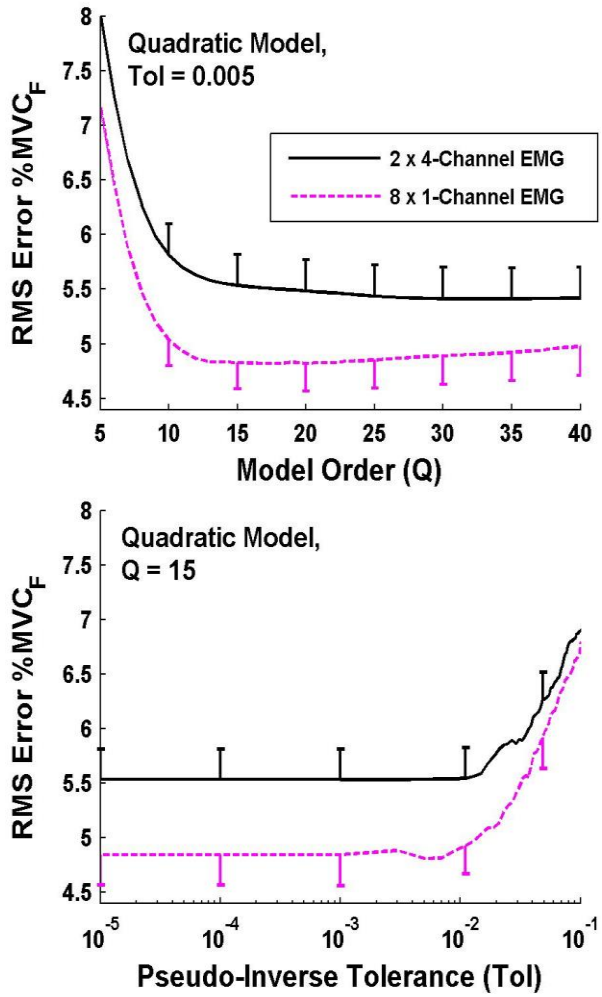

Fig. 4. Baseline Model vs. EMG Channel Selection: Average RMS errors from 65 subjects, EMGσ-only feature set. Single-sided standard error bars shown for selected Q values. Top: Results vs. quadratic model order (Q), using pseudo-inverse tolerance of Tol= 0.005. Bottom: Results vs. pseudo-inverse tolerance, with quadratic model order Q=15.

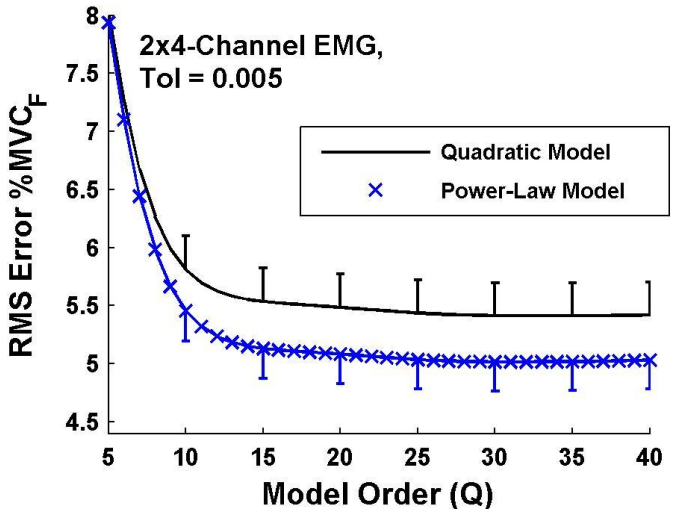

Fig. 5. Baseline Model vs. Power-Law Model: Average RMS errors from 65 subjects, EMGσ-only feature set. Results vs. model order (Q). Quadratic model used pseudo-inverse tolerance of Tol=0.005. Single-sided standard error bars shown for selected Q values.

6.3.2 One Improvement Technique vs. Two

We concluded from the above results that each of the three techniques improved EMG-torque performance *individually*. Thus we next evaluated *pairs* of techniques, comparing each pair to the individual improvements. For EMG feature sets, we only retained two options, EMGσ only and all features. The results above showed that the other feature set options had performance that fell between these two. Also, we eliminated the reporting of *post hoc* statistical evaluation for model order and tolerance, as their roles were well established by the results above and prior literature results [31]. Doing so placed our focus on the three improvement techniques.

EMG Feature Set & EMG Channel Selection: Above, Fig. 3 showed the error improvements from the baseline technique due to EMG feature set and Fig. 4 to EMG channel selection. Here, Fig. 6 repeats both of these individual results, then adds the results when these techniques are combined (quadratic model with all features and eight individual EMG channels). For the results shown in Fig. 6, top, a two-way ANOVA (Factors: model order, the three techniques) was significant for both main effects [$F(35, 70)=8.7$, $p=10^{-6}$ for model order; $F(2, 70)=23$, $p=10^{-6}$ for technique], without interaction. *Post hoc* Tukey evaluation of technique found that using all EMG features with four-channel EMG had higher error than the other two techniques (EMGσ only, eight individual channels; all features, eight individual channels). At Q=15, the technique with all features and eight individual EMG channels had an error mean ± std. of 4.8 ± 2.2 $\%MVC_F$. The error results shown in Fig. 6, bottom, are high for all techniques

for large tolerance values and climb when using all features and eight individual channels for tolerances $\leq 10^{-3}$. A two-way ANOVA (Factors: tolerance values $\leq$0.011, the three techniques) was only significant for technique [F(2, 20)=4.2, p=0.02; no interaction]. *Post hoc* Tukey evaluation of technique found that using EMGσ only with eight individual channels exhibited lower error than the other two techniques. Nonetheless, Fig. 6 shows similar performance specifically in the region of the optimum tolerance value (e.g., *Tol* = 0.005), when comparing the technique of EMGσ only with eight individual channels to the technique of all features with eight individual channels.

EMG Feature Set & Model Form: Above, Fig. 3 showed the error improvements due to EMG feature set and Fig. 5 to model form. Here, Fig. 7 repeats both of these individual results, then adds the results when these techniques are combined (four-channel EMG with all features and the power-law model). A two-way ANOVA (Factors: model order, the three techniques) was significant for the main effect of model order [F(35, 70)=13, $p=10^{-6}$], but not significant for the main effect of technique [F(2, 70)=2.8, p=0.06], without interaction. Thus, this paired set of improvements did not reduce error beyond that found from each individual technique. At Q=15, each of the three techniques had an error mean ± std. of approximately 5.1 ± 2.1 %MVC$_F$.

EMG Channel Selection & Model Form: Above, Fig. 4 showed the error improvements due to eight individual EMG channels and Fig. 5 to model form. Here, Fig. 8 repeats both of these individual results, then adds the results when these techniques are combined (EMGσ-only feature with eight individual EMG channels and the power-law model). A two-way ANOVA (Factors: model order, the three techniques) was significant for both main effects [F(35, 70)=14, $p=10^{-6}$ for model order; F(2, 70)=21, $p=10^{-6}$ for technique], without interaction. *Post hoc* Tukey evaluation of technique found that using four-channel EMG with the power-law model had higher error than the other two techniques. At Q=15, the technique with eight individual EMG channels and the power-law model had an error mean ± std. of 4.7 ± 2.0 %MVC$_F$.

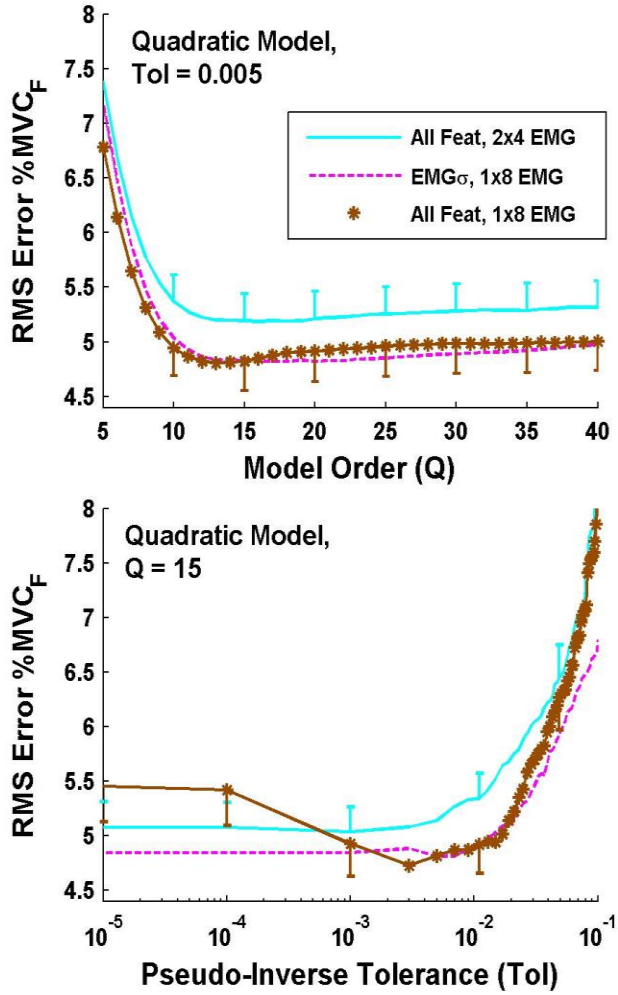

Fig. 6. Quadratic Model: All Features vs. Eight Individual EMG vs. Both. Average RMS errors from 65 subjects. Legend refers to both plots. Single-sided standard error bars shown for two of three feature sets (standard errors were similar for the third feature set) for selected Q values. Top: Results vs. quadratic model order (Q), using pseudo-inverse tolerance of Tol=0.005. Bottom: Results vs. pseudo-inverse tolerance, with quadratic model order Q=15.

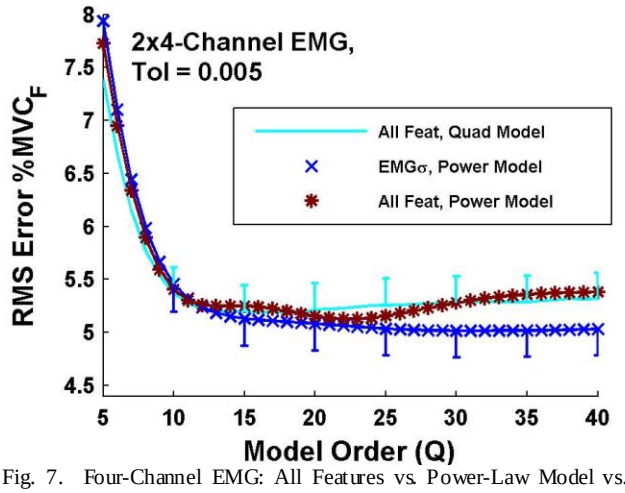

Fig. 7. Four-Channel EMG: All Features vs. Power-Law Model vs. Both. Average RMS errors from 65 subjects. Results vs. model order (Q). Quadratic model used pseudo-inverse tolerance of Tol=0.005. Single-sided standard error bars shown for two of three feature sets (standard errors were similar for the third feature set) for selected Q values.

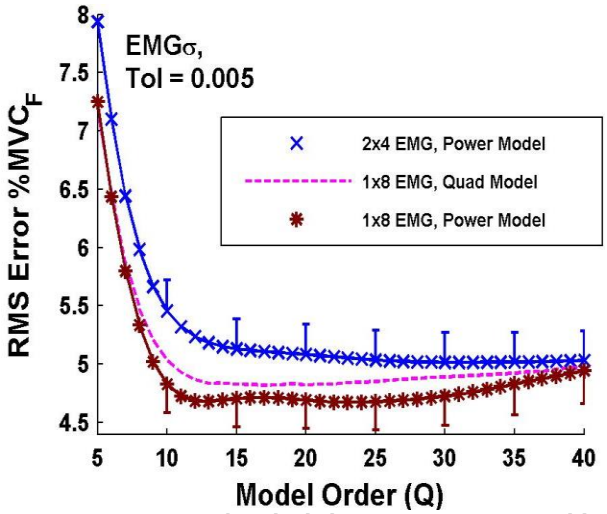

Fig. 8. EMGσ Feature: Eight Individual EMG vs. Power-Law Model vs. Both. Average RMS errors from 65 subjects. Results vs. model order (Q). Quadratic model used pseudo-inverse tolerance of Tol=0.005. Single-sided standard error bars shown for two of three feature sets (standard errors were similar for the third feature set) for selected Q values.

6.4 Discussion

This study evaluated three techniques to reduce error in the EMG-torque relationship about the elbow—additional EMG features, EMG channel selection and EMG-force model form. Figs. 3–5 (and their associated statistical analyses) show that *each* of these techniques *individually* improved upon a "baseline" model that used only the EMGσ feature, four-channel EMG for each of the biceps and

triceps, and the quadratic polynomial model. Note that this baseline model already optimizes several processing steps, including using EMG signal whitening, selecting the degree of the polynomial model and selecting the pseudo-inverse tolerance [15, 16, 31]. Whitening has previously been shown to reduce the variance of EMGσ estimates [13-16], e.g. providing an ≈63% improvement in SNR for constant-posture, constant-force elbow contractions when using a 245 ms smoothing window [15]. EMG whitening leads to significant performance improvements in EMG-torque estimation [17, 31], e.g. a 14.1% reduction in RMS error during constant-posture, repetitive elbow exertions [17]. Whitening has also been shown to reduce the variance of WL and (to some extent) ZC estimates [55] (leading to performance improvements in multifunction prosthesis control [55]). The variance reduction is attributed to an increase in signal statistical bandwidth provided by whitening [13, 55]. Therefore, we would expect similar variance reduction in whitened estimates of the SSC feature.

Of the three techniques, Figs. 6 and 8 show that using eight individual EMGs (as opposed to a four-channel EMG for each of the biceps and triceps) provides the clearest advantage. The concept of combining the information from multiple electrodes sited over a large muscle assumes that the spatially diverse information represents different statistical samples of the same underlying stochastic process [12, 13]. The elbow contractions used herein were constrained to a single plane, reinforcing this assumption. Certainly, prior work has shown that four-channel EMG over the biceps and triceps leads to lower EMG-torque error than if only one biceps and one triceps EMG were used [12, 13, 30, 31], attributed largely to lower EMGσ variance [12, 13, 15-17]. However, our current results show that further error reduction is realized if the multiple EMG channels are used as separate inputs to the system identification model. Several concepts could explain this further improvement, all challenging the assumption that each electrode is stochastically sampling the same distribution. First, the individual electrodes could be sampling from distinct spatial regions with distinct neuromuscular control (i.e., neuromuscular compartments [46-48]). Second, we have anecdotally noticed that electrodes placed further from the muscle midline are more prone to crosstalk from the antagonist muscles, and that the EMG from such electrodes leads to a poorer EMG-torque estimate. The use of individual electrodes would permit the system identification model to de-emphasize those EMG channels that contribute less to reducing the EMG-torque error. Third, the quality of the EMG signal (e.g., signal to noise ratio) can vary electrode-to-electrode. When used as individual channels, the system identification model can de-emphasize the noisy electrodes; but when combined into a four-channel EMG, the emphasis of

individual channels is purposely equalized [12, 16]. Future research should examine which EMG channels are more heavily weighted in these identified models.

Because the decrease in EMG-force error due to eight individual EMG channels was robust to model form, it may be especially applicable to other nonlinear models used in the literature, such as parallel-cascade models [24] and neural networks [40, 42, 44, 45, 50]. All model forms, however, become increasingly ill-conditioned as more fit parameters are added, the relative importance of which may vary model form to model form.

Figs. 6–8 show that the remaining two improvement techniques (EMG feature sets and EMG-force model form) each provide approximately the same error reduction—Fig. 6, top, shows that all features, eight individual EMG channels and the quadratic model (Q=15, Tol=0.005) had an error mean ± std. of 4.8 ± 2.2 %MVC$_F$.; while Fig. 8 shows that the EMGσ-only feature, eight individual EMG channels and the power-law model (Q=15) had an error mean ± std. of 4.7 ± 2.0 %MVC$_F$. These error performances represent an ≈15% reduction in error compared to the baseline model error of 5.5 ± 2.3 %MVC$_F$. The power-law model has the advantage of fulfilling the static EMG-force nonlinearity found by Vredenbregt and Rau [1] with a single exponential parameter per EMG channel, but the disadvantage of requiring significantly more computation time for determining fit coefficients via nonlinear least squares. A concern with using additional EMG features is their effect on the conditioning of the linear/nonlinear least squares fit, since conditioning is inversely related to the number of fit coefficients [49]. In particular, Fig. 6, bottom, shows error increasing for tolerances below 10^{-3} when all four features for each of eight individual channels are fit using the quadratic model (64 coefficients in total). Tolerances below 10^{-3} provide progressively less regularization, the opposite of what is needed when the number of fit coefficients grows. Hence, model error grows, likely due to overfitting. As a result, the range of tolerance values over which error is minimum shrinks, making the modeling less reliable.

Considering systematic errors in the EMG-torque techniques, the use of multiple features expands the model shapes that can be fit (i.e., beyond the shapes that can be accommodated when only using EMGσ as an input). The performance of EMG-torque models also suffer from random errors due to the stochastic nature of EMG. The uncorrelated components of the four EMG features would tend to average and reduce variance errors. (E.g., when one feature value is randomly above its "true" value, another feature might be below.) Hence, both systematic and stochastic improvements can result. Of course, a challenge is to improve EMG-torque performance due to these advantages, in spite of the

detrimental effects of overfitting (due to the increased number of parameters) and feature correlation (which, combined with overfitting, degrade the conditioning of the least squares fit). Future modeling might consider a compromise approach that only utilizes a sub-set of the additional features.

For the quadratic polynomial model, we focused our attention on a model order of Q=15 and a tolerance of Tol=0.005. Our ANOVA results showed statistical differences (reductions) in error as model order increased from Q=5 to Q=7 or 8 (depending on the condition). Nonetheless, all of our graphical results show continuing decline in error up to about Q=15. Although we had a large sample size of 65 subjects, it is likely that statistical power limited our ability to find statistical differences for orders above 8. In particular, paired statistical tests can be more powerful when assessing different treatments (i.e., EMG-force techniques) applied to the same data. For example, consider the technique that demonstrated the lowest average error: EMGσ-only feature, eight individual channels and the power-law model (Fig. 8). If we successively compute paired sign tests [58] between adjacent model orders at/above Q=8, we find statistical differences (p<0.01) until comparing orders Q=12 to 13. Such comparisons support our choice of Q=15 (and are more fully detailed in [31]). A similar argument supports our use of Tol=0.005.

Within the literature, it is difficult to directly compare EMG-torque results between studies, since error is a function of many variables, including the experimental conditions (e.g., constant-posture vs. freely moving) and experimental tasks (e.g., random, broadband torques vs. sinusoidal). Further, several different error measures are used within the literature. However, relative changes in performance in the same dataset, evaluated with the same error measure, should be more robust when compared. To that end, we have studied sub-portions of this data set in several published studies. The highest error of 19.2 ± 11.2 $\%MVC_F$ was found when supplying single-channel, unwhitened EMGσ to a simple second-order Butterworth model, calibrated from 50% constant-force contractions [31]. Our results herein reduced the error to 8.9 ± 3.0 $\%MVC_F$ when the single-channel, unwhitened EMGσ supplied to the Butterworth model was calibrated from two dynamic contractions. This error was reduced to 5.5 ± 2.3 $\%MVC_F$ with our "baseline" method that used four-channel, whitened EMG and a quadratic nonlinearity (and FIR linear model). Finally, error was reduced to 4.7 ± 2.0 $\%MVC_F$ (the primarily work reported herein) by substituting individual EMG channels (rather than grouping them, separately, from the biceps and triceps muscle groups) and the power-law model (or reduced to 4.8 ± 2.2 $\%MVC_F$ by substituting individual EMG channels and all features). Thus, dramatic reduction in EMG-torque error has been

achieved overall. In many applications in clinical biomechanics and ergonomics assessment, electrodes would be mounted on a subject, calibration data recorded and then a clinical/experimental task completed in a single session. Since appropriate EMG-torque calibration data is required for these scenarios and computation is readily available, all of the performance gains realized by these modeling techniques could be utilized. For prosthesis control, however, there is some evidence that improved off-line classification results do not always translate into improved on-line classification performance when assessed on standard prosthesis tasks [59, 60]. Although our research involved EMG-torque estimation and not EMG-based classification, similar concerns exist [61].

We limited this work to constant-posture contractions in order to reduce the complexity of a problem that already considers many modeling variables. In so doing, our results are directly relevant to prosthesis control when EMG is observed over remnant muscles whose posture is constrained (e.g., secured at both ends to the same bone), and in clinical/ergonomic assessments in which such postural constraint is appropriate. But, when joint angle is varied, additional study will be necessary. That said, the reduction in RMS error can be thought of as a reduction of two error components: a variance error and a bias error. Those processing techniques that generally reduce variance (e.g., whitening, averaging due to multiple EMG channels, averaging due to multiple EMG features) should reduce EMG-torque error regardless of the experimental conditions. Techniques that reduce bias would likely need to be substituted with appropriate posture-varying models. The relative magnitude of variance vs. bias error can also change in posture-varying contractions. Nonetheless, our results should be informative to future studies of the reduction of both components of the RMS error in posture-varying contractions.

6.5 Conclusion

Our baseline technique for relating EMG to torque—EMGσ feature only, four-channel EMG from each of the biceps and triceps and a dynamic, quadratic nonlinear model—produced an error mean $\pm$ std. on this dataset of 5.5 $\pm$ 2.3 %MVC$_F$. This baseline technique already includes several technique optimizations, including EMG signal whitening, multi-site EMG and the use of the quadratic nonlinearity [31]. Three technique improvements were individually applied. These improvements were: additional EMG features, the use of eight individual EMG channels and a power-law model. Each technique individually lowered EMG-torque fit error. Combining the techniques of additional features and individual channels reduced error to 4.8 $\pm$ 2.2 %MVC$_F$, while combining individual channels with

the power-law model reduced error to 4.7 ± 2.0 %MVC$_F$. These error performances represent an ≈15% reduction in error compared to the baseline model. Hence, these combined techniques represent a substantial improvement in performance. These results should be informative to application areas, including prosthesis control, clinical biomechanics and ergonomics assessment.

References

[1] J. Vredenbregt and G. Rau, "Surface electromyography in relation to force, muscle length and endurance," *New Developments Electromyogr. Clin. Neurophysiol.*, vol. 1, pp. 607–622, 1973.

[2] V. T. Inman, H. J. Ralston, J. B. Saunders, B. Feinstein, and E. W. Wright, "Relation of human electromyogram to musculuar tension," *EEG Clin. Neurophysiol.*, vol. 4, pp. 187–194, 1952.

[3] J. H. Lawrence and C. J. De Luca, "Myoelectric signal versus force relationship in different human muscles," *J. Appl. Physiol.: Respirat. Environ. Exercise Physiol.*, vol. 54, pp. 1653–1659, 1983.

[4] Z. Hasan and R. M. Enoka, "Isometric torque-angle relationship and movement-related activity of human elbow flexors: Implications for the equilibrium-point hypothesis," *Exp. Brain Res.*, vol. 59, pp. 441–450, 1985.

[5] C. W. Heckathorne and D. S. Childress, "Relationships of the surface electromyogram to the force, length, velocity, and contraction rate of the cineplastic human biceps," *Am. J. Phys. Med.*, vol. 60, pp. 1–19, 1981.

[6] D. Staudenmann, K. Roeleveld, D. F. Stegeman, and J. H. van Dieen, "Methodological aspects of EMG recordings for force estimation—A tutorial and review," *J Electromyogr Kinesiol*, vol. 20, pp. 375–387, 2010.

[7] R. H. Messier, J. Duffy, H. M. Litchman, P. R. Raslay, J. F. Soechting, and P. A. Stewart, "The electromyogram as a measure of tension in the human biceps and triceps muscles," *Int. J. Mech. Sci.*, vol. 13, pp. 585–598, 1971.

[8] K. N. An, W. P. Cooney, E. Y. Chao, L. J. Askew, and D. J. R., "Determination of forces in extensor pollicis longus and flexor pollicis longus of the thumb," *J Appl Physiol*, vol. 54, pp. 714–719, 1983.

[9] M. Solomonow, A. Guzzi, R. Baratta, H. Shoji, and R. D'Ambrosia, "EMG-force model of the elbows antagonistic muscle pair," *Am. J. Phys. Med.*, vol. 65, pp. 223–244, 1986.

[10] E. A. Clancy and N. Hogan, "Relating agonist-antagonist electromyograms to joint torque during isometric, quasi-isotonic, non-fatiguing contractions," *IEEE Trans. Biomed. Eng.*, vol. 44, pp. 1024–1028, 1997.

[11] D. G. Thelen, A. B. Schultz, S. D. Fassois, and J. A. Ashton-Miller, "Identification of dynamic myoelectric signal-to-force models during isometric lumber muscle contractions," *J. Biomech.*, vol. 27, pp. 907–919, 1994.

[12] N. Hogan and R. W. Mann, "Myoelectric signal processing: Optimal estimation applied to electromyography—Part I: Derivation of the optimal myoprocessor," *IEEE Trans. Biomed. Eng.*, vol. 27, pp. 382–395, 1980.

[13] N. Hogan and R. W. Mann, "Myoelectric signal processing: Optimal estimation applied to electromyography—Part II: Experimental demonstration of optimal myoprocessor performance," *IEEE Trans. Biomed. Eng.*, vol. 27, pp. 396–410, 1980.

[14] M. I. A. Harba and P. A. Lynn, "Optimizing the acquisition and processing of surface electromyographic signals," *J. Biomech. Eng.*, vol. 3, pp. 100–106, 1981.

[15] E. A. Clancy and N. Hogan, "Single site electromyograph amplitude estimation," *IEEE Trans. Biomed. Eng.*, vol. 41, pp. 159–167, 1994.

[16] E. A. Clancy and N. Hogan, "Multiple site electromyograph amplitude estimation," *IEEE Trans. Biomed. Eng.*, vol. 42, pp. 203–211, 1995.

[17] J. R. Potvin and S. H. M. Brown, "Less is more: High pass filtering, to remove up to 99% of the surface EMG signal power, improves EMG-based biceps brachii muscle force estimates," *J. Electromyo. Kinesiol.*, vol. 14, pp. 389–399, 2004.

[18] D. Staudenmann, I. Kingma, A. Daffertshofer, D. F. Stegeman, and J. H. van Dieen, "Heterogeneity of muscle activation in relation to force direction: A multi-channel surface electromyography study on the triceps surae muscle," *J. Electromyo. Kinesiol.*, vol. 19, pp. 882–895, 2009.

[19] J. Hashemi, E. Morin, P. Mousavi, and K. Hashtrudi-Zaad, "Enhanced dynamic EMG-force estimation through calibration and PCI modeling," *IEEE Trans. Neural Sys. Rehabil. Eng.*, vol. 23, pp. 41–50, 2015.

[20] D. Staudenmann, I. Kingma, A. Daffertshofer, D. F. Stegeman, and J. H. Van Dieen, "Improving EMG-based muscle force estimation by using a high-density EMG grid and principal component analysis," *IEEE Trans. Neural Sys. Rehabil. Eng.*, vol. 53, pp. 712–719, 2006.

[21] D. Staudenmann, I. Kingma, D. F. Stegeman, and J. H. van Dieen, "Towards optimal multi-channel EMG electrode configurations in muscle force estimation: A high density EMG study," *J. Electromyo. Kinesiol.*, vol. 15, pp. 1–11, 2005.

[22] G. L. Gottlieb and G. C. Agarwal, "Dynamic relationship between isometric muscle tension and the electromyogram in man," *J Appl Physiol*, vol. 30, pp. 345–351, 1971.

[23] T. D. Sanger, "Bayesian filtering of myoelectric signals," *J. Neurophysiol.*, vol. 97, pp. 1839–1845, 2007.

[24] J. Hashemi, E. Morin, P. Mousavi, K. Mountjoy, and K. Hashtrudi-Zaad, "EMG-force modeling using parallel cascade identification," *J Electromyogr Kinesiol*, vol. 22, pp. 469–477, 2012.

[25] A. L. Hof and J. Van den Berg, "EMG to force processing I: An electrical analogue of the Hill muscle model," *J. Biomech.*, vol. 14, pp. 747–758, 1981.

[26] E. P. Doheny, M. M. Lowery, D. P. FitzPatrick, and M. J. O'Malley, "Effect of elbow joint angle on force-EMG relationships in human elbow flexor and extensor muscles," *J Electromyogr Kinesiol*, vol. 18, pp. 760–770, 2008.

[27] J. Hashemi, E. Morin, P. Mousavi, and K. Hashtrudi-Zaad, "Surface EMG force modeling with joint angle based calibration," *J Electromyogr Kinesiol*, vol. 23, pp. 416–424, 2013.

[28] P. Liu, L. Liu, F. Martel, D. Rancourt, and E. A. Clancy, "Influence of joint angle on EMG-torque model during constant-posture quasi-constant-torque contractions," *J. Electromyo. Kinesiol.*, vol. 23, pp. 1020–1028, 2013.

[29] P. Liu, L. Liu, and E. A. Clancy, "Influence of joint angle on EMG-torque model during constant-posture, torque-varying contractions," *IEEE Trans. Neural Sys. Rehabil. Eng.*, vol. 23, pp. 1039–1046, 2015.
[30] E. A. Clancy, O. Bida, and D. Rancourt, "Influence of advanced electromyogram (EMG) amplitude processors on EMG-to-torque estimation during constant-posture, force-varying contractions," *J. Biomech.*, vol. 39, pp. 2690–2698, 2006.
[31] E. A. Clancy, L. Liu, P. Liu, and D. V. Moyer, "Identification of constant-posture EMG-torque relationship about the elbow using nonlinear dynamic models," *IEEE Trans. Biomed. Eng.*, vol. 59, pp. 205–212, 2012.
[32] R. W. Mann and S. D. Reimers, "Kinesthetic sensing for the EMG controlled "Boston Arm"," *IEEE Trans. Man-Mach. Sys.*, vol. 11, pp. 110–115, 1970.
[33] P. Parker, K. Englehart, and B. Hudgins, "Myoelectric signal processing for control of powered limb prostheses," *J. Electromyo. Kinesiol.*, vol. 16, pp. 541–548, 2006.
[34] C. A. M. Doorenbosch and J. Harlaar, "A clinically applicable EMG-force model to quantify active stabilization of the knee after a lesion of the anterior cruciate ligament," *Clin. Biomech.*, vol. 18, pp. 142–149, 2003.
[35] C. Disselhorst-Klug, T. Schmitz-Rode, and G. Rau, "Surface electromyography and muscle force: Limits in sEMG-force relationship and new approaches for applications," *Clin. Biomech.*, vol. 24, pp. 225–235, 2009.
[36] S. Kumar and A. Mital, *Electromyography in Ergonomics*. Briston, PA: Taylor & Francis, 1996.
[37] G. M. Hagg, B. Melin, and R. Kadefors, "Applications in ergonomics," in *Electromyography: Physiology, Engineering, and Noninvasive Applications*, R. Merletti and P. A. Parker, Eds., ed: IEEE Press/Wiley-Interscience, 2004, pp. 343–363.
[38] B. Hudgins, P. Parker, and R. N. Scott, "A new strategy for multifunction myoelectric control," *IEEE Trans. Biomed. Eng.*, vol. 40, pp. 82–94, 1993.
[39] S. Micera, J. Carpaneto, and S. Raspopovic, "Control of hand prostheses using peripheral information," *IEEE Rev. Biomed. Eng.*, vol. 3, pp. 48–68, 2010.
[40] J. L. Nielsen, S. Holmgaard, N. Jiang, K. B. Englehart, D. Farina, and P. Parker, "Simultaneous and proportional force estimation for multifunction myoelectric prostheses using mirrored bilateral training," *IEEE Trans. Biomed. Eng.*, vol. 58, pp. 681–688, 2011.
[41] E. N. Kamavuako, K. B. Englehart, W. Jensen, and D. Farina, "Simultaneous and proportional force estimation in multiple degrees of freedom from intramuscular EMG," *IEEE Trans. Biomed. Eng.*, vol. 59, pp. 1804–1807, 2012.
[42] N. Jiang, J. L. G. Vest-Nielsen, S. Muceli, and D. Farina, "EMG-based simultaneous and proportional estimation of wrist/hand kinematics in uni-lateral trans-radial amputees," *J. NeuroEng. Rehabil.*, vol. 9:42, 2012.
[43] N. Jiang, S. Muceli, B. Graimann, and D. Farina, "Effect of arm position on the prediction of kinematics from EMG in amputees," *Med. Biol. Eng. Comput.*, vol. 51, pp. 143–151, 2013.
[44] A. Ameri, E. J. Scheme, E. N. Kamavuako, K. B. Englehart, and P. A. Parker, "Real-time, simultaneous myoelectric control using force and position-based training paradigms," *IEEE Trans. Biomed. Eng.*, vol. 61, pp. 279–287, 2014.
[45] A. Ameri, E. N. Kamavuako, E. J. Scheme, K. B. Englehart, and P. Parker, "Support vector regression for improved real-time, simultaneous myoelectric control," *IEEE Trans. Neural Sys. Rehabil. Eng.*, vol. 22, pp. 1198–1209, 2014.
[46] A. W. English, S. L. Wolf, and R. L. Segal, "Compartmentalization of muscles and their motor nuclei: The partitioning hypothesis," *Phys. Ther.*, vol. 73, pp. 857–867, 1993.
[47] A.-T. Liu, B.-L. Liu, L.-X. Lu, G. Chen, D.-Z. Yu, L. Zhu, *et al.*, "Architectural properties of the neuromuscular compartments in selected forearm skeletal muscles," *J. Anat.*, vol. 225, pp. 12–18, 2014.
[48] U. Windhorst, T. M. Hamm, and D. G. Stuart, "On the function of muscle and reflex partitioning," *Behav. Brain Sci.*, vol. 12, pp. 629–645, 1989.
[49] L. Ljung, *System Identification: Theory for the User*. Upper Saddle River, NJ: Prentice-Hall, 1999, pp. 491–519.
[50] S. Muceli and D. Farina, "Simultaneous and proportional estimation of hand kinematics from EMG during mirrored movements at multiple degrees-of-freedom," *IEEE Trans. Neural Sys. Rehabil. Eng.*, vol. 20, pp. 371–378, 2012.
[51] E. A. Clancy, "Electromyogram amplitude estimation with adaptive smoothing window length," *IEEE Trans. Biomed. Eng.*, vol. 46, pp. 717–729, 1999.
[52] E. A. Clancy and K. A. Farry, "Adaptive whitening of the electromyogram to improve amplitude estimation," *IEEE Trans. Biomed. Eng.*, vol. 47, pp. 709–719, 2000.
[53] P. Prakash, C. A. Salini, J. A. Tranquilli, D. R. Brown, and E. A. Clancy, "Adaptive whitening in electromyogram amplitude estimation for epoch-based applications," *IEEE Trans. Biomed. Eng.*, vol. 52, pp. 331–334, 2005.
[54] J. S. Bendat and A. G. Piersol, *Random Data: Analysis and Measurement Procedures*. New York: John Wiley and Sons, Inc., 1971, pp. 277–281.
[55] L. Liu, P. Liu, E. A. Clancy, E. Scheme, and K. B. Englehart, "Electromyogram whitening for improved classification accuracy in upper limb prosthesis control," *IEEE Trans. Neural Sys. Rehabil. Eng.*, vol. 21, pp. 767–774, 2013.
[56] K. Koirala, M. Dasog, P. Liu, and E. A. Clancy, "Using the electromyogram to anticipate torques about the elbow," *IEEE Trans. Neural Sys. Rehabil. Eng.*, vol. 23, pp. 396–402, 2015.
[57] W. H. Press, B. P. Flannery, S. A. Teukolsky, and W. T. Vetterling, *Numerical Recipies in C*, 2nd ed. New York: Cambridge Univ. Press, 1994, pp. 671–681.
[58] I. Miller and J. E. Freund, in *Probability and Statistics for Engineers, 2nd edition*, ed: Prentice-Hall, Inc., 1977, pp. 272–275.
[59] B. A. Lock, K. Englehart, and B. Hudgins, "Real-time myoelectric control in a virtual environment to relate usability vs. accuracy," in *Myoelectric Controls/Powered Prosthetics Symposium*, New Brunswick, Canada, 2005.
[60] L. Hargrove, Y. Losier, B. Lock, K. Englehart, and B. Hudgins, "A real-time pattern recognition based myoelectric control usability study implemented in a virtual environment," in *29th IEEE Eng. Med. Biol. Conf.*, 2007.
[61] N. Jiang, I. Vujaklija, H. Rehbaum, B. Graimann, and D. Farina, "Is accurate mapping of EMG signals on kinematics needed for precise online myoelectric control?," *IEEE Trans. Neural Sys. Rehabil. Eng.*, vol. 22, pp. 549–558, 2014.

Chapter 7: Two degrees of freedom quasi-static EMG-force at the wrist using a minimum number of electrodes

This chapter has been submitted as: Edward A. Clancy, Carlos Martinez-Luna, Marek Wartenberg, Chenyun Dai, Todd R. Farrell, "*Two degrees of freedom quasi-static EMG-force at the wrist using a minimum number of electrodes*."

***Abstract*—Surface electromyogram-controlled powered hand/wrist prostheses return partial upper-limb function to limb-absent persons. Typically, one degree of freedom (DoF) is controlled at a time, with mode switching between DoFs. Recent research has explored using large-channel EMG systems to provide simultaneous, independent and proportional (SIP) control of two joints—but such systems are not practical in current commercial prostheses. Thus, we investigated optimal selection of a minimum number of EMG sites, targeting four sites for a two DoF controller. In a laboratory experiment with 10 able-bodied subjects and three limb-absent subjects, 16 conventional electrodes were placed about the proximal forearm. Subjects produced 1-DoF and 2-DoF slowly force-varying contractions up to 30% maximum voluntary contraction (MVC). EMG standard deviation was related to forces via regularized regression. Backward stepwise selection was used to optimally retain progressively fewer electrodes. For 1-DoF models using two optimally retained electrodes (which mimics the current state of the art), subjects had average RMS errors of (depending on the DoF): 7.1–9.5 %MVC for able-bodied and 13.7–17.1 %MVC for limb-absent subjects. For 2-DoF models, subjects using four electrodes had errors on 1-DoF trials of 6.7–8.5 %MVC for able-bodied and 11.9–14.0 %MVC for limb-absent; and errors on 2-DoF trials of 9.9–11.2 %MVC for able-bodied and 15.8–16.7 %MVC for limb-absent subjects. For each model, retaining more electrodes did not statistically improve performance. These results suggest that as few as four optimally sited electrodes could control two DoFs of SIP control at the wrist.**

***Keywords*—EMG, EMG-force, EMG signal processing, Electromyogram, Myoelectric control, Prosthesis, Prosthesis control**

7.1 Introduction

Most upper-limb absence is transradial or more distal (Dillingham et al., 2002). Typical commercial myoelectric hand-wrist prostheses return partial function by using residual forearm muscle surface electromyogram (EMG) signals to control hand closing/opening. Additional degrees of freedom (DoF), e.g. wrist rotation, are not controlled simultaneously; rather, mode switching sequentially activates additional DoFs (Parker et al., 2006). This limitation is problematic (Atkins et al., 1996; Pezzin et al., 2004), as many basic daily tasks require the simultaneous activation and control of two or more joints.

Three notable techniques to provide multi-DoF control have been emerging. First, Kuiken and colleagues (Kuiken et al., 2004; Kuiken et al., 2009) pioneered "targeted muscle reinnervation" surgery in which certain muscles (e.g., pectoralis) are denervated, and then nerves which formerly innervated absent upper limb muscles are grafted to them. EMGs from the grafted muscles provide simultaneous, independent and proportional (SIP) control. The invasive and costly surgery and long recovery period (3–6 months) likely make this technique most attractive to those with bilateral and proximal limb-loss.

Second, multifunction pattern recognition (recently commercialized (Coapt, Chicago, IL)) uses forearm EMGs to select between a small set of predefined movements (Boostani and Moradi, 2003; Englehart and Hudgins, 2003; Graupe and Cline, 1975; Hudgins et al., 1993; Parker, Englehart, 2006; Powell et al., 2014). All functions are comprised of one DoF of movement at a time—although this degree can be multi-joint.

Third, studies have related forearm surface EMG to multiple DoF finger (Liu et al., 2013; Smith et al., 2009; Smith et al., 2008) and/or hand-wrist (Ameri et al., 2014a; Ameri et al., 2014b; Jiang et al., 2009; Jiang et al., 2012b; Muceli and Farina, 2012; Muceli et al., 2014; Nielsen et al., 2011) forces or kinematics, primarily in able-bodied subjects. Preliminary studies utilized high-density electrode arrays (32–64^{+} channels) (Liu, Brown, 2013; Muceli and Farina, 2012; Muceli, Jiang, 2014) or indwelling electrodes (Kamavuako et al., 2012; Kamavuako et al., 2014; Smith and Hargrove, 2014). These studies demonstrated that intact forearm EMG encodes multiple DoFs of SIP information—but the high-density EMG arrays/indwelling electrodes are not viable in commercial prosthetic systems. Recently, conventional (bipolar) surface EMG systems with as few as 7–8 electrodes have been reported—an electrode quantity that is still high for most practical prosthesis systems. The electrodes are generally equally-spaced about the circumference of the forearm. Jang *et al.* (Jiang, Englehart, 2009) related eight electrodes to wrist forces of 11 able-bodied subjects, achieving a multivariate R^2 index of 77.5 ± 10.9% for two DoF tasks utilizing extension-flexion (Ext-Flx) and radial-ulnar deviation (Rad-Uln). Nielson *et al.* (Nielsen, Holmgaard, 2011) related multiple EMG features from seven electrodes to wrist Ext-Flx with Rad-Uln forces, achieving

R^2 values that exceeded 90% in 10 able-bodied subjects and averaged 72% in their one subject with congenital malformation. Jiang *et al.* (Jiang, Vest-Nielsen, 2012b) related seven electrodes to the kinematics of all three wrist DoFs. Three amputees with a long residual limb (≥20 cm) achieved a R^2 performance of 62.5 ± 8.50%, while five able-bodied subjects achieved a R^2 performance of 72.0 ± 8.29%. Ameri *et al.* (Ameri, Kamavuako, 2014a) related eight EMG signals to 1- and 2-DoF target displacements. Ten able-bodied subjects achieved average R^2 values from 82–90% and two limb-deficient subjects from 76–84%, depending on the DoF. Fougner *et al.* (Fougner et al., 2014) applied only five electrodes over selected anatomical locations, and implemented a form of hybrid control between multi-level control and proportional control. Two able-bodied subjects could actuate a hand, a wrist or simultaneously activate both at a fixed-ratio co-active rate. This approach does not provide independent proportional control, but does provide simultaneous control and represents an improvement step that may be easier for the user to control. Amsuess *et al.* (Amsuess et al., 2016) used eight electrodes and combined sequential-simultaneous control to improve activity of daily living performance tasks in five able-bodied subjects and two amputees.

Throughout all of this work, many different modeling techniques were evaluated (e.g., regression, regularized regression, neural networks, support vector machines), and studies used a wide selection of force or kinematic trajectories as the model output variable (Ameri *et al.* (Ameri, Scheme, 2014b) contrasted force vs. kinematic outputs; Jiang, Muceli and colleagues (Jiang et al., 2014; Muceli, Jiang, 2014) developed models requiring minimal supervision). Recent studies have even combined EMG inputs with other modalities, such as kinematic signals (Blana et al., 2016). Most studies found that performance is inversely related to the number of DoFs/classes modeled and positively correlated to the number of EMG channels.

No study has specifically targeted two DoFs of SIP control from a *minimum number of conventional surface electrodes*. In particular, if as few as four electrodes could be used to provide 2-DoF control, this number of conventional electrodes is already within the capability of commercial prostheses. Of course, determining the optimal location of a limited number of electrodes *a priori* is difficult (Cavanaugh et al., 1983) for two DoF control. Hence, our research applied 16 electrodes packed tightly about the circumference of the proximal forearm and then used backward stepwise selection (off-line) to progressively reduce the number of electrodes—optimally removing the least useful electrode at each step. This proximal location was selected since it is applicable to the broadest range of residual forearm lengths. Clinically, we foresee a procedure in which the optimal four of 16 electrode sites are determined via our technique during the fitting stage by a prosthetist; then these four optimal sites are fixed into the final prosthesis socket. Herein, we studied 2-DoF combinations of the three possible wrist DoFs: Ext-Flx, Rad-

Uln and pronation-supination (Pro-Sup). We did so because the literature is unclear as to which DoF pair is best for prosthesis control. We elicited *slowly force/moment-varying contractions ("quasi-static")* for this initial exploration, so as to avoid the additional complexity of dynamical system modeling. Our results suggest that optimal selection of electrode sites may lead to a viable four-channel prosthesis that can provide SIP control of two wrist DoFs.

7.2 Methods

7.2.1 Experimental apparatus and procedures

Experiments were approved and supervised by the New England IRB (Newton, MA). Each subject provided written informed consent. Ten able-bodied subjects (6 female, 4 male; aged 22–61 years) and three subjects with transradial limb absence (3 male; aged 24–60 years; 8–50 years of limb absence) each successfully completed one experiment lasting 3–4 hours. Data from two additional limb-absent subjects were excluded, one due to unusable MVC values and one due to poor EMG quality.

Able-Bodied Subjects, Setup: Skin about the proximal forearm of the dominant arm was scrubbed vigorously with an alcohol wipe and a bead of electrode gel was applied. Sixteen bipolar EMG electrodes were placed equidistant in a row, transversely about the forearm, each centered 5 cm distal from the crease of the elbow, with one electrode aligned at the most dorsal aspect. Each electrode pair consisted of 5 mm diameter, stainless steel, hemispherical contacts separated 1 cm edge-to-edge, oriented along the forearm's long axis. The average transverse spacing between bipolar electrodes was 1.6 ± 0.24 cm. A reference electrode was gelled and secured on the ventral forearm, just distal to the row of bipolar electrodes. The EMG signals from each bipolar electrode were cabled to a differential amplifier circuit (Liberating Technologies, Inc. BE328 amplifier; pass band from 30–500 Hz, CMRR > 100 dB over the pass band) and then selectable gain was applied to maximize ADC resolution without signal saturation. The RMS EMG signal level at rest (representing equipment and electrode-skin interface noise plus ambient physiological activity) averaged 7.1 ± 6.4% (median of 3.8%) of the RMS EMG at 50% maximum voluntary contraction (MVC). This rest level is marginally higher than that of our previous laboratory work (Clancy et al., 2005; Clancy and Farry, 2000; Liu et al., 2015), perhaps due to cabling the EMG pre-amplifiers 16 cm from the electrode contacts in a standard "remote" prosthesis configuration (as opposed to using cased electrodes with embedded pre-amplifiers in past work).

Able-bodied subjects sat at the experimental apparatus, as shown in Fig. 1 (top). A thermo-formable plastic hand splint was rigidly attached to a load cell (AMTI, Watertown, MA; model MC3A-100

transducer, Gen 5 signal conditioner). The metacarpal region of the dominant hand was tightly secured to the hand splint using Velcro straps, while leaving the phalanges free. The palm of the hand was perpendicular with the plane of the floor, the hand was in a neutral position with respect to the wrist, the forearm was parallel to the plane of the floor and the shoulder was flexed 45° forward from the anatomical position along the sagittal plane. The elbow was supported just distal to the olecranon process. The load cell measured three DoFs, which were displayed on a computer screen in front of the subject via an arrowhead in which wrist Ext-Flx force specified its *x*-axis location, Rad-Uln force its *y*-axis location and Pro-Sup moment its rotation. A second computer-generated target arrowhead could also be displayed. The three load cell signals and the 16 EMG channels were each sampled at 2048 Hz with 16-bit resolution.

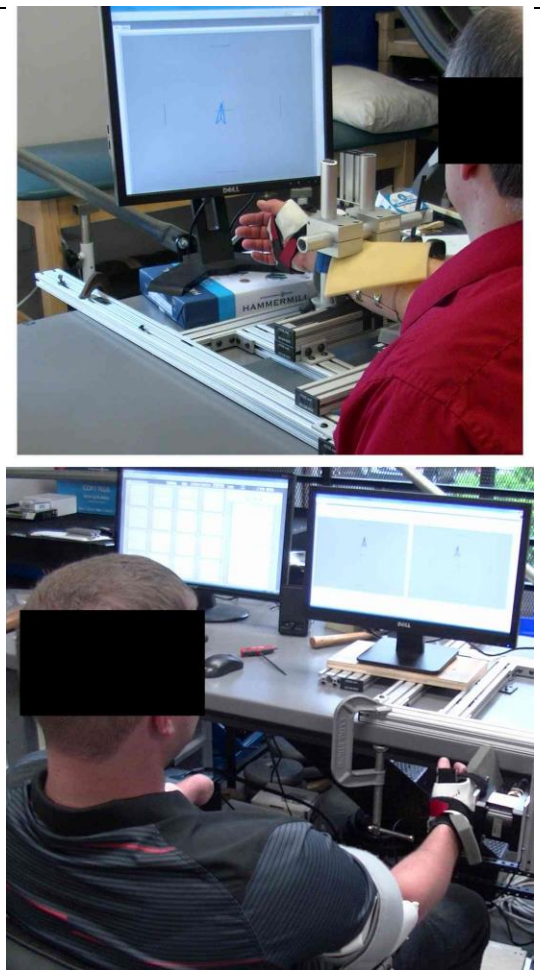

Fig. 1. Experimental apparatus. Dominant/able hand was tightly secured via thermo-formable plastic and Velcro to six-axis load cell. Sixteen electrodes (not visible) were secured about the proximal aspect of the dominant/limb-absent forearm. Top: Able-bodied configuration. Wrist was maintained in a neutral position by a padded restraint. Bottom: Limb-absent configuration. Mirrored display screen at right.

Able-Bodied Subjects, Contractions: Contractions were constant-posture about the wrist. Subjects were instructed to relax all muscles not involved in the task (including their phalanges). Trials were conducted at an interval of at least two minutes, to avoid accumulated fatigue. Subjects were released from

the hand cuff for rest between experiment stages. Initially, subjects practiced the contraction tasks for 10–20 minutes to become familiar with the apparatus and experimental protocol. Next, subjects performed MVCs in each of wrist extension, flexion, radial deviation, ulnar deviation, pronation and supination. Subjects increased force to their maximum over 2–3 s, then maintained maximum for 5 s. Verbal encouragement was provided. The average load cell value during the contraction plateau was the MVC.

One-DoF quasi-static trials were then conducted separately for each DoF (Fig. 2). For Ext-Flx, subjects followed the target arrowhead as it took 30 s to linearly ramp from zero force, to *Peak* force level in flexion, to *Peak* force level in extension, back to *Peak* force level in flexion and then back to zero force. This *Peak* force, in N, equaled half the 30 %MVC Ext-Flx force range: *Peak* = (|30 %MVC Flx| + |30 %MVC Ext|)/2. This trajectory provided a consistent, subject-scaled force range and a constant rate of change of force (within subject) in physical units. The subject-controlled arrowhead was only permitted to move along the active DoF, to avoid distraction from unused DoFs. Analogous ramp trajectories were used for Rad-Uln and Pro-Sup trials, four trials per DoF (12 trials total, block randomized by DoF).

Next, 2-DoF quasi-static ramp trials were conducted (Fig. 4). Two DoFs were active and their target effort levels were coincident. Thus, both active DoFs had their effort levels rise and fall simultaneously. The same *"quasi-static"* 30 s ramp trajectory was used. Two sets of six (block randomized) trials were conducted (12 trials total), the trials being identified by the contraction directions associated with the first effort direction during the ramp (Flx coincident with Uln, Flx with Rad, Flx with Pro, Flx with Sup, Uln with Pro, Uln with Sup). The subject-controlled arrowhead was only permitted to move/rotate along the two active DoFs.

Limb-Absent Subjects: The same general procedure was used, with a few differences. For warm-up, subjects practiced mirrored movements for the three DoFs using a mirror box (Mirror Box Therapy, Stockport, England; Hand/Wrist model) prior to more extensive practice of constant-posture tasks in the experimental apparatus. Their sound-side wrist was secured to the load cell that was re-positioned such that their elbow angle was reduced to 100° (Fig. 1, bottom). A cupped support contacted the proximal edge of the olecranon process and distal portion of the upper arm, securing the upper arm via taught-fitting Velcro. This posture facilitated bilateral symmetry, since the arm on their limb-absent side was similarly supported and secured, and the 16 electrodes placed on this forearm. Limb-absent subjects completed mirrored contractions, using forces/moment on their sound side for feedback (Ameri, Scheme, 2014b; Clancy et al., 2015; Hahne et al., 2014; Jiang, Vest-Nielsen, 2012b; Muceli and Farina, 2012; Nielsen, Holmgaard, 2011). Additionally, a mirrored screen display showed two graphs, one showing the subject-controlled and target arrowheads for the sound side and a second which mirrored this display for the limb-absent side. Subjects

were instructed to use the muscles in the forearm on their limb-absent side to mirror the forces/moment actually generated on their sound side. EMG from their limb-absent side was related to forces generated on their sound side.

7.2.2 Methods of analysis

Pre-Processing: Analysis was performed offline in MATLAB (The MathWorks, Inc., Natick, MA) and used causal processing, appropriate for future real-time implementation. Each EMG channel was highpass filtered (fifth-order Butterworth, cut-off at 15 Hz) and notch filtered at the power line frequency (second-order IIR filter at 60 Hz, notch bandwidth of 1 Hz). The narrow notch bandwidth greatly attenuated power line interference, with limited loss of signal power. An estimate of EMG standard deviation (EMGσ) was formed as the mean absolute value of the notched signal followed by decimation to 4.096 Hz. Decimation, (MATLAB "decimate" function) incorporated lowpass filtering at 1.6 Hz (Chebyshev Type 1 filter, ninth-order, 0.05 dB peak-to-peak passband ripple). This lowpass filter served the same function as a smoothing window. Ext-Flx force was normalized to the Ext-Flx MVC ranges. Rad-Uln force and Pro-Sup moment were similarly normalized. Each mechanical signal was then decimated to 4.096 Hz. Thus, the complete input-output data set for EMG-force modeling was sampled at 4.096 Hz—approximately ten times the bandwidth of the output force/moment signal (which is preferred for system identification (Clancy et al., 2006; Ljung, 1999)).

One-DoF Models: For comparison to existing prosthesis control, 1-DoF linear models were fit for each subject, using the 1-DoF trials. For Ext-Flx, EMGσs were least squares fit to Ext-Flx force (the remaining force and moment were ignored), initially using all 16 electrodes. Dynamics were not included in the model due to the slow rate of change of forces. The pseudo-inverse technique was used to regularize the least squares fit, in which singular values were removed if the ratio of that singular value to the largest singular value in the design matrix was less than a tolerance value. Via preliminary analysis, a tolerance value of 0.01 was selected, consistent with prior work (Clancy et al., 2012; Press et al., 1994). Two 1-DoF trials for Ext-Flx were used for model training, with performance taken as the RMS error between the known force and the EMG-estimated force, averaged across these two training trials. This error was expressed in %MVC. Previous research has shown lower test error when combining multiple training trials into one longer training set (Clancy, Liu, 2012). Backward stepwise selection was then used to progressively reduce the number of EMG channels (i.e., leaving out the channel whose absence resulted in the lowest error), making all decisions only on the training data. In this manner, the complete training operation—including electrode selection—is conducted with the training data. The two remaining 1-DoF

trials were used for testing at each step (normalized RMS error, average of the two trials). The entire process was repeated after switching training and testing data, with the average RMS error from this two-fold cross validation used as the overall error. Noting that correlated models are less statistically efficient, two-fold cross validation was selected for computational efficiency in lieu of exhaustive cross validation. The analogous process was used for 1-DoF models relating EMG to Rad-Uln force and Pro-Sup moment.

Two-DoF Models: Next, 2-DoF linear models were fit. The EMG-force model and backward stepwise selection were applied identically, except that the model always simultaneously estimated two mechanical DoFs (the third, unused mechanical force/moment was ignored). Each model fit produced two sets of coefficients, one per DoF. The model training data either consisted of two 1-DoF trials from each of the two DoFs (representing the simplest method by which a prosthesis controller might be trained), or two 2-DoF trials from each of the two DoF pairs, or both of these trial groupings (representing the most exhaustive method by which a prosthesis controller might be trained). During backward selection, RMS error was assessed on the training data (both DoFs). For testing, RMS error was assessed on the remaining trials, separately for 1-DoF trials (four trials) and 2-DoF trials (four trials). In either case, error was always assessed across the two available DoFs. (When assessing 1-DoF trials for these 2-DoF models, the second mechanical dimension would be expected to remain near a zero value throughout the trial.) The 1-DoF assessments were useful to compare vs. typical prostheses, which only control 1-DoF at a time. Ideally, the addition of 2-DoF control would not serve as a detriment to 1-DoF tasks. The trial data were switched and the overall error assigned as the average of the two-fold cross validation.

Statistics: Statistical evaluation used multivariate ANOVA, with *post hoc* pair-wise comparisons conducted using Tukey's honestly significant difference test (which adjusts for multiple comparisons). A significance level of $p = 0.05$ was used.

7.3 Results

Our analysis and models evaluated three 1-DoF contractions (Ext-Flx, Rad-Uln, Pro-Sup), their three 2-DoF co-contraction combinations (with different training conditions) and the number of electrodes used (1–16). Results are reported separately for able-bodied and amputee subjects.

7.3.1 One-DoF models, able-bodied subjects

Fig. 2 shows sample time-series EMG-force test results for the 1-DoF models (i.e., separate models formed for each DoF from trials that only excited each respective DoF) for an able-bodied subject. Table 1

and Fig. 3 show summary results. A two-way ANOVA was computed (factors: DoF and number of electrodes). Both main effects were significant ($p<10^{-6}$), with no interaction. Tukey *post hoc* comparisons found that Pro-Sup errors were significantly higher than the other two DoFs ($p<0.01$), and that the only statistical differences between number of channels was when comparing one channel (highest error) to each other number of channels ($p<10^{-6}$ for each pair). In addition, Table 1 (row 1) shows these RMS errors for two electrodes—typical in a commercial 1-DoF prosthesis controller. Two-channel results for 1-DoF represent the state-of-the art *for this contraction task*.

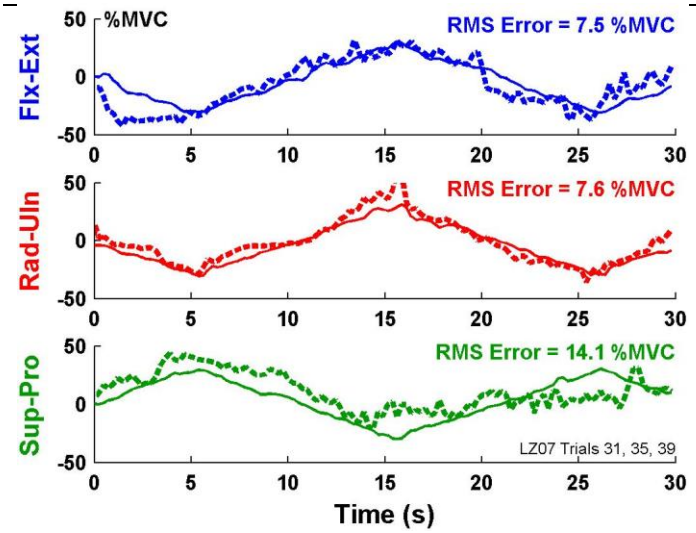

Fig. 2. Example time-series plots of 1-degree-of-freedom models, able-bodied subject. Solid lines are actual forces/moment, dashed lines are estimated using two EMG channels.

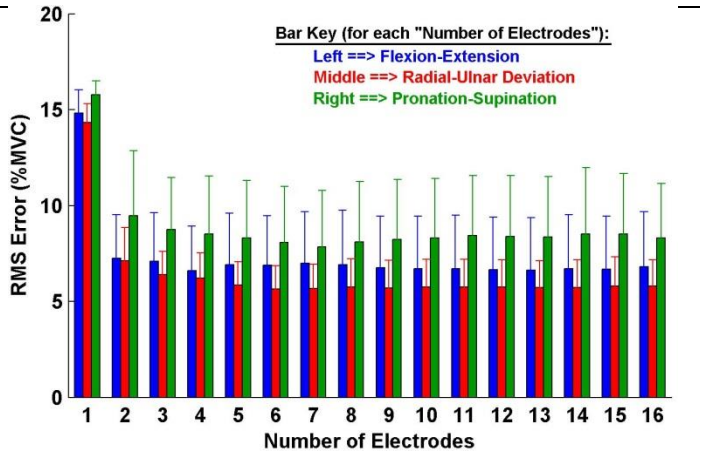

Fig. 3. Summary results: 1-degree-of-freedom models, ten able-bodied subjects. Error lines show one standard deviation above the mean.

7.3.2 Two-DoF models, able-bodied subjects

Two-DoF models always estimated both DoFs simultaneously. Fig. 4 shows sample time-series EMG-force test results during 2-DoF (co-contraction) trials from an able-bodied subject. Table 1 and Fig. 5 show summary results.

For 2-DOF model errors assessed on the 1-DoF trials (Fig. 5, top), a three-way ANOVA (factors: DoF, number of electrodes and training condition—either 1-DoF trials, 2-DoF trials or both) found that training condition interacted with number of electrodes. Thus, separate two-way ANOVAs were computed with each of the training conditions fixed. Results when training with 2-DoF trails were inconclusive, due to interaction. Results when training with 1-DoF trials or both were similar. Both main factors (DoF and number of electrodes) were significant ($p<10^{-6}$), without interaction. Tukey *post hoc* analysis of DoF found

Ext-Flx with Pro-Sup to have higher errors than either of the other two DoF combinations ($p<10^{-6}$). For number of electrodes, one electrode always exhibited higher error than more than one ($p<10^{-6}$); and two electrodes exhibited higher error than either three or more (when training with 1-DoF trials, $p<0.02$), or four or more (when training with 1- and 2-DoF trials, $p<0.002$) electrodes. Thus, performance improved as the selected number of channels increased from one channel, with performance stabilizing (statistically) at 3–4 channels. In addition, Table 1 (row 2) shows these RMS errors for four electrodes (the goal minimum number of electrodes for a commercial 2-DoF prosthesis controller). Lastly, we also computed a two-way ANOVA with number of electrodes fixed at the preferred value of four. Both main factors (DoF, training condition) were significant ($p\leq0.01$), without interaction. Tukey *post hoc* analysis found Ext-Flx with Pro-Sup DoF to have higher errors than either of the other two DoF combinations ($p\leq0.03$) and training with only 2-DoF trials to have higher errors than either of the other two training conditions ($p<10^{-6}$).

For 2-DoF model errors assessed on the 2-DoF trials (Fig. 5, bottom), a three-way ANOVA (factors: DoF, number of electrodes and training condition) found that training condition interacted with DoF and number of electrodes. Thus, separate two-way ANOVAs were computed with each of the training conditions fixed. Results found no interactions. When training with 1-DoF trials, only the main effect of DoF was significant, with Tukey *post hoc* analysis finding Ext-Flx with Rad-Uln to have lower errors than either of the other two DoF combinations ($p<10^{-3}$). When training with either 2-DoF trials or both 1- and 2-DoF trials, only the main effect of number of electrodes was significant. In both ANOVAs, Tukey *post hoc* analysis found that selection down to one electrode gave higher error than three or more electrodes ($p<10^{-5}$) and selection down to two electrodes gave higher error than six or more electrodes ($p\leq0.03$). Errors when selecting down to three electrodes did not differ from when selecting four or more electrodes. In addition, Table 1 (rows 3–4) shows these RMS errors for four electrodes. Overall, performance improved when increasing from one electrode to approximately 3–6. Lastly we also computed a two-way ANOVA with number of electrodes fixed at the preferred value of four (factors: DoF and training condition). Only the main effect of training condition was significant ($p<10^{-3}$), without interaction. Tukey *post hoc* analysis found that training with only 1-DoF trials had higher errors than either of the other two training conditions ($p<0.004$).

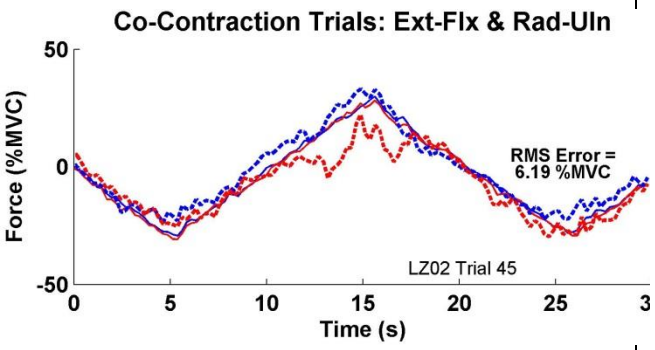

Fig. 4. Example time-series plots of 2-degree-of-freedom models applied to co-contraction trials from able-bodied subject. Key: solid lines=actual forces, dashed=estimated using four EMG channels; blue=Ext-Flx, red=Rad-Uln. Positive %MVC corresponds to Ext-Rad. Four EMG channels and training from both 1- and 2-DoF trials.

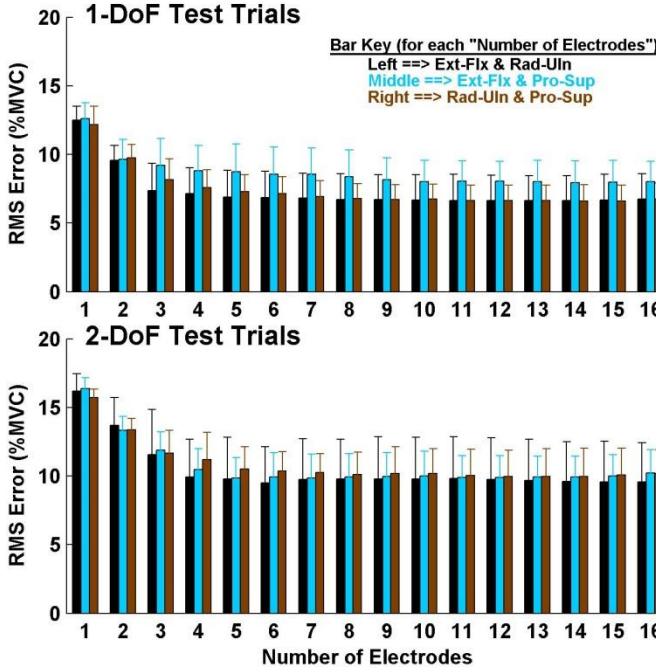

Fig. 5. Summary results: 2-degree-of-freedom (DoF) models, ten able-bodied subjects, training from both 1- and 2-DoF models. Top: tested on 1-DoF trials. Bottom: tested on 2-DoF trials. Error lines show one standard deviation above the mean.

Table 1
Mean ±std. dev. RMS errors (%MVC), ten able-bodied subjects.

Condition	DoF(s)		
1-DoF Models (2 electrodes)	**Ext-Flx**	**Rad-Uln**	**Pro-Sup**
Assessed on 1-DoF trials	7.3 ±2.4	7.1 ±1.8	9.5 ±3.6
2-DoF Models (4 electrodes)	**Ext-Flx & Rad-Uln**	**Ext-Flx & Pro-Sup**	**Rad-Uln & Pro-Sup**
Assessed on 1-DoF trials:			
Train with 1-DoF trials	6.7 ±2.0	8.5 ±2.2	7.4 ±1.5
Train with 2- DoF trials	12.5 ±5.2	14.0 ±2.7	11.0 ±1.0
Train with 1-, 2-DoF trials	7.1 ±2.0	8.8 ±2.0	7.6 ±1.4
Assessed on 2-DoF trials:			
Train with 1-DoF trials	13.1 ±5.4	15.5 ±4.0	15.7 ±7.2
Train with 2-DoF trials	11.7 ±5.4	11.3 ±3.0	10.6 ±2.1
Train with 1-, 2-DoF trials	9.9 ±2.9	10.5 ±1.6	11.2 ±2.1

7.3.3 Interposing electrode distance, able-bodied subjects

It is useful to describe the extent to which the algorithm is selecting electrodes from diverse locations about the forearm. For 1-DoF models with two electrodes, there are two distances between the selected electrodes, measured in number of interposing electrodes. The average interposing distance must equal 8

electrodes (out of 16 total). The left plot of Fig. 6 shows the distribution of the *minimum* interposing distances, aggregating the separate results from electrode selection from the three DoFs, two cross-validations and ten subjects. The mean ± std. dev. distance was 31 ± 14% of forearm circumference. For 2-DoF models, we considered the case of training with both 1- and 2-DoF trials and selection to four electrodes. Thus, there are four interposing distances whose average must equal 4 electrodes. The right plot of Fig. 6 shows the distribution from *each* such interposing distance, aggregating the separate results from electrode selection from the three DoFs, two cross-validations and ten subjects. The mean ± std. dev. distance was 25 ± 14% of forearm circumference. Note that when an interposing space of, for example, 11 electrodes is found, the remaining three interposing spaces from that model must be small, such that the sum of the four interposing spaces from that model equals 16. Overall, the selected electrodes tended not to be adjacent, but were also not necessarily equally-spaced about the forearm.

Fig. 6. Distribution of interposing distances, all degrees-of-freedom (DoFs). Left shows proportion of *minimum* distances for the 1-DoF models using two electrodes. Right shows the proportion of *each* of the four interposing distances for the 2-DoF models, trained using both 1- and 2-DoF trials, using four electrodes. Total of 16 electrodes/subject.

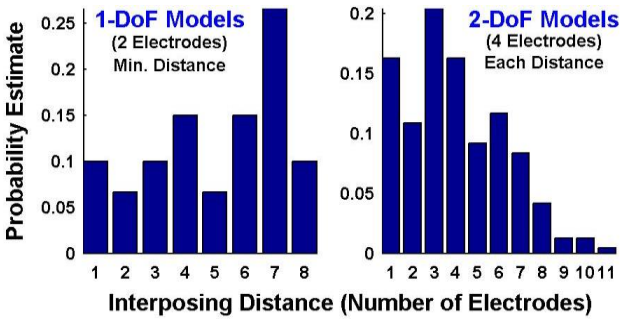

7.3.4 One-DoF models, limb-absent subjects

Fig. 7 shows sample time-series EMG-force test results for the 1-DoF models (i.e., separate models formed for each DoF from trials that only excited each respective DoF) from a limb-absent subject. Fig. 8 shows summary results. Table 2 shows RMS error for 1-DoF models using two electrodes and 2-DoF models using four electrodes. All of the errors were large compared to those of the able-bodied subjects. A two-way ANOVA (factors: DoF and number of electrodes) found the main effect of DoF was significant $\left(p<10^{-6}\right)$, with no interaction. Tukey *post hoc* analysis found Rad-Uln to have higher error then either of Ext-Flx or Pro-Sup (p<0.02).

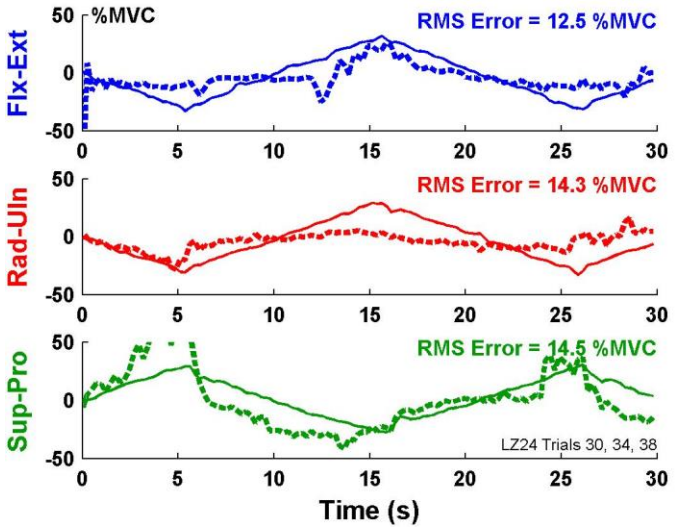

Fig. 7. Example time-series plots of 1-degree-of-freedom models, limb-absent subject. Solid lines are actual forces/moment from sound side, dashed lines are estimated using two EMG channels of limb-absent side.

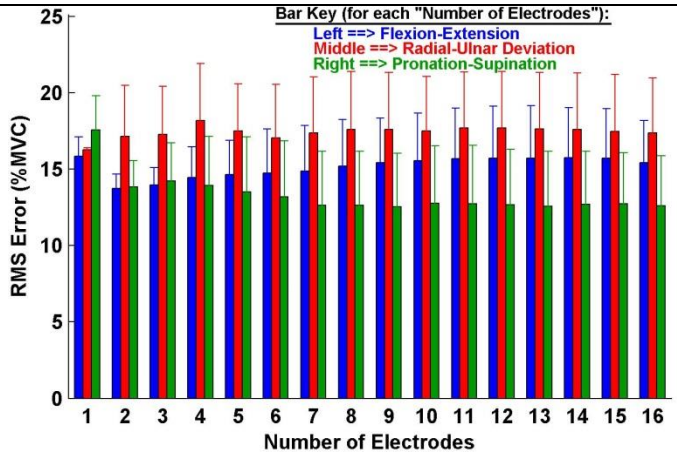

Fig. 8. Summary results: 1-degree-of-freedom models, three limb-absent subjects. Error lines show one standard deviation above the mean. Note y-axis scale differs from that of other bar plot result figures.

Table 2

Mean ± std. dev. RMS errors (%MVC), three limb-absent subjects.

Condition	DoF(s)		
1-DoF Models (2 electrodes)	**Ext-Flx**	**Rad-Uln**	**Pro-Sup**
Assessed on 1-DoF trials	13.7 ±1.2	17.1 ±4.1	13.8 ±2.1
2-DoF Models (4 electrodes)	**Ext-Flx & Rad-Uln**	**Ext-Flx & Pro-Sup**	**Rad-Uln & Pro-Sup**
Assessed on 1-DoF trials:			
Train with 1-DoF trials	11.9 ±1.3	14.0 ±2.7	12.5 ±2.5
Train with 2- DoF trials	38.4 ±7.2	35.9 ±18.6	19.5 ±3.4
Train with 1-, 2- DoF trials	12.3 ±1.4	13.9 ±2.4	11.9 ±2.1
Assessed on 2-DoF trials:			
Train with 1-DoF trials	20.2 ±2.5	21.0 ±5.4	17.9 ±3.9
Train with 2-DoF trials	24.2 ±2.2	20.0 ±3.2	16.6 ±1.8
Train with 1-, 2-DoF trials	16.3 ±1.0	16.7 ±2.8	15.8 ±0.4

7.3.5 Two-DoF models, limb-absent subjects

Fig. 9 shows sample time-series test results of simultaneous EMG-based estimation of Ext-Flx forces with Pro-Sup moments during 2-DoF (co-contraction) trials from a limb-absent subject. Table 2 and Fig. 10 show summary results. All errors were large when compared to the able-bodied subjects.

For 2-DoF model errors assessed with the 1-DoF trials (Fig. 10, top), a three-way ANOVA (factors: DoF, number of electrodes and training condition) found that training condition interacted with DoF and number of electrodes. Thus, separate two-way ANOVAs were computed with each of the training conditions fixed. These three ANOVAs each found a significant difference only for the main effect of DoF (p<0.01), without interactions. Tukey *post hoc* analysis found Ext-Flx with Pro-Sup to have higher errors

than either of the other two DoF combinations when training with 1-DoF, or 1- and 2-DoF trials ($p<0.03$); and for Rad-Uln with Pro-Sup to have lower errors than either of the other two DoF combinations when training with 2-DoF trials ($p<0.03$) Lastly, we also computed a two-way ANOVA with number of electrodes fixed at the preferred value of four (factors: DoF and training condition). This comparison was only significant for training condition ($p<10^{-6}$), with no interaction. Tukey *post hoc* analysis showed that training with only the 2-DoF trials had higher error than both of the other training conditions ($p<10^{-4}$).

For 2-DoF model errors assessed with the 2-DoF trials (Fig. 10, bottom), a three-way ANOVA (factors: DoF, number of electrodes and training condition) found an interaction between DoF and training condition. Thus, separate two-way ANOVAs were computed with each of the training conditions fixed. None found interactions. When training with 1-DoF trials, no main effects were found. When training with 2-DoF trials, the main effect of DoF was significant ($p<10^{-6}$); and Tukey *post hoc* analysis found Ext-Flx with Rad-Uln to have higher errors than either of the other two DoF combinations ($p<10^{-6}$). When training with 1- and 2-DoF trials, the main effect of DoF was significant ($p=0.01$); and Tukey *post hoc* analysis found Ext-Flx with Pro-Sup to have higher errors than Rad-Uln with Pro-Sup ($p=0.01$). Lastly we also computed a two-way ANOVA with number of electrodes fixed at the preferred value of four (factors: DoF and training condition). Only the main effect of training condition was significant ($p=0.02$), without interaction. Tukey *post hoc* analysis found that training with only 2-DoF trails had higher error than training with both 1- and 2-DoF trials ($p=0.02$)

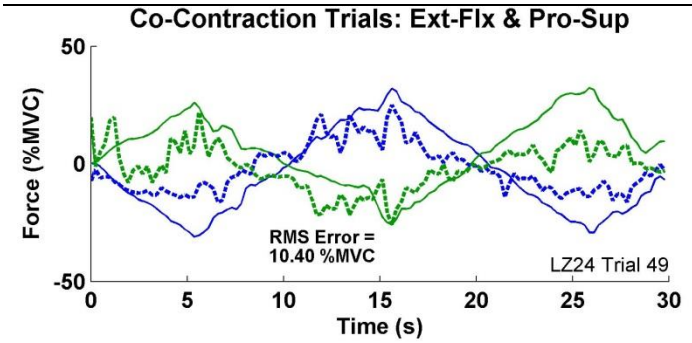

Fig. 9. Example time-series plots of 2-degree-of-freedom (DoF) models applied to co-contraction trials from limb-absent subject. Key: solid lines=actual forces from sound side, dashed=estimated from four EMG channels of limb-absent side; blue=Ext-Flx, green=Pro-Sup. Positive %MVC corresponds to Ext/Pro. Four EMG channels, training from both 1- and 2-DoF trials.

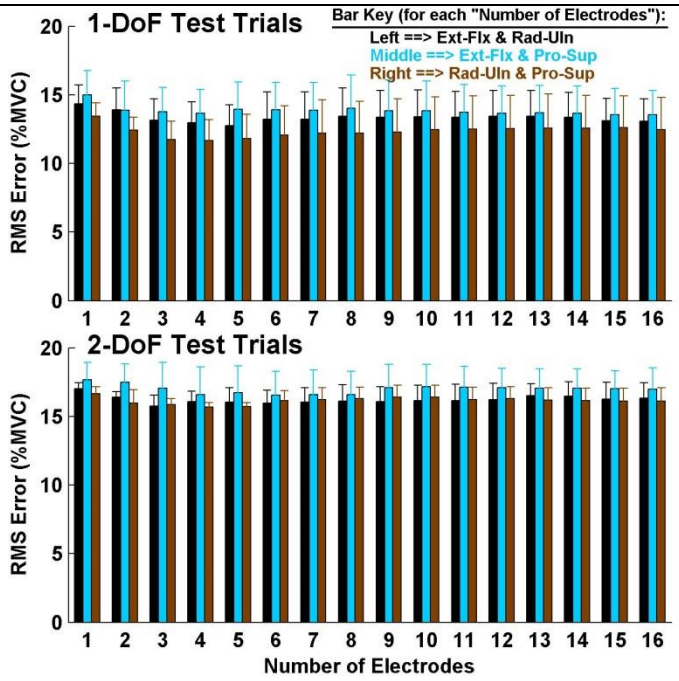

Fig. 10. Summary results: 2-degree-of-freedom models, three limb-absent subjects, training from both 1- and 2-DoF trials. Top: tested on 1-DoF trials. Bottom: tested on 2-DoF trials. Error lines show one standard deviation above the mean.

7.3.6 Interposing electrode distance, limb-absent subjects

Methods identical to those for the able-subjects were used to produce these results. Distribution plots were not developed, since the samples size is much smaller for limb-absent subjects. For 1-DoF models with two electrodes, the mean ± std. dev. of the *minimum* distances between selected electrodes was 28 ± 14% of forearm circumference. For 2-DoF models, trained with both 1- and 2-DoF trials and selection to four electrodes, the mean ± std. dev. of *each* distance was 25 ± 15% of forearm circumference. These results are similar to those of the able-bodied subjects.

7.4 Discussion

7.4.1 Discussion of able-bodied results

An existing prosthesis control strategy is the use of two electrodes to provide proportional control of one DoF. When our 1-DoF tasks were used to produce 1-DoF models, Table 1 shows average EMG-force errors for able-bodied subjects of 7.1–9.5 %MVC, depending on the DoF. Our interest was in the design of EMG-based controllers using as few as four electrodes that could perform comparably in two DoFs. The

second row of Table 1 shows that SIP estimation of two DoFs assessed with the same 1-DoF tasks exhibited average errors between 6.7–8.5 %MVC, depending on the DoFs. (Ideally, we desire that 2-DoF control retains low error even when operated on only 1-DoF tasks.) Direct comparison of these RMS values is not appropriate—during 1-DoF tasks, our 2-DoF models simultaneously assess errors in both DoFs, however only one DoF is active while the second DoF has forces near zero. Nonetheless, low errors were achieved in the 2-DoF models with four electrodes; additional electrodes provided no statistically significant advantage.

When a 2-DoF task was used for assessment, the errors grew. This increase is consistent with an increase in the average effort level—both DoFs were active. Four-channel versions of these 2-DoF models performed poorest when trained from only 1-DoF trials (bottom row of Table 1). This result is unfortunate, as training from 1-DoF trials would be simpler. Lower errors when including 2-DoF trials may be due to the wider range of the model space explored, or simply due to the noise averaging effect of a larger training set when using both 1- and 2-DoF trials (Clancy, Liu, 2012). These overall results are consistent with much of the developing EMG-force research related to the wrist, extending acceptable 2-DoF performance to a minimum number of electrodes (e.g., four). In particular, for 1-DoF models (Fig. 3), the able-bodied results show that using two *optimally sited* electrodes are significantly better than one, and additional electrodes beyond two provide limited benefit. For 2-DoF models (Fig. 5), errors generally decreased progressively as the number of selected electrodes increased from one to four, with little additional improvement thereafter. Of the three possible DoF combinations that could be utilized for control, our results suggested some (limited) preference *for* Ext-Flx paired with Rad-Uln and *against* Ext-Flx paired with Pro-Sup.

7.4.2 Discussion of limb-absent results

As found in prior studies (Ameri, Kamavuako, 2014a; Jiang, Vest-Nielsen, 2012b; Nielsen, Holmgaard, 2011), force estimation errors for the limb-absent subjects were universally much higher than those from the able-bodied subjects. Average errors above 15 %MVC are particularly problematic, as they are more than half the experimental force range. Our models require an output signal (force/moment) in order to estimate the model parameters; but, limb-absent subjects cannot directly provide this information. We, therefore, utilized bilateral mirrored contractions. An alternative approach is for the subject to only use their phantom limb on their affected side to match the effort associated with the location and/or orientation of the computer screen target (Ameri, Kamavuako, 2014a; Ameri, Scheme, 2014b). In neither case does a limb-absent subject benefit from afferent feedback. Hence, less accurate muscular activation and measurement is likely, leading to higher EMG-force errors. A better understanding of the limitations

imposed by these surrogate force measures might lead to better EMG-force performance. In addition, limb-absent subjects may require substantially more training than was made available to them in this single-session study (Hahne et al., 2015; Powell, Kaliki, 2014). Each of our limb-absent subjects was new to lab-based EMG-force experimentation.

Increasing the number of electrodes did not statistically improve performance. For 1-DoF models, Rad-Uln and Ext-Flx results in Fig. 8 even suggest that higher numbers of electrodes might lead to *increased* error, if sufficient statistical power existed. Such contrary results could exist since models with higher numbers of electrodes *require* retaining electrodes in the model's training set, even if their corresponding EMG signals have no useful relation to the output forces. (Such a situation is not uncommon due to the altered anatomy of limb-loss subjects.) However, results from the independent test trials (shown in the figure) would demonstrate the poor performance of such models.

7.4.3 Limitations and extensions

Direct comparison of *absolute* error performance to prior studies can be misleading due to differences in the types of contractions produced (e.g., more forceful contractions will necessarily produce higher errors, measured either in physical units or %MVC; dynamic contractions are generally more challenging to model than static contractions), the measure of error, the subject population, the experimental conditions and numerous other factors. Nonetheless, *relative* error performance should be a more consistent metric for inter-study comparison. In that regard, it is most useful to observe that 1-DoF models (Figs. 3, 8) experienced no statistically significant benefit when using more than two optimally-sited electrodes and 2-DoF models (Figs. 5, 10) saw little or no benefit when using more than four optimally-sited electrodes. Given that EMGσ is a non-negative measure, it is not expected that fewer than four electrode sites could successfully provide 2-DoFs of SIP control. The prior literature (see Introduction section) has related progressively fewer EMG signals to 2-DoF forces at the wrist; our results help set a lower limit.

Several limitations should be noted. First, the successful results were primarily observed in able-bodied subjects, with poorer results in limb-absent subjects. Multi-session training could lead to lower errors in limb-absent subjects (Hahne, Dahne, 2015; Powell, Kaliki, 2014). Second, low EMG-force errors in the laboratory do not necessarily transfer to improved prosthesis usability (Jiang et al., 2012a). We utilized the controlled (and inexpensive) laboratory setting—a common paradigm in this field—to demonstrate performance of electrode site selection via the backward stepwise selection method. Future work should investigate its performance by limb-loss subjects performing more functional tasks. Third, the relative merits of bilateral mirrored contractions vs. screen tracking in limb-absent subjects are not well

understood. Fourth, we examined a single fixed posture, but Jiang *et al.* (Jiang et al., 2013) showed that arm pose influences performance of a simultaneous and proportional myoelectric control algorithm. Fifth, our results were from within a single session. If electrodes are re-applied, the effect of subtle shifts in electrode locations is unclear (Muceli, Jiang, 2014; Simon et al., 2012). Sixth, the selection of optimal electrodes (from the available 16) may not be unique. In fact, the two distinct training sets from our two cross validation folds may have selected different electrodes. Alternative optimized electrode site selection schemes are possible (including simply selecting four equally-spaced electrodes), as well as anatomically-based schemes (e.g., (Fougner, Stavdahl, 2014)). Anecdotally, we made preliminary evaluation of *forward* stepwise selection of electrode sites, finding rather similar performance to the backward stepwise selection results shown herein. Nonetheless, a more complete study is appropriate as future work. Seventh, our contractions were limited to slowly force-varying (quasi-static), so that we could concentrate on optimal selection of the electrode sites. Future work should include dynamic contraction trials and models (Clancy, Liu, 2012; Hashemi et al., 2012; Thelen et al., 1994), and this research will clearly need to progress to implementation and testing in prosthetic devices.

7.5 Conclusions

This initial study is encouraging for the use of as few as four conventional electrodes for 2-DoF of SIP prosthesis control at the wrist. Two-DoF EMG-force models using four electrodes, trained from both 1- and 2-DoF trials, had average RMS errors of 9.9–11.2 %MVC on able-bodied subjects and 15.8–16.7 %MVC on limb-absent subjects, depending on the DoF. Additional electrodes, up to a total of 16, provided no statistically significant benefit. Electrodes were automatically selected over a reasonably diverse (generally non-adjacent) extent of the forearm. In able-bodied subjects, there was some preference for lower errors when utilizing Ext-Flx, and higher errors when utilizing Pro-Sup. Transition of these results beyond a laboratory task and into prosthesis testing and implementation is necessary, and may require substantive training in limb-absent subjects.

Conflict of interest

The authors (except C. Dai) are/were employees of Liberating Technologies, Inc., which may benefit from this research.

Acknowledgements

The authors thank Debra Latour, OT, and Thane Hunt for help with the experiments involving limb-absent subjects.

References

Ameri A, Kamavuako EN, Scheme EJ, Englehart KB, Parker P. Support vector regression for improved real-time, simultaneous myoelectric control. IEEE Trans Neural Sys Rehabil Eng. 2014a;22:1198–209.

Ameri A, Scheme EJ, Kamavuako EN, Englehart KB, Parker PA. Real-time, simultaneous myoelectric control using force and position-based training paradigms. IEEE Trans Biomed Eng. 2014b;61:279–87.

Amsuess S, Vujaklija I, Goebel P, Roche AD, Graimann B, Aszmann OC, et al. Context-dependent upper limb prosthesis control for natural and robust use. IEEE Trans Neural Sys Rehabil Eng. 2016;24:744–53.

Atkins DJ, Heard DCY, Donovan WH. Epidemilogic overview of individuals with upper-limb loss and their reported research priorities. J Prosthet Orthot. 1996;8:2–11.

Blana D, Kyriacou T, Lambrecht JM, Chadwick EK. Feasibility of using combined EMG and kinematic signals for prosthesis control: A simulation study using a virtual reality environment. J Electromyo Kinesiol. 2016;29:21–7.

Boostani R, Moradi MH. Evaluation of the forearm EMG signal features for the control of a prosthetic hand. Physiol Meas. 2003;24:309–19.

Cavanaugh KT, Clancy EA, Natrillo JA, Paquette RJ, Looft FJ. Optimal site selection for prosthetic control. IEEE 1983 Frontiers Eng Comput Health Care. 1983:565–9.

Clancy EA, Bida O, Rancourt D. Influence of advanced electromyogram (EMG) amplitude processors on EMG-to-torque estimation during constant-posture, force-varying contractions. J Biomech. 2006;39:2690–8.

Clancy EA, Dai C, Wartenberg M, Martinez-Luna C, Hunt TR, Farrell TR. A pilot study assessing ipsilateral vs. contralateral feedback in EMG-force models of the wrist for upper-limb prosthesis control. IEEE Signal Proc Med Biol Conf. Temple University, Philadelphia, PA, 2015.

Clancy EA, Farina D, Merletti R. Cross-comparison of time- and frequency-domain methods for monitoring the myoelectric signal during a cyclic, force-varying, fatiguing hand-grip task. J Electromyo Kinesiol. 2005;15:256–65.

Clancy EA, Farry KA. Adaptive whitening of the electromyogram to improve amplitude estimation. IEEE Trans Biomed Eng. 2000;47:709–19.

Clancy EA, Liu L, Liu P, Moyer DV. Identification of constant-posture EMG-torque relationship about the elbow using nonlinear dynamic models. IEEE Trans Biomed Eng. 2012;59:205–12.

Coapt, LLC. Chicago, ILChicago, IL.

Dillingham TR, Pezzin LE, MacKenzie EJ. Limb Amputation and Limb Deficiency: Epidemiology and Recent Trends in the United States. South Med J. 2002;95:875–83.

Englehart K, Hudgins B. A robust, real-time control scheme for multifunction myoelectric control. IEEE Trans Biomed Eng. 2003;50:848–54.

Fougner AL, Stavdahl O, Kyberd PJ. System training and assessment in simultaneous proportional myoelectric prosthesis control. J NeuroEng Rehabil. 2014;11:75.

Graupe D, Cline WK. Functional separation of EMG signals via ARMA identification methods for prosthesis control purposes. IEEE Trans Sys Man Cyber. 1975;5:252–9.

Hahne JM, Biebmann, F., Jiang N, Rehbaum H, Farina D, Meinecke FC, et al. Linear and nonlinear regression techniques for simultaneous and proportional myoelectric control. IEEE Trans Neural Sys Rehabil Eng. 2014;22:269–79.

Hahne JM, Dahne S, Hwang H-J, Muller K-R, Parra LC. Concurrent adaptation of human and machine improves simultaneous and proportional myoelectric control. IEEE Trans Neural Sys Rehabil Eng. 2015;24:618–27.

Hashemi J, Morin E, Mousavi P, Mountjoy K, Hashtrudi-Zaad K. EMG-force modeling using parallel cascade identification. J Electromyogr Kinesiol. 2012;22:469–77.

Hudgins B, Parker P, Scott RN. A new strategy for multifunction myoelectric control. IEEE Trans Biomed Eng. 1993;40:82–94.

Jiang N, Dosen S, Muller K-R, Farina D. Myoelectric control of artificial limbs—Is there a need to change focus? IEEE Signal Proc Mag. 2012a;29:152–0.

Jiang N, Englehart KB, Parker PA. Extracting simultaneous and proportional neural control information for multiple-DOF prostheses from the surface electromyographic signal. IEEE Trans Biomed Eng. 2009;56:1070–80.

Jiang N, Muceli S, Graimann B, Farina D. Effect of arm position on the prediction of kinematics from EMG in amputees. Med Biol Eng Comput. 2013;51:143–51.

Jiang N, Rehbaum H, Vujaklija I, Graimann B, Farina D. Intuitive, online, simultaneous, and proportional myoelectric control over two degrees-of-freedom in upper limb amputees. IEEE Trans Neural Sys Rehabil Eng. 2014;22:501–10.

Jiang N, Vest-Nielsen JLG, Muceli S, Farina D. EMG-based simultaneous and proportional estimation of wrist/hand kinematics in uni-lateral trans-radial amputees. J NeuroEng Rehabil. 2012b;9:42.

Kamavuako EN, Englehart KB, Jensen W, Farina D. Simultaneous and proportional force estimation in multiple degrees of freedom from intramuscular EMG. IEEE Trans Biomed Eng. 2012;59:1804–7.

Kamavuako EN, Scheme EJ, Englehart KB. On the usability of intramuscular EMG for prosthetic control: A Fitt's Law approach. J Electromyo Kinesiol. 2014;24:770–7.

Kuiken TA, Dumanian GA, Lipschutz RD, Miller LA, Stubblefield KA. The use of targeted muscle reinnervation for improved myoelectric prosthesis control in a bilateral shoulder disarticulation amputee. Prosthet Orthot Int. 2004;28:245–53.

Kuiken TA, Li G, Lock BA, Lipschutz RD, Miller LA, Stubblefield KA, et al. Targeted muscle reinnervation for real-time myoelectric control of multifunction artificial arms. J Am Med Assoc. 2009;301:619–28.

Liu P, Brown DR, Clancy EA, Martel F, Rancourt D. EMG-force estimation for multiple fingers. IEEE Sig Proc Med Biol Symp. 2013.

Liu P, Liu L, Clancy EA. Influence of joint angle on EMG-torque model during constant-posture, torque-varying contractions. IEEE Trans Neural Sys Rehabil Eng. 2015;23:1039–46.

Ljung L. System Identification: Theory for the User. Upper Saddle River, NJ: Prentice-Hall; 1999. p. 491–519.

Muceli S, Farina D. Simultaneous and proportional estimation of hand kinematics from EMG during mirrored movements at multiple degrees-of-freedom. IEEE Trans Neural Sys Rehabil Eng. 2012;20:371–8.

Muceli S, Jiang N, Farina D. Extracting signals robust to electrode number and shift for online simultaneous and proportional myoelectric control by factorization algorithms. IEEE Trans Neural Sys Rehabil Eng. 2014;22:623–33.

Nielsen JL, Holmgaard S, Jiang N, Englehart KB, Farina D, Parker P. Simultaneous and proportional force estimation for multifunction myoelectric prostheses using mirrored bilateral training. IEEE Trans Biomed Eng. 2011;58:681–8.

Parker P, Englehart K, Hudgins B. Myoelectric signal processing for control of powered limb prostheses. J Electromyo Kinesiol. 2006;16:541–8.

Pezzin LE, Dillingham TR, MacKenzie EJ, Ephraim P, Rossbach P. Use and satisfaction with prosthetic limb devices and related services. Arch Phys Med Rehabil. 2004;85:723–9.

Powell MA, Kaliki RR, Thakor NV. User training for pattern recognition-based myoelectric prostheses: Improving phantom limb movement consistency and distinguishability. IEEE Trans Neural Sys Rehabil Eng. 2014;22:522–32.

Press WH, Flannery BP, Teukolsky SA, Vetterling WT. Numerical Recipies in C. 2nd ed. New York: Cambridge Univ. Press; 1994. p. 671–81.

Simon AM, Lock BA, Stubblefield KA. Patient training for functional use of pattern recognition-controlled prostheses. J Prosthet Orthot. 2012;24:56–64.

Smith LH, Hargrove LJ. Surface versus intramuscular EMG for linear regression-based myoelectric control of the wrist and hand. Myoelec Controls Symp. 2014:244–8.

Smith RJ, Huberdeau D, Tenore F, Thakor NV. Real-time myoelectric decoding of individual finger movements for a virtual target task. Ann Int Conf IEEE EMBS. 2009:2376–9.

Smith RJ, Tenore F, Huberdeau D, Etienne-Cummings R, Thakor NV. Continuous decoding of finger position from surface EMG signals for the control of powered prostheses. Ann Int Conf IEEE EMBS. 2008:197–200.

Thelen DG, Schultz AB, Fassois SD, Ashton-Miller JA. Identification of dynamic myoelectric signal-to-force models during isometric lumber muscle contractions. J Biomech. 1994;27:907–19.

Chapter 8: Two Degrees of Freedom, Dynamic, Hand-Wrist EMG-Force Using a Minimum Number of Electrodes

***Abstract*— Commercial hand-wrist prostheses provide partial function for limb-absent persons, often controlled via surface electromyogram (EMG) from the residual forearm. Traditional prostheses only control one degree of freedom (DoF) at a time, regulating the hand or wrist sequentially. Recent studies realized simultaneous, independent and proportional (SIP) estimation of kinetics/kinematics from two joints using a large number of EMG channels, which is not practical for commercial prostheses. Hence, our research provides evidence for the feasibility of controlling two DoFs—hand open-closed paired with one wrist DoF, simultaneously—using as few as four electrodes. Experimental data from nine able-bodied subjects were analyzed. Subjects produced 1-DoF and 2-DoF uniform random forces (bandlimited to 0.75 Hz) up to 30% maximum voluntary contraction (MVC). EMG standard deviation (EMGσ) was related to force using linear dynamic models were via least squares. For 1-DoF forces, the average RMS errors ranged from 8.3–9.0 %MVC, depending on the DoF, and indicated that two electrodes were required. For 2-DoFs, overall performance was best when training from both 1- and 2-DoF trials. When doing so, average RMS errors were 9.2 %MVC for each DoF pair (hand open-close paired with one wrist DoF), using four electrodes. For each model, more electrodes showed no statistical improvement. The results suggest that 2-DoF SIP hand-wrist control with a small number of electrodes may be feasible.**

***Index Terms*—EMG-force, EMG signal processing, electromyogram, myoelectric control, prosthesis control**

8.1 Introduction

It is estimated that 41,000 people in the U.S. experienced upper-limb loss in 2005 [1] and that 95% of traumatic upper-limb extremity amputations are transradial or more distal [2]. For several decades, commercial myoelectric prostheses have used surface electromyogram (EMG) activity from residual muscles to control prosthesis movement, thereby realizing partial replacement function [3-5]. However, substantial issues exist for prosthesis control. A fundamental challenge is that only one degree of

freedom (DoF) is typically controlled at a time, with mode switching used between them [3]. Prosthesis users recognize this limitation [6], since even simple daily tasks can require simultaneous use of multiple DoFs—e.g. opening a door requires hand grip of the door knob with simultaneous wrist rotation. Another related issue is that most EMG-based laboratory studies of multi–DoF control have utilized a large quantity of specialized electrodes (upwards of 32–64). High density electrode arrays can extract more information and decrease the error in EMG-force/kinematics estimation [7-9], but they are not practical for commercial prostheses.

To improve multi-DoF control of prostheses, Kuiken and colleagues [10, 11] developed targeted muscle reinnervation surgery. Surface EMG electrodes sense the actual muscle contractions of reinnervated residual muscle regions to provide simultaneous, independent and proportional (SIP) control of multiple prosthesis joints (e.g., hand, wrist, elbow). The high cost, invasive surgery and long recovery period (3–6 months) likely limit its acceptability. Another improvement technique is based on the multifunction pattern recognition approach to select desired movements of the hand and/or wrist via EMG signals from the forearm [12-16] (recently commercialized [17]). Multi-joint control is facilitated, but still only 1-DoF is operated at a time. The performance of this method degrades with the number of functions selected and increases with the number of electrodes applied.

Recent studies have explored EMG-based multiple DoF EMG-force/kinematics (or direct prosthesis control) using 7–8 conventional electrodes, equally-spaced transversely about the forearm [18-22]; and one study has placed 5 electrodes over anatomically-selected locations in able-bodied subjects [23]. However, none of these works explored the influence or feasibility of reducing the quantity of conventional EMG channels to its minimum number. Further, very little work has studied 2-DoF SIP hand-wrist control [i.e., hand open-close (Opn-Cls) combined with one wrist DoF] using a surface EMG-force approach. Limiting the number of applied electrodes is an important goal, since electrode site selection and cabling remain difficult tasks faced by prosthetists who must custom fit each prosthetic device to its user. This problem grows with the number of electrodes used. In addition, when more electrodes are used in a preparation, the odds of a failure increase, with a single failing electrode channel potentially degrading the entire system [24]. Combining hand Opn-Cls with one wrist DoF could be immediately mapped to existing hand-wrist prostheses (with the one wrist DoF being mapped to rotation of the prosthetic wrist). Improvement to 2-DoF control would then be available immediately to a wide range of existing commercial prosthetic devices.

Hence, our work studied the feasibility of estimating 2 DoFs—hand Opn-Cls force in conjunction with one wrist DoF—using as few conventional electrodes as possible. In particular, each 2-DoF contraction trial, which produced random forces queued by a computer-generated target, incorporated hand Opn-Cls force with one of either extension-flexion (Ext-Flx), radial-ulnar deviation (Rad-Uln) or pronation-supination (Pro-Sup). In a prosthesis controller, the one best performing of these wrist DoFs would be utilized. Backward stepwise selection was utilized to progressively reduce the number of EMG channels. In practice, selection of the optimal electrode sites and best performing wrist DoF would occur in the fitting stage by a prosthetist, with the optimal EMG locations then used to produce the final prosthesis socket. The electrode sites would then be fixed during fielded prosthesis use. Our results show that 2-DoF control had similar error levels when compared to 1-DoF control and required as few as four electrodes.

8.2 Methods

8.2.1 Experimental Data and Apparatus

Experimental data from nine able-bodied subjects (five males, four females; aged 27±9.7 years) were acquired at Liberating Technologies, Inc. (Holliston, MA) and approved by the New England Independent Review Board (Newton, MA). All subjects provided written informed consent. Data from one additional subject were excluded from analysis due to erroneous EMG values.

Data Collection, Setup: Subjects sat at the experimental apparatus. The back of the dominant hand was tightly cuffed to a six-DoF load cell (MC3A-100 transducer with Gen 5 signal conditioner, AMTI, Watertown, MA) using a thermo-formable plastic mold, to measure force/torque generated at the wrist. A single-axis load cell (LCR-150 with DMD-465WB amplifier, Omega Engineering, Inc., Stamford, CT) was secured around the distal thumb via a rigid tube and, separately on the opposing side of the cell, Velcro-secured to the proximal aspects of the four fingers to measure grip force during attempted hand Opn-Cls (see Fig. 1). The palm of the hand was perpendicular with the plane of the floor, the wrist was relaxed in a neutral position with respect to the hand and the shoulder was flexed 45^{o} forward from the anatomical position along the sagittal plane. The elbow was supported just distal to the olecranon process. The skin surface about the forearm was scrubbed with an alcohol wipe and electrode gel was applied. Sixteen bipolar EMG electrodes were equidistantly placed in a row, transversely around the forearm (one electrode aligned at the most dorsal aspect) with the mid-point between bipolar contacts

situated 5 cm distal to the elbow crease; and then held in place with bandaging. Each electrode pair consisted of 5 mm diameter, stainless steel, hemispherical contacts separated 1 cm edge-to-edge, oriented along the long axis of the forearm. A reference electrode was gelled and secured on the ventral forearm, just distal to the row of active electrodes. Each bipolar EMG signal was differentially amplified (Liberating Technologies, Inc. BE328 amplifier; 30–500 Hz pass band, CMRR > 100 dB over the pass band) and then selectable gain was applied. The average ratio of resting RMS EMG to the RMS EMG at 50% maximum voluntary contraction (MVC) was 8.1 ± 5.4%. A real-time feedback signal from the load cells was shown via an arrowhead on the computer screen in front of the subject. The arrowhead displayed four different DoFs—*x*-axis location for Ext-Flx force, *y*-axis location for Rad-Uln force, rotation for Pro-Sup moment, and size for hand Opn-Cls. A second arrowhead displayed in another color was a computer-controlled target that guided the subject to complete different experimental tasks. Four load cell signals and 16 EMG channels were each sampled at 2048 Hz with 16-bit resolution.

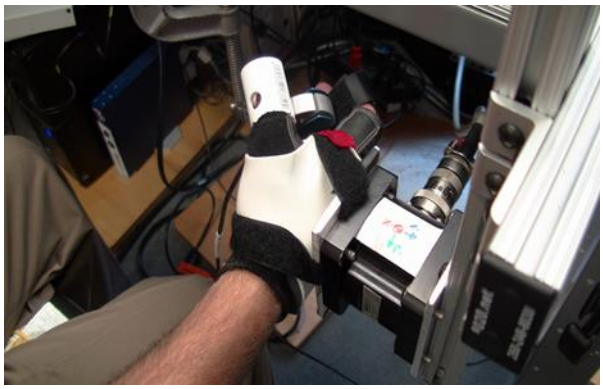

Fig. 1. Experimental apparatus. Dominant hand was tightly secured via thermo-formable plastic and Velcro to six-axis load cell. Sixteen electrodes (not visible) were secured about the distal aspect of the dominant forearm.

Data Collection, Contractions: All contractions were constant-posture. A minimum two-minute rest interval was provided between contractions to prevent muscle fatigue. After a warm-up period, MVC was measured separately for both directions (e.g., open vs. close) for each of the four DoFs. A subject took 2–3 seconds to ramp up their effort to MVC, maintaining that effort for two seconds. The plateau level of this force/ moment was measured as the MVC. Lastly, rest trials were recorded for noise level evaluation.

Next, subjects proceeded to 1-DoF dynamic tracking trials. Each of the four DoFs was tested separately. Subject feedback only modified the arrowhead according to changes in the specified DoF.

For Ext-Flx, the guide arrowhead generated a random target moving between ±(|30 %MVC Flx| + |30 %MVC Ext|)/2 on the screen, and subjects were asked to track the movement of the target by controlling the load cell force. The random target was a 0.75 Hz band-limited, white and uniform random process. Preliminary testing was used to select this bandwidth as the widest in which subjects could maintain target tracking for these tasks. Four trials of 40 s duration each were collected. The equivalent experiment was applied for the three remaining DoFs (16 total trials). The order of presentation of the DoFs was randomized.

Lastly, 2-DoF trials were conducted in which two different DoFs were tracked simultaneously. We only considered three combinations: hand Opn-Cls combined with one of the three wrist DOFs (Ext-Flx, Rad-Uln or Pro-Sup)—targeting control of a prosthetic hand/terminal device with a wrist rotator. The same random target style was used, but with two independent random instances (one per DoF). Four trials of 40 s duration were tested for each hand-wrist combination (12 total trials).

8.2.2 Methods of Analysis

Pre-Processing: Data analysis was performed offline in MATLAB (The MathWorks, Inc., Natick, MA). Once designed, all filters were implemented using MATLAB function "filtfilt()", which applied filters in the forward and reverse time directions to achieve a noncausal, zero-phase and magnitude squared response. An estimate of EMG standard deviation (EMGσ) was computed for each EMG channel. Raw EMG was highpass filtered to avoid motion artifact (fifth-order Butterworth, cut-off at 15 Hz), notch filtered to attenuate power-line interference with little loss of signal power (second-order IIR filter at 60 Hz, notch bandwidth of 1Hz), rectified and downsampled (after lowpass filtering at 16 Hz; Chebyshev Type 1 filter, ninth-order, 0.05 dB peak-to-peak passband ripple) from 2048 Hz to 40.96 Hz. This resulting frequency is suitable for system identification of EMG-force dynamic models [25, 26]. The lowpass filter can be regarded as a smoothing window. Each force/moment signal (Opn-Cls, Ext-Flx, Rad-Uln and Pro-Sup) was normalized by its corresponding MVC level pair. For example, Ext-Flx was normalized by: $\left(\left|MVC_{Ext}\right|+\left|MVC_{Flx}\right|\right)/2$.

One-DoF Dynamic Models: The processed extension and flexion EMGσ values were related to Ext-Flx wrist force via a 1-DoF linear dynamic model as:

$$T_{E-F}[m]=\sum_{q=0}^{Q}\sum_{e=1}^{E}c_{e,q}\,EMG\sigma_e[m-q]$$

where $T_{E\text{-}F}$ was wrist Ext-Flx force, m was the decimated discrete-time sample index, E was the number of electrodes used in the fit (initially set to 16), Q was the maximum lag of the model (set to 20 based on [27] and preliminary evaluation of these data) and $c_{e,q}$ were the fit coefficients. Two of four trials were used for coefficient training, using the known EMGσ values and force. The linear least squares pseudo-inverse method [28] was performed for model training, in which singular values of the design matrix were removed if the ratio of that singular value to the largest was less than a tolerance value, *Tol* (set to 0.01 based on [27] and preliminary evaluation of these data). The remaining two trials were used for testing (RMS error between the estimated and measured torques). The training and testing sets were flipped for two-fold cross-validation, and the average of these two results reported. Two-fold cross validation was selected for computational efficiency, and because the remaining four folds would necessarily yield correlated results (which are statistically less efficient). Since the mechanical signals were normalized by MVC, the final RMS error was in %MVC. The backward stepwise method was utilized for electrode selection. All 16 EMG channels were entered initially. Then, the channel whose absence resulted in the lowest RMS error was excluded for each step. Stepping continued until only one electrode remained. Identical modeling was separately performed for the other three DoFs (Opn-Cls, Rad-Uln and Pro-Sup).

Two-DoF Models: Similar 2-DoF EMG-force models were evaluated (including backward stepwise selection of EMG channels) for each of the three pairs of dimensions tested (Opn-Cls paired with one wrist DoF), except these models always estimated two DoFs simultaneously. Thus, each EMG channel contributed to each DoF. All six combinations of three different training paradigms and two testing paradigms were performed to evaluate the best modeling strategy. The training paradigms were: training with 1-DoF trials, with 2-DoF trials or with both 1- and 2-DoF trials. The testing paradigms were: testing on 1-DoF trials or on 2-DoF trials. When testing on 1-DoF trials for these 2-DoF models, the non-used dimension would be expected to remain near a zero value throughout the trial. These 1-DoF tests were intended to determine if 2-DoF models could still perform well when encountering 1-DoF tasks (common to prosthesis use).

Statistics: Performance differences were tested statistically using multivariate ANOVA, with *post hoc* pair-wise comparisons conducted using Tukey's honestly significant difference test. A significance level of $p = 0.05$ was used.

8.3 Results

8.3.1 One-DoF Models

Fig. 2 shows sample time-series EMG-force test results for the 1-DoF models (i.e., separate models formed for each DoF from trials that only examined each respective DoF). Fig. 3 shows summary results as a function of number of electrodes selected. Using all the results of one-DoF models, a two-way ANOVA was computed (factors: DoF; and number of electrodes, E). Both main effects were significant (p<0.001), without interactions. Tukey *post hoc* comparisons for DoF only found that Rad-Uln errors were significantly higher than Ext-Flx (p=0.001) and Opn-Cls (p=0.01). For number of electrodes, 1 optimally-sited electrode always exhibited higher error than 2 or more electrodes $\left(p < 10^{-6}\right)$. There were no other significant differences. Table I shows the RMS errors for 2 optimally-sited electrodes (typical in a commercial 1-DoF prosthesis controller), for each DoF.

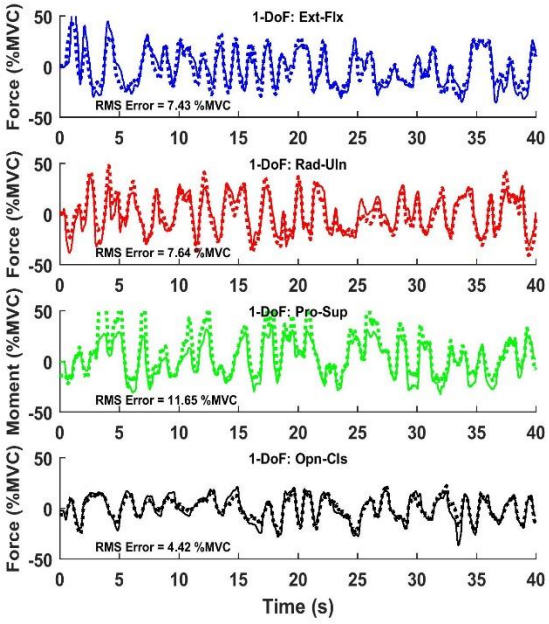

Fig. 2. Example time-series plots of 1-degree-of-freedom models, two electrodes (Subject 46, Trials 31, 35, 39 and 43). Solid lines are actual forces/moment, dashed lines are EMG-estimated.

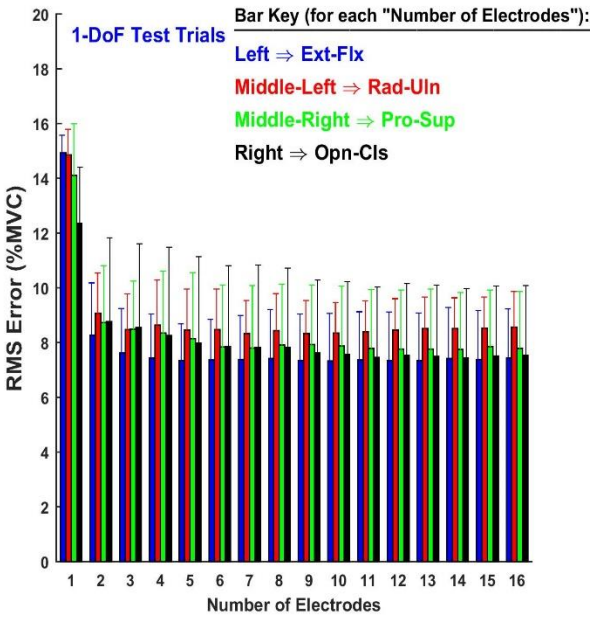

Fig. 3. Summary results: 1-degree-of-freedom models, nine subjects. Error lines show one standard deviation above the mean.

8.3.2 Two-DoF Models

Two-DoF models always estimated Opn-Cls with one other DoF (Ext-Flx, Rad-Uln or Pro-Sup) simultaneously. Fig. 4 shows sample time-series EMG-force test results during 2-DoF trials. Fig. 5 shows a set of summary results.

For 2-DoF models assessed on the 1-DoF trials, a three-way ANOVA (factors: DoF, number of electrodes and training condition—either 1-DoF trials, 2-DoF trials or both) found interactions between training condition and each of the two other factors. Thus, separate two-way ANOVAs were computed with each of the training conditions fixed. We fixed the training condition because it had the smallest number of degrees of freedom and represented different variants on how a prosthetist might perform electrode site selection. There were no interactions. Results when training with 1-DoF trials or both (Fig. 5, top) were similar. Both main factors (DoF, number of electrodes) were significant $\left(p < 10^{-5}\right)$. Tukey *post hoc* analysis of DoF only found Opn-Cls with Ext-Flx to have lower errors than the other two DoF combinations $\left(p \le 10^{-4}\right)$. For number of optimally-sited electrodes, 1 electrode exhibited higher error than more than 1 (p<0.01), 2 electrodes exhibited higher error than 4 or more (p<0.01), 3 electrodes exhibited higher error than 9 or more (p<0.045), and there were no significant differences when comparing 4 electrodes to more than 4 electrodes (p>0.06). Results when training with 2-DoF trials were only significant for DoF (p=0.001). Tukey *post hoc* analysis only found Opn-Cls with Pro-Sup to have higher errors than the other two DoF combinations (p≤0.03). Table I shows the RMS errors for 4 optimally-sited electrodes (preferred for a commercial prosthesis controller). Lastly, we also computed a two-way ANOVA with number of electrodes fixed at the preferred value of four (factors: DoF, training condition). Only the main effect of training condition was significant ($p = 10^{-6}$), without interaction. Tukey *post hoc* analysis found that training with only 2-DoF trials had higher errors than either of the other two training conditions $\left(p \le 10^{-6}\right)$.

For 2-DoF models assessed on the 2-DoF trials, a three-way ANOVA (factors: DoF, number of electrodes and training condition) found interactions between training condition and each of the two other factors. Thus, separate two-way ANOVAs were again computed with each of the training conditions fixed. There were no interactions. Results when training with 1-DoF trials were only significant for DoF $\left(p = 10^{-5}\right)$, with Tukey *post hoc* analysis only finding that Opn-Cls with Pro-Sup had higher errors than the other two DoF combinations (p<0.001). Results when training with 2-DoF trials were significant for both factors (p<0.01). Tukey *post hoc* analysis of DoF only found that Opn-Cls with

Ext-Flx had higher errors than the other two DoF combinations (p<0.01). Tukey *post hoc* analysis of number of optimally-sited electrodes only found that 1 electrode exhibited higher error than more than one (p<0.002), and 2 electrodes exhibited higher error than nine or more (p<0.045). Results when training with 1- and 2-DoF trials were only significant for number of electrodes $\left(p=10^{-6}\right)$; with Tukey *post hoc* analysis finding that 1 optimally-sited electrode exhibited higher error than more than one (p<0.002), 2 electrodes exhibited higher error than five or more (p<0.02), 3 electrodes exhibited higher error than 11 or more (p<0.005), and there were no significant differences when comparing 4 electrodes to more than 4 electrodes (p>0.64). Table I shows the RMS errors for 4 electrodes. Lastly, we also computed a two-way ANOVA with number of optimally-sited electrodes fixed at the preferred value of four (factors: DoF, training condition). Only the main effect of training condition was significant $\left(p=10^{-6}\right)$, without interaction. Tukey *post hoc* analysis found that training with only 1-DoF trials had higher errors than either of the other two training conditions $\left(p\le 10^{-4}\right)$.

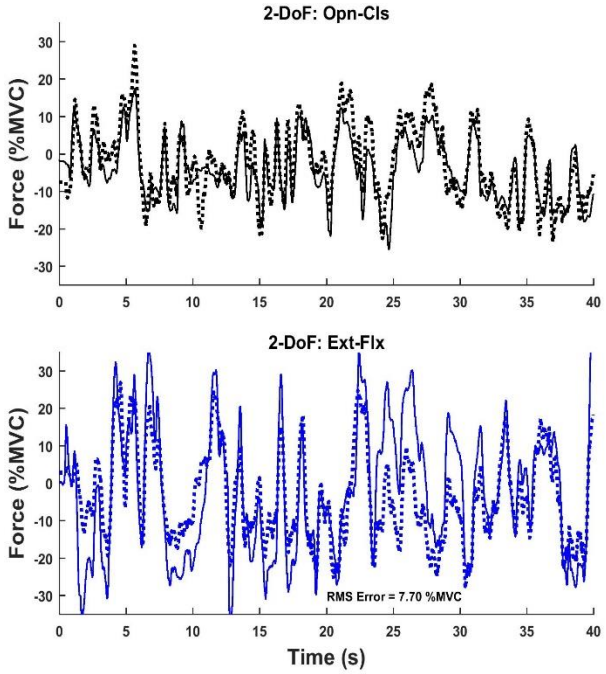

Fig. 4. Example time-series plots of 2-degree-of-freedom models applied to co-contraction trials from subject 46, trial 51 (four electrodes). Key: solid lines=actual forces, dashed=estimated; blue=Ext-Flx, black=Opn-Cls. Positive %MVC corresponds to Ext-Rad. Four EMG channels and training from both 1- and 2-DoF trials.

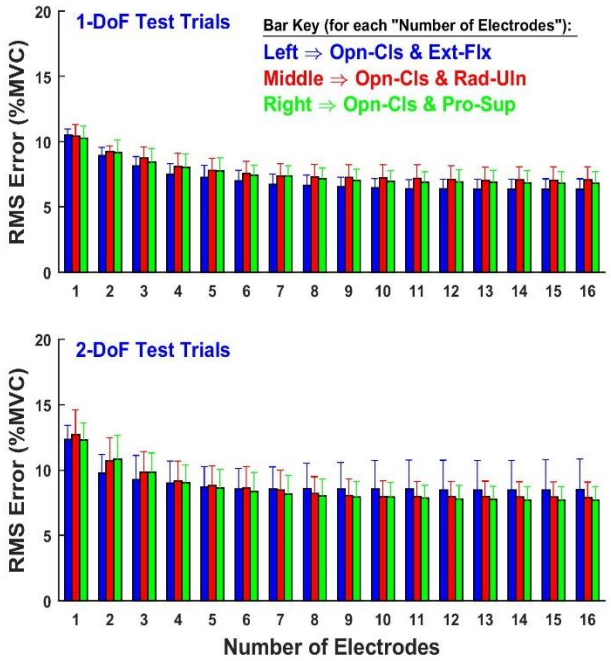

Fig. 5. Summary results: 2-degree-of-freedom (DoF) models, nine subjects. Top: testing on 1-DoF trials. Bottom: Models trained from both 1- and 2-DoF trials, tested on 2-DoF trials. Error lines show one standard deviation above the mean.

8.3.3 Interposing Electrode Distances

It is helpful to characterize the extent to which the selected electrode locations were distributed about the forearm. When selecting to two electrodes in 1-DoF models, there exist two interposing electrode distances. The average distance must equal 8 electrodes (out of 16 total). Fig. 6-left shows the distribution of the *minimum* interposing distance, aggregating the results across four DoFs, two cross-validations and nine subjects. The mean ± std. distance was 31 ± 12% of forearm circumference. When selecting to four electrodes in 2-DoF models, there exist four interposing distances (with an average distance of 4 electrodes). Fig. 6-right shows the distribution of *each* interposing distance (same aggregation), when training with both 1- and 2-DoF trials. The mean ± std. distance was 25 ± 17% of forearm circumference. Overall, the selected electrodes were rarely adjacent, but not necessarily spaced equally about the forearm.

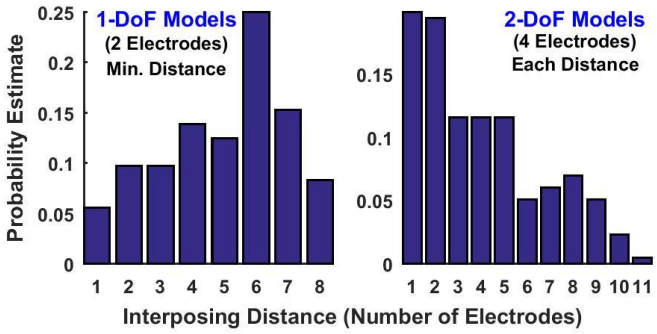

Fig. 6. Distribution of interposing electrode distances, aggregated across all DoFs, two cross-validations and nine subjects. Left shows proportion of *minimum* distances for the 1-DoF models with two electrodes. Right shows proportion of *each* of distance for the 2-DoF models, trained with 1- and 2-DoF trials, with four electrodes. Total of 16 electrodes per subject.

8.4 Discussion

8.4.1 One-DoF Models

One-DoF models were studied to quantify the existing state of the art in 1-DoF EMG-force, at least as assessed on these tasks and with this protocol. Fig. 3 and its associated statistical results show, as expected, rather poor performance when only one electrode is retained in the models. EMGσ is a non-negative (unipolar) quantity, yet 1-DoF wrist force/moment is bipolar (spanning a range of 30 %MVC); thus, one would not expect one EMG channel to accurately relate to these outputs when using linear models. It is for this reason that common 1-DoF proportional EMG controllers utilize the difference

between agonist and antagonist EMGσ values [3, 29], forming a bipolar signal from two unipolar signals. Our results herein confirm the need for two *optimally-sited* EMG channels [30], and show statistically that additional channels (beyond two) provide no benefit. Our results also suggest higher relative errors for Rad-Uln, as compared to Ext-Flx and Opn-Cls. With two optimally-sited electrodes, the mean errors ranged from 8.3–9.0 %MVC, depending on the DoF.

8.4.2 Two-DoF Models

We initially assessed our 2-DoF models on 1-DoF tasks, since 2-DoF prosthesis controllers would still be operated for use in 1-DoF tasks. When training with 1-DoF trials, or both 1- and 2-DoF trials, error was reduced as the selected number of electrodes increased from one until four. And, there was preference for *lower* errors when combining Opn-Cls with Ext-Flx. When the number of electrodes was fixed at four, training with only 2-DoF trials produced higher errors. We next assessed our 2-DoF models on 2-DoF tasks. In general, Table I shows that higher average errors were found. However, direct comparison between 1-DoF assessment and 2-DoF assessment is not appropriate. In 1-DoF assessment, errors in the second DoF were assessed, but their truth values were near zero (as the second DoF was not active). Hence, higher errors are expected in the 2-DoF assessments, since the average %MVC level (across both DoFs) is much higher. (Both DoFs were active, and higher effort levels produce higher errors, in general.) When training with 2-DoF trials or both 1- and 2-DoF trials, error was reduced as the selected number of electrodes increased from two until 4–9. Fig. 5 suggests that most of the improvement happened when the number of electrodes was less than 4–5. And, there was preference for *higher* errors when combining Opn-Cls with Ext-Flx. When the number of electrodes was fixed at four, training with only 1-DoF trials produced higher errors.

For model training, a single training procedure is required, after which the model is used on both 1-DoF and 2-DoF tasks. The summary of results in the prior paragraph shows that the clearly advantageous training technique is to use both 1- and 2-DoF trials. This result is unfortunate, since training would be simpler if only 1-DoF trials were required. Substantial concentration is required to track a random target in two dimensions; simpler tracking is found with only 1-DoF targets. It is, however, not overly surprising that training on both 1- and 2-DoF trials provides the best performance when assessing across both 1- and 2-DoF tasks [25]. And, as mentioned previously, training trials of sufficiently long duration so as to permit electrode site selection are only required during the prosthesis fitting task.

For number of optimally-sited electrodes, there was generally no statistical advantage in the 2-DoF models to having more than four electrodes. Fig. 5 shows a *trend* for some (limited) improvement due to more than four electrodes. A larger sample size might have borne out this trend statistically, although the likely strength of the error reduction seems small (once the number of electrodes exceeds four). Again, since two bipolar DoFs are being estimated, it is not surprising that at least four unipolar EMGσ channels are appropriate.

Our goal was to facilitate 2-DoF EMG-force, which could be mapped to 2-DoF SIP control of a hand-wrist prosthesis. However, which pair of DoFs to utilize was not assumed *a priori*. We required hand Opn-CLS to be one of the DoFs, but examined pairings with Ext-Flx or Rad-Uln or Pro-Sup. Some previous literature has found higher errors when including the Pro-Sup DoF [18, 20]. In our work, no preferred DoF pair seemed to emerge.

8.4.3 Limitations

This study was an initial examination into using the backward stepwise selection method to optimally site a minimum number of electrodes for simultaneous estimation of *force-varying* hand grip (Opn-Cls) and one wrist DoF. The target application was SIP control of a conventional hand-wrist prosthesis, although results can be helpful to the general 2-DoF EMG-force problem. Several limitations are evident. First, low error in a laboratory setting has not necessarily reflected improved performance in a prosthesis [31]. That fact noted, laboratory studies represent an established and inexpensive initial step in the development of new technologies, a method that is particularly adept at screening out unsuccessful approaches and refining algorithms before undertaking expensive applied/field evaluations. For example, the results of the work herein recommend the use of both 1- and 2-DoF trials for training and the use of a minimum of four optimally-cited electrodes. Second, this EMG-force training technique was only studied in able-bodied subjects during a single session. Evaluation in limb-loss subjects should follow; including multi-session training, which has been shown to produce better performance [16, 32]. Third, we studied fixed-posture, dynamic contraction with a bandwidth of 0.75 Hz. Varying posture can alter the interpretation of EMG intent [33], and the re-donning of a prosthesis can produce subtle shifts in EMG sites and channel gains which may confound prosthesis control [9, 34]. Fourth, our backward selection method for choosing the optimal electrodes (as a subset of the available 16) may not be unique or represent the only successful method. Further, the two distinct folds (from cross-validation) did not necessarily select the same electrodes. When choosing 4 electrodes from 16 total, there are 1820

combinations. Thus, a non-exhaustive search method seems advantageous. But, alternatives to backward selection exist, including selection based on anatomical locations [23] (appropriate for able-bodied subjects but perhaps problematic for limb-loss subjects who may have altered remnant anatomy), forward stepwise selection and backward-forward stepwise combinations. Fifth, direct comparison of our *absolute* performance results to those of other studies is quite difficult, as performance is a function of many factors, including: contractions used for training/testing (wider bandwidth contractions and more forceful contractions should each lead to higher average errors, at least as measured in %MVC or physical units), the subject population (young vs. aged able-bodied subjects, vs. limb-loss subjects), the experimental conditions and tasks (ADLs [35-38] vs. EMG-force measures), and the manner by which error is measured. Regardless, *relative* performance should be more interpretable across studies. In particular, our relative results suggest that: two electrodes are the minimum number for EMG-force estimation of our 1-DoF hand-wrist tasks, and additional electrodes do not reduce error; four electrodes are the minimum number for our 2-DoF tasks, with a few additional electrodes perhaps providing some limited improvement; training for a 2-DoF model should include both 1-DoF and 2-DoF trials; and that we found no substantial evidence to either prefer or dissuade the pairing of the hand grip DoF with any of the three wrist DoFs when forming a 2-DoF hand-wrist EMG-force estimator.

8.4.4 Implications for Prosthesis Control

The long-term implications for prosthetic control may best be understood via prosthesis testing in limb-loss subjects. But, the implication from able-bodied subjects is that as few as four optimally-sited electrodes—trained from both 1- and 2-DoF trials—may provide 2-DoF EMG-force estimates that are as good (or nearly so) as those from 16 electrodes placed equidistant about the circumference of the forearm. The automated backward selection algorithm is not biased towards *a priori* site locations, thus the altered anatomy of many limb-loss subjects may not adversely influence this site selection method, so long as the necessary information is available in the surface EMG—an assumption that will require evaluation.

Although we have evaluated site selection, training techniques and DoF pairing with an EMG-force/moment task, many prosthesis controllers map EMGσ to joint velocity (rather than joint torque). And, controllers routinely maintain a "dead zone" at EMGσ values near zero, so that the prosthesis does not actuate in response to EMG measurement noise at rest [23]. These distinctions will need to be added to a controller that is based on our calibration method.

Our modeling techniques require measurement of an output force/moment. No such signal is available from limb-loss subjects. As a surrogate measure, unilateral limb-loss subjects can produce force/moment on the sound side and relate it to EMG produced on the limb-loss side during mirrored contractions [8, 19, 20, 39, 40]. Alternatively, all limb-loss subjects can directly activate their phantom limb to track a desired target effort pattern, and then relate EMGσ from the affected limb directly to this target (without feedback) [21, 39]. In either case, one disadvantage is the lack of proprioceptive feedback from the phantom limb.

Training duration is an important issue for prosthesis users. As noted previously, we envision a protocol in which optimal site selection of the preferred number of electrodes (e.g., optimal four of 16 candidate electrode sites) is performed by a prosthetist when fitting a permanent socket. During such a fitting, the several minutes of training time (or more) required when using our data collection protocol would not seem problematic, as the current process of manually siting two electrodes within a socket is already time consuming. Thereafter, a fielded prosthesis would only need an ability to calibrate the permanent (e.g., four) electrode channels. Further, it is also possible that the dynamics of each channel might be fixed during fitting, leaving only the channel gains for field calibration—existing prostheses have fixed dynamics that are the same for all users, only permitting gain adjustments of each EMG channel. In either case, such a small number of free parameters might be trained in only a few seconds [25, 27]. Reasonable field recalibration might be facilitated.

While we limited ourselves to hand grip in combination with one wrist DoF, the long-term goal is the development of upper-limb prostheses that also control individual finger actuation. Limited efforts have been made to do so based on surface EMG from the forearm [7, 41-46].

8.5 Conclusions

This laboratory study provided evidence that 2-DoF EMG-force estimation in the hand-wrist can be successfully accomplished with the use of four electrodes, which are optimally selected from 16 electrodes via backward stepwise selection. These models should be calibrated using both 1- and 2-DoF trials and there did not seem to be a preference as to which wrist DoF to pair with hand grip. With this training, Table I shows that 2-DoF estimation had average RMS testing errors of 9.2 %MVC for each DoF pair. Transition of these techniques to testing in hand-wrist prosthesis users is an appropriate next step.

References

[1] K. Ziegler-Graham, E. J. MacKenzie, P. L. Ephraim, T. G. Travison, and R. Brookmeyer, "Estimating the prevalence of limb loss in the United States: 2005 to 2050," *Arch. Phys. Med. Rehabil.*, vol. 89, pp. 422–429, 2008.

[2] T. R. Dillingham, L. E. Pezzin, and E. J. MacKenzie, "Limb Amputation and Limb Deficiency: Epidemiology and Recent Trends in the United States," *South. Med. J.*, vol. 95, pp. 875–883, 2002.

[3] P. Parker, K. Englehart, and B. Hudgins, "Myoelectric signal processing for control of powered limb prostheses," *J. Electromyo. Kinesiol.*, vol. 16, pp. 541–548, 2006.

[4] D. Farina, N. Jiang, H. Rehbaum, A. Holobar, B. Graimann, H. Dietl, *et al.*, "The extraction of neural information from the surface EMG for the control of upper-limb prostheses: Emerging avenues and Challenges," *IEEE Trans. Neural Sys. Rehabil. Eng.*, vol. 22, pp. 797–809, 2014 2014.

[5] R. W. Mann and S. D. Reimers, "Kinesthetic sensing for the EMG controlled "Boston Arm"," *IEEE Trans. Man-Mach. Sys.*, vol. 11, pp. 110–115, 1970.

[6] D. J. Atkins, D. C. Y. Heard, and W. H. Donovan, "Epidemilogic overview of individuals with upper-limb loss and their reported research priorities," *J. Prosthet. Orthot.*, vol. 8, pp. 2–11, 1996.

[7] P. Liu, D. R. Brown, E. A. Clancy, F. Martel, and D. Rancourt, "EMG-force estimation for multiple fingers," *IEEE Sig. Proc. Med. Biol. Symp.*, 2013.

[8] S. Muceli and D. Farina, "Simultaneous and proportional estimation of hand kinematics from EMG during mirrored movements at multiple degrees-of-freedom," *IEEE Trans. Neural Sys. Rehabil. Eng.*, vol. 20, pp. 371–378, 2012.

[9] S. Muceli, N. Jiang, and D. Farina, "Extracting signals robust to electrode number and shift for online simultaneous and proportional myoelectric control by factorization algorithms," *IEEE Trans. Neural Sys. Rehabil. Eng.*, vol. 22, pp. 623–633, 2014.

[10] T. A. Kuiken, G. A. Dumanian, R. D. Lipschutz, L. A. Miller, and K. A. Stubblefield, "The use of targeted muscle reinnervation for improved myoelectric prosthesis control in a bilateral shoulder disarticulation amputee," *Prosthet. Orthot. Int.*, vol. 28, pp. 245–253, 2004.

[11] T. A. Kuiken, G. Li, B. A. Lock, R. D. Lipschutz, L. A. Miller, K. A. Stubblefield, *et al.*, "Targeted muscle reinnervation for real-time myoelectric control of multifunction artificial arms," *J. Am. Med. Assoc.*, vol. 301, pp. 619–628, 2009.

[12] D. Graupe and W. K. Cline, "Functional separation of EMG signals via ARMA identification methods for prosthesis control purposes," *IEEE Trans. Sys. Man Cyber.*, vol. 5, pp. 252–259, 1975.

[13] B. Hudgins, P. Parker, and R. N. Scott, "A new strategy for multifunction myoelectric control," *IEEE Trans. Biomed. Eng.*, vol. 40, pp. 82–94, 1993.

[14] R. Boostani and M. H. Moradi, "Evaluation of the forearm EMG signal features for the control of a prosthetic hand," *Physiol. Meas.*, vol. 24, pp. 309–319, 2003.

[15] K. Englehart and B. Hudgins, "A robust, real-time control scheme for multifunction myoelectric control," *IEEE Trans. Biomed. Eng.*, vol. 50, pp. 848–854, 2003.

[16] M. A. Powell, R. R. Kaliki, and N. V. Thakor, "User training for pattern recognition-based myoelectric prostheses: Improving phantom limb movement consistency and distinguishability," *IEEE Trans. Neural Sys. Rehabil. Eng.*, vol. 22, pp. 522–532, 2014.

[17] Coapt, LLC. (Chicago, IL, accessed 6 June 2015). Available: http://www.coaptengineering.com.

[18] N. Jiang, K. B. Englehart, and P. A. Parker, "Extracting simultaneous and proportional neural control information for multiple-DOF prostheses from the surface electromyographic signal," *IEEE Trans. Biomed. Eng.*, vol. 56, pp. 1070–1080, 2009.

[19] J. L. Nielsen, S. Holmgaard, N. Jiang, K. B. Englehart, D. Farina, and P. Parker, "Simultaneous and proportional force estimation for multifunction myoelectric prostheses using mirrored bilateral training," *IEEE Trans. Biomed. Eng.*, vol. 58, pp. 681–688, 2011.

[20] N. Jiang, J. L. G. Vest-Nielsen, S. Muceli, and D. Farina, "EMG-based simultaneous and proportional estimation of wrist/hand kinematics in uni-lateral trans-radial amputees," *J. NeuroEng. Rehabil.*, vol. 9:42, 2012.

[21] A. Ameri, E. N. Kamavuako, E. J. Scheme, K. B. Englehart, and P. Parker, "Support vector regression for improved real-time, simultaneous myoelectric control," *IEEE Trans. Neural Sys. Rehabil. Eng.*, vol. 22, pp. 1198–1209, 2014.

[22] S. Amsuess, I. Vujaklija, P. Goebel, A. D. Roche, B. Graimann, O. C. Aszmann, *et al.*, "Context-dependent upper limb prosthesis control for natural and robust use," *IEEE Trans. Neural Sys. Rehabil. Eng.*, vol. 24, pp. 744–753, 2016.

[23] A. L. Fougner, O. Stavdahl, and P. J. Kyberd, "System training and assessment in simultaneous proportional myoelectric prosthesis control," *J. NeuroEng. Rehabil.*, vol. 11:75, 2014.

[24] E. A. Clancy and N. Hogan, "Multiple site electromyograph amplitude estimation," *IEEE Trans. Biomed. Eng.*, vol. 42, pp. 203–211, 1995.

[25] L. Ljung, "System Identification: Theory for the User," ed Upper Saddle River, NJ: Prentice-Hall, 1999, pp. 408–452, 491–519.

[26] E. A. Clancy, O. Bida, and D. Rancourt, "Influence of advanced electromyogram (EMG) amplitude processors on EMG-to-torque estimation during constant-posture, force-varying contractions," *J. Biomech.*, vol. 39, pp. 2690–2698, 2006.

[27] E. A. Clancy, L. Liu, P. Liu, and D. V. Moyer, "Identification of constant-posture EMG-torque relationship about the elbow using nonlinear dynamic models," *IEEE Trans. Biomed. Eng.*, vol. 59, pp. 205–212, 2012.

[28] W. H. Press, B. P. Flannery, S. A. Teukolsky, and W. T. Vetterling, "Numerical Recipies in C," 2nd ed New York: Cambridge Univ. Press, 1994, pp. 671–681.

[29] R. W. Mann, "Cybernetic limb prosthesis: The ALZA distinguished lecture," *Ann. Biomed. Eng.*, vol. 9, pp. 1–43, 1981.

[30] K. T. Cavanaugh, E. A. Clancy, J. A. Natrillo, R. J. Paquette, and F. J. Looft, "Optimal site selection for prosthetic control," *IEEE 1983 Frontiers Eng. Comput. Health Care*, pp. 565–569, 1983.

[31] N. Jiang, S. Dosen, K.-R. Muller, and D. Farina, "Myoelectric control of artificial limbs—Is there a need to change focus?," *IEEE Signal Proc. Mag.*, vol. 29, pp. 152–150, 2012.

[32] J. M. Hahne, S. Dahne, H.-J. Hwang, K.-R. Muller, and L. C. Parra, "Concurrent adaptation of human and machine improves simultaneous and proportional myoelectric control," *IEEE Trans. Neural Sys. Rehabil. Eng.*, vol. 24, pp. 618–627, 2015.

[33] N. Jiang, S. Muceli, B. Graimann, and D. Farina, "Effect of arm position on the prediction of kinematics from EMG in amputees," *Med. Biol. Eng. Comput.*, vol. 51, pp. 143–151, 2013.

[34] A. M. Simon, B. A. Lock, and K. A. Stubblefield, "Patient training for functional use of pattern recognition-controlled prostheses," *J. Prosthet. Orthot.*, vol. 24, pp. 56–64, 2012.

[35] C. M. Light, P. H. Chappell, and P. J. Kyberd, "Establishing a standardized clinical assessment tool of pathologic and prosthetic hand function: Normative data, reliability, and validity," *Arch. Phys. Med. Rehabil.*, vol. 83, pp. 776–783, 2002.
[36] R. D. Lipschutz, T. A. Kuiken, L. A. Miller, and G. A. Dumanian, "Shoulder disarticulation externally powered prosthetic fitting following targeted muscle reinnervation for improved myoelectric control," *J. Prosthet. Orthot.*, vol. 18, pp. 28–34, 2006.
[37] A. M. Simon, L. J. Hargrove, B. A. Lock, and T. A. Kuiken, "Target achievement control test: Evaluating real-time myoelectric pattern-recognition control of multifunctional upper-limb prostheses," *J. Rehabil. Res. Devel.*, vol. 48, pp. 619–628, 2011.
[38] L. H. Smith, T. A. Kuiken, and L. J. Hargrove, "Real-time simultaneous and proportional myoelectric control using intramuscular EMG," *J. Neural. Eng.*, vol. 11, p. 066013, 2014.
[39] A. Ameri, E. J. Scheme, E. N. Kamavuako, K. B. Englehart, and P. A. Parker, "Real-time, simultaneous myoelectric control using force and position-based training paradigms," *IEEE Trans. Biomed. Eng.*, vol. 61, pp. 279–287, 2014.
[40] J. M. Hahne, Biebmann, F., N. Jiang, H. Rehbaum, D. Farina, F. C. Meinecke, *et al.*, "Linear and nonlinear regression techniques for simultaneous and proportional myoelectric control," *IEEE Trans. Neural Sys. Rehabil. Eng.*, vol. 22, pp. 269–279, 2014.
[41] R. N. Khushaba, S. Kodagoda, M. Takruri, and G. Dissanayake, "Toward improved control of prosthetic fingers using surface electromyogram (EMG) signals," *Exp. Sys. App.*, vol. 39, pp. 10731–10738, 2012.
[42] C. Cipriani, C. Antfolk, M. Controzzi, G. Lundborg, M. C. Carrozza, and F. Sebelius, "Online myoelectric control of a dexterous hand prosthesis by transradial amputees," *IEEE Trans. Neural Sys. Rehabil. Eng.*, vol. 19, pp. 260–270, 2011.
[43] R. J. Smith, D. Huberdeau, F. Tenore, and N. V. Thakor, "Real-time myoelectric decoding of individual finger movements for a virtual target task," *Ann. Int. Conf. IEEE EMBS*, pp. 2376–2379, 2009.
[44] R. J. Smith, F. Tenore, D. Huberdeau, R. Etienne-Cummings, and N. V. Thakor, "Continuous decoding of finger position from surface EMG signals for the control of powered prostheses," *Ann. Int. Conf. IEEE EMBS*, pp. 197–200, 2008.
[45] H.-P. Huang and C.-Y. Chen, "Development of a myoelectric discrimination system for a multi-degree prosthetic hand," *Proc. IEEE Int. Conf. Robotics Automat.*, pp. 2392–2397, 1999.
[46] C. Cipriani, F. Zaccone, S. Micera, and M. C. Carozza, "On the shared control of an EMG-controlled prosthetic hand: Analysis of user-prosthesis interaction," *IEEE Trans. Robotics*, vol. 24, pp. 170–184, 2008.

Chapter 9: A Pilot Study Assessing Ipsilateral vs. Contralateral Feedback in EMG-Force Models of the Wrist for Upper-Limb Prosthesis Control

This chapter has been published as: Edward A. Clancy, Chenyun Dai, Marek Wartenberg, Carlos Martinez Luna, Thane R. Hunt and Todd R. Farrell, "*A Pilot Study Assessing Ipsilateral vs. Contralateral Feedback in EMG-Force Models of the Wrist for Upper-Limb Prosthesis Control*," 2015 IEEE Signal Processing in Medicine and Biology Symposium (SPMB), Temple University, Philadelphia, PA, 12 December 2015. Color versions of one or more of the figures in this paper are available online at http://ieeexplore.ieee.org/stamp/stamp.jsp?tp=&arnumber=7002963.

***Abstract*—Many advanced EMG-based upper-limb prosthesis control methods require model training in which subjects produce supervised forces/movements. Since unilateral limb-absent subjects cannot produce forces/movements on their affected side, one technique (mirrored bi-lateral training) relates forces/motions produced on the sound side to EMG on the affected side. However, the efforts made by the phantom limb may not fully reflect those of the sound limb. To understand this issue, three able-bodied subjects produced mirrored bi-lateral forces during constant-posture contraction at the wrist. EMG-force models were formed for 1- and 2-degree of freedom tasks and results compared to previous trials in which ipsilateral training had been conducted. We found that contralateral training generally, but not always, produced errors (in percent maximum voluntary contraction) that were 6–56% larger than those found from ipsilateral training. Our results suggest that a substantial portion—but not all—of the errors found in mirrored tasks may be due to contralateral tracking errors. Further study with a larger population is indicated.**

Keywords—EMG, electromyogram, prosthesis, prosthesis control, myoelectric control, EMG signal processing

9.1 Introduction

Many people with transradial limb absence use electromyogram (EMG)-controlled, powered hand and wrist prostheses to provide partial functional replacement. Existing commercial EMG-controlled prostheses typically use EMG from the residual flexors and extensors of the forearm to actuate prosthetic hand closing and opening, respectively. Wrist rotation is not controlled simultaneously, rather some form of mode switching (via EMG or mechanical switch) is used to sequence between hand and wrist activation [1]. This lack of proportional, simultaneous and independent control represents a substantial limitation of existing upper-limb prosthetic systems [2].

To improve upper-limb prosthesis control, Kuiken and colleagues [3, 4] have developed targeted muscle reinnervation surgery, in which muscles of the chest wall are denervated, after which nerves formerly associated with the lost limbs are grafted to these chest muscles. Activation of the phantom limb causes actual contraction of chest muscles, providing proportional, simultaneous and independent control signals. The cost and lengthy rehabilitation (3–6 months) required by this technique may make it most appropriate for bilateral limb-absent patients and those with high-level unilateral limb absence. Alternatively, pattern recognition techniques have related EMG from the residual forearm to a set of preselected hand-wrist movements [1, 5-9]. Multiple-joint movement is possible, albeit still generally comprised of only one degree of freedom (DoF). This method recently became available in a commercial system (COAPT LLC, Chicago, IL).

For a large class of transradial limb-absent persons, there is a need for proportional, simultaneous and independent EMG-based prosthesis control using the residual forearm musculature. Several studies have addressed this problem, primarily in able-bodied volunteers. Initial studies largely focused on the scientific establishment of a hand/wrist EMG-force relationship. These studies applied high-density electrodes to the forearm (often 64+ electrodes), studying finger forces/pose or wrist forces [10-12]. A convincing, multiple-DoF EMG-force relationship in the wrist was demonstrated in able-bodied subjects. Nonetheless, high-density electrodes were never intended for commercial prosthetic use.

In the past few years, research has focused on adapting the EMG-force modeling for use with conventional bipolar electrodes and commercial prosthesis systems [13-18]. Most modeling methods are supervised, thus some form of subject "output" (i.e., subject force, position or effort) must exist to which the (input) EMG signal is related. In persons with limb absence, finding an appropriate output is challenging, as no limb is available on the affected side to produce hand/wrist forces or movement. One method uses only the affected side and a target on the computer screen [15, 18]. The subject produces an

effort in their phantom limb to match the effort associated with the location and/or orientation of the target. This method is direct, but does not provide any feedback.

The interest of this work is in another training method known as mirrored bi-lateral (contralateral) contractions, in which the affected hand/wrist mirrors the contraction profile of the sound side hand/wrist [11, 14, 17-19]. EMG recordings from the affected side are related to the actual forces/ movements measured on the sound side. Feedback is available, but only from the contralateral side. This method is only available to those with unilateral limb-absence. Past research work suggests that performance when using the contralateral training approach is poorer than that found in identical tasks using an ipsilateral training approach [17, 18]. These past studies investigated forces in the wrist, applying 7–8 bipolar electrodes, performing specific tasks (1- and 2-DoF wrist movement or isometric attempted movement or sinusoidal contractions) using the coefficient of determination (R^2) for assessment. We have been studying constant-posture EMG-force in the wrist with either quasi-constant-force contractions that span ±30% maximum voluntary contraction (MVC) or band-limited uniform random dynamic force contractions that span this same force range. Our studies also reduce the number of bipolar electrodes used from 16 to 4 for 2-DoF tasks. A subset of three able-bodied subjects completed both ipsilateral training and mirrored bi-lateral (contralateral) training. Herein we compare their EMG-force performance with our assessment metric—RMS EMG-force error, normalized to MVC.

9.2 Methods

9.2.1 Experimental Apparatus and Procedures

Experiments and data analysis were approved by the New England IRB (Newton, MA) and the WPI IRB. Each of three male subjects (aged 25, 37 and 53 years) provided written informed consent. Each subject participated in two, half-day experiments on separate days, with ~6 months between the two sessions. Subjects performed ipsilateral training in the first session and contralateral training in the second session.

For the first experimental session (ipsilateral trials), skin about the proximal forearm of the dominant arm (right arm for each subject) was scrubbed with an alcohol wipe and electrode gel was massaged into the skin. Sixteen bipolar electrodes were mounted equidistant in a row, transversely about the forearm, each centered 5 cm distal from the elbow crease. One electrode pair was aligned at the most

dorsal aspect. Each electrode pair consisted of 5 mm diameter, stainless steel, hemispherical contacts separated 1 cm edge-to-edge, oriented along the long axis of the forearm. The average transverse spacing between bipolar electrode pairs was 1.9 cm center-to-center. A reference electrode was gelled and secured on the ventral side of the forearm, just distal to the bipolar electrodes. Each bipolar EMD signal was differentially amplified (Liberating Technologies, Inc. BE328 amplifier; pass band from 30–500 Hz, CMRR > 100 dB over the pass band) and selectable gain applied. EMG were acquired at 2048 Hz using a 16-bit ADC.

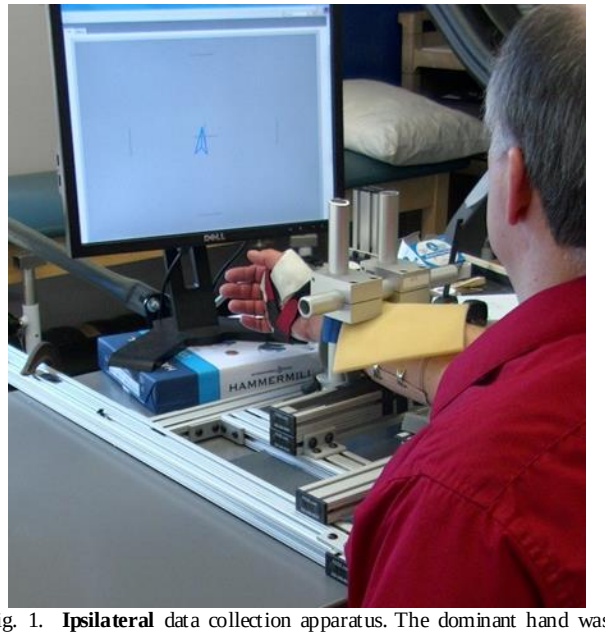

Fig. 1. **Ipsilateral** data collection apparatus. The dominant hand was tightly secured via a thermo-formable plastic splint and Velcro to a six-axis load cell. The wrist was maintained in a neutral position by a padded restraint. Sixteen electrodes (not visible) were secured about the proximal aspect of the forearm. Display screen is visible in front of the subject.

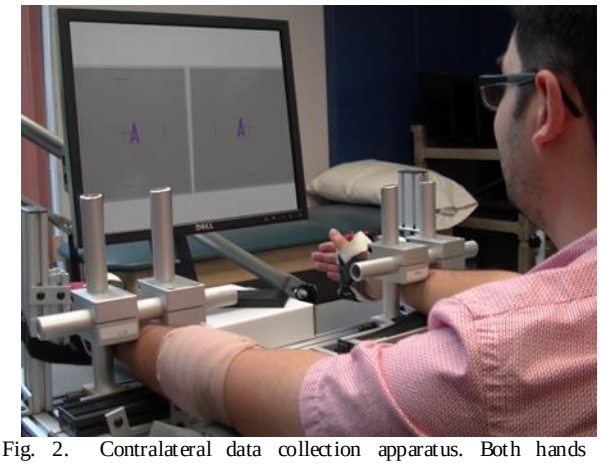

Fig. 2. Contralateral data collection apparatus. Both hands are constrained, but load cell measurements are only made from the dominant (right) side. Electrodes mounted about non-dominant (left) forearm.

As shown in Fig. 1, subjects sat and extended their dominant arm to place their hand in a thermo-formable plastic splint that was rigidly attached to a load cell (AMTI, Watertown, MA; model MC3A-100 transducer, Gen 5 signal conditioner). The metacarpal region of the hand was tightly secured to the splint using Velcro, while the phalanges were free. This attachment isolated measurement of forces at the wrist. The palm of the hand was perpendicular to the plane of the floor, the hand was in a neutral position with respect to the wrist, the elbow was extended and the upper arm was rotated ~45o forward from the anatomical position. The arm was supported just distal to the olecranon process. The load cell measured three DoFs, which were displayed on a computer screen directly in front of the subject via an arrowhead cursor. Wrist extension-flexion (Ext-Flx) specified the x-axis location of the arrowhead,

radial-ulnar deviation (Rad-Uln) the y-axis location and pronation-supination (Pro-Sup) moment the angular rotation. A second computer-generated target arrowhead could also be displayed. The three load cell signals were also sampled at 2048 Hz at 16-bit resolution.

MVCs and 50% MVCs were measured in each of wrist extension, flexion, radial and ulnar deviation, pronation and supination, along with a rest recording. These calibration contractions were used for force normalization, EMG noise assessment and calibration of advanced EMG processing techniques [20, 21]. Contractions for model training and testing followed. First, 1-DoF quasi-static trials were conducted separately for Ext-Flx, Rad-Uln and Pro-Sup. For Ext-Flx, subjects followed the computer screen force target as it took 30 s to linearly ramp from the force midpoint, to 30% MVC flexion, to 30% MVC extension, back to 30% MVC flexion and then back to the force range midpoint. Analogous ramp trajectories were used for Rad-Uln and Pro-Sup trials. Four trials per DoF were recorded (12 trials in total), randomized by DoF. During each trial, the on-screen arrowhead cursor that was controlled by the subject was only permitted to move along the active DoF. Second, 2-DoF quasi-static trials were conducted by eliciting ramp co-contraction of pairs of contraction directions. Two DoFs were active and their target effort levels were coincident. The same 30 s ramp trajectory was used. Two repetitions of six randomized trials were conducted (12 trials in total), the trials being identified by the contraction directions associated with the first 30% MVC co-contraction achieved. The subject-controlled arrowhead was only permitted to move/rotate along the two active DoFs. Third, 40-s duration, 1-DoF dynamic force trials were conducted separately for each of the three DoFs. For Ext-Flx, the target followed a random, uniform trajectory between 30% MVC extension and 30% MVC flexion, band-limited between 0–1 Hz. Three such trials were conducted for each DoF, randomized by DoF. The subject-controlled arrowhead was only permitted to move along the active DoF. Fourth, 40-s duration, 2-DoF dynamic force trials were conducted for each of the three pairs of DoFs. For these 2-DoF tasks, the target moved randomly and independently in each DoF. Three such trials were conducted for each DoF pair, randomized in order. All four sets of contractions were conducted at an interval of at least two minutes, to avoid accumulated fatigue. Subjects were released from the hand cuff between experiment stages.

For the second experimental session (contralateral trials), the apparatus differed only in that the electrodes were mounted on the contralateral forearm and that the contralateral arm was identically constrained with its hand secured to a second hand cuff (Fig. 2). Load cell measurement was still only

provided for the dominant hand. MVC calibrations were not repeated; rather, the values from the first experimental session were used. Subjects completed the 50% MVC trials and the four sets of contractions for model training and testing (see previous paragraph). Subjects were provided load cell feedback from their dominant arm and instructed to mirror this effort level on their non-dominant (contralateral) side.

9.2.2 Methods of Analysis

Analysis was performed offline using MATLAB (The MathWorks, Inc., Natick, MA). Only causal algorithms were studied. EMG amplitude was estimated from each EMG signal. Each EMG signal was highpass filtered (5th-order Butterworth, cut-off at 15 Hz), notch filtered at the power-line frequency of 60 Hz (2nd-order notch filter, 1 Hz bandwidth) and rectified. Data from quasi-static trials were then lowpass filtered (cut-off frequency of 1.6 Hz; Chebyshev Type 1 filter, 9th-order, 0.05 dB peak-to-peak passband ripple) and downsampled to 4.096 Hz. Data from dynamic force trials were then lowpass filtered (cut-off frequency of 16 Hz; Chebyshev Type 1 filter, 9th-order, 0.05 dB peak-to-peak passband ripple) and downsampled to 40.96 Hz. Separately, the three mechanical signals were each normalized to their respective MVC value per DoF, and then similarly decimated depending on the trial type (to 4.096 Hz for quasi-static trials and to 40.96 Hz for dynamic trials). Hence, the input-output data sets available for EMG-force modeling were sampled at a rate that was approximately ten times the bandwidth of the output, which is appropriate for system identification [22, 23].

First, 1-DoF models were fit for each subject, using the quasi-static 1-DoF trials. For Ext-Flx, EMGs were least squares fit to Ext-Flx force (the remaining mechanical measures were ignored) via the model:

$$T_{E-F}[m] = \sum_{e=1}^{E} \sum_{q=0}^{Q} c_{e,q}\, \sigma_e[m-q] \quad , \tag{1}$$

Where T_{E-F} was Ext-Flx force, m was the decimated discrete-time sample index, E was the number of electrodes (initially set to 16), $c_{e,q}$ were the fit coefficients and $\sigma_e[m-q]$ were the EMG amplitude values. Model order Q was set to 0, since the quasi-static trials had essentially no dynamics. Fit coefficients were determined using least squares via the pseudo-inverse technique, in which singular values were removed if the ratio of that singular value to the largest singular value in the design matrix was less than a tolerance value of 0.01. This tolerance was selected after some initial evaluation over a range of tolerance values. Two quasi-static trials were used to train a model. Backward stepwise

selection was then used to progressively reduce the number of EMG channels (i.e., omit the channel whose absence resulted in the lowest error), making all decisions only on the training trials. The two remaining 1-DoF trials were used for testing at each step (normalized RMS error in %MVC, averaged across the two trials). This process was repeated after exchanging the training and testing trials, for cross-validation. The average of the cross-validated results is reported. An identical process was then repeated for 1-DoF models relating EMG to Rad-Uln force and, separately, Pro-Sup moment.

Second, 2-DoF models were fit for each subject, using the quasi-static trials and the static model of (1). The EMG-force model and backward stepwise selection were applied identically, except that the model always simultaneously estimated two mechanical DoFs (the third, unused mechanical force/moment was ignored). Model training optionally consisted of 1-DoF trials (the first repetition of two trials from each relevant DoF), or 2-DoF trials (the first repetition of four trials, one per 2-DoF contraction direction), or both. For testing, RMS error was assessed separately for 1-DoF test trials and 2-DoFs trials, always for the two available mechanical dimensions. (During 1-DoF trials, the second mechanical dimension remained near zero throughout the trial.) The trial repetitions were switched and the overall error assigned as the average of the two-fold cross validation.

Third, 1-DoF models were fit for each subject, using the dynamic trials and the model of (1), with model order selected as Q = 25 [24]. For each DoF, three trials were available. Two were used for training and one for testing, with full cross-validation. The average cross-validated result is reported.

Fourth, 2-DoF models were fit for each subject, using the dynamic trials and model order Q = 25. For each pair of DoFs, three trials were available. Two were used for training and one for testing, with full cross-validation and the averaged result reported. As before, training from 1-DoF, 2-DoF or both trials was separately pursued.

Note that statistical comparisons will not be presented, as only three subjects participated in this study. Rather, trends will be noted in the EMG-force errors. In addition, direct comparison of the absolute error values between 1-DoF models and 2-DoF trials must be approached cautiously, since the underlying data differ.

9.3 Results

Quasi-Static Models: Fig. 3 shows sample time-series test results of contralateral EMG-force for the 1-DoF models based on the quasi-static trials. Fig. 4 shows similar (contralateral) results for the 2-

DoF models based on quasi-static trials and training from both 1- and 2-DoF trials. Table 1 shows summary quasi-static results for the three subjects, where we have concentrated on two-channel systems for the 1-DoF models and four-channel systems for the 2-DoF models. Table I shows that each 1-DoF model had average errors that were 10–56% higher for contralateral-trained models. If effect size is taken as the difference of the paired means divided by their average standard deviation, then it ranges from 0.29–0.69. When assessing on 2-DoF models, overall lower errors were achieved when training from both 1- and 2-DoF trials. And, these average performance differences were similar in percentage as to the 1-DoF models, with contralateral-trained models performing 3–65% poorer (effect size: 0.08–1.04).

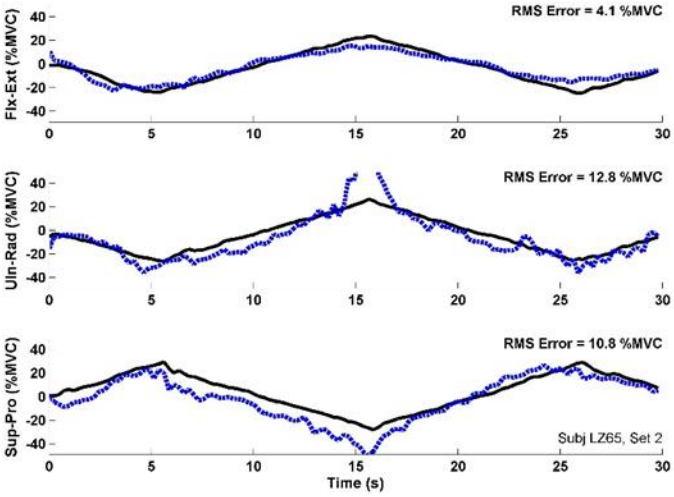

Fig. 3. **Contralateral, 1-DoF Model, Quasi-Static:** Example time-series plots of one-degree-of-freedom models, contralateral trials, quasi-static, two electrodes. Solid black lines are actual forces/moment, dashed blues lines are EMG-estimated.

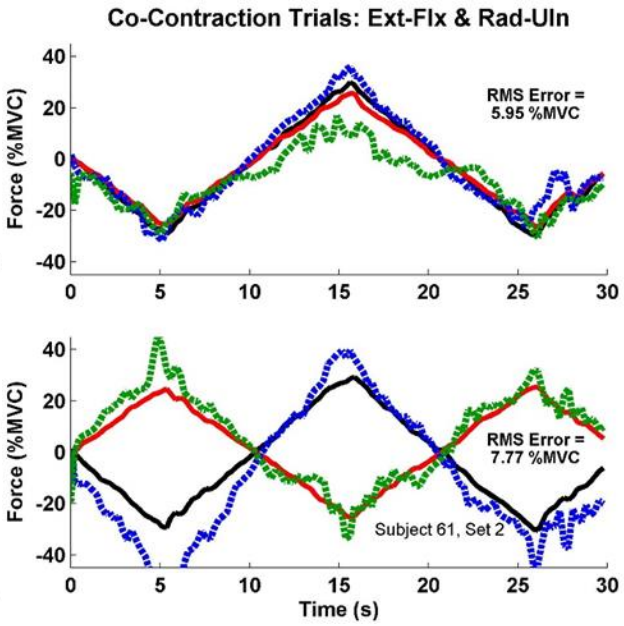

Fig. 4. **Contralateral, 2-DoF Model, Quasi-Static:** Example time-series plots of two-degree-of-freedom models. Contralateral trials, quasi-static, four electrodes. Training was from both 1- and 2-DoF trials. Key: solid black = actual Ext-Flx, dashed blue = estimated Ext-Flx, solid red = actual Rad-Uln, dash green = estimated Rad-Uln. Positive %MVC corresponds to Ext/Rad.

Dynamic Models: Fig. 5 shows sample time-series test results of contralateral EMG-force for the 2-DoF models based on the dynamic trials. Fig. 6 shows dynamic model contralateral results as a function of the number of electrodes for 2-DoF models, when training was from only the 2-DoF trials. Results when training from only the 1-DoF trials or from both followed the same trends. For all three DoF pairs, average errors varied little as the number of electrodes was reduced from 16 down to 4. Further

decreases in electrodes led to progressive increases in the average error. For Rad-Uln & Pro-Sup, errors were always larger (compared to the other DoF pairs), particularly for 2-DoF assessment. Tables II and III show summary dynamic results for the three subjects. For 1-DoF models (Table II), contralateral-trained models performed better for Ext-Flx, but poorer for the two other DoFs. With two electrodes, the differences ranged from 6–19%. As the number of electrodes was increased, some limited error improvement seemed to result. For 1-DoF models (Table III), contralateral training errors using four electrodes were 9–18% higher, except when pairing Rad-Uln with Pro-Sup (errors were both higher and lower). Note that the Rad-Uln & Pro-Sup errors were larger than those of the other two pairings, thus this 2-DoF pairing would seem to be least valuable for use in prosthesis control. Again, as the number of electrodes was increased, there appeared to be some limited reduction in error.

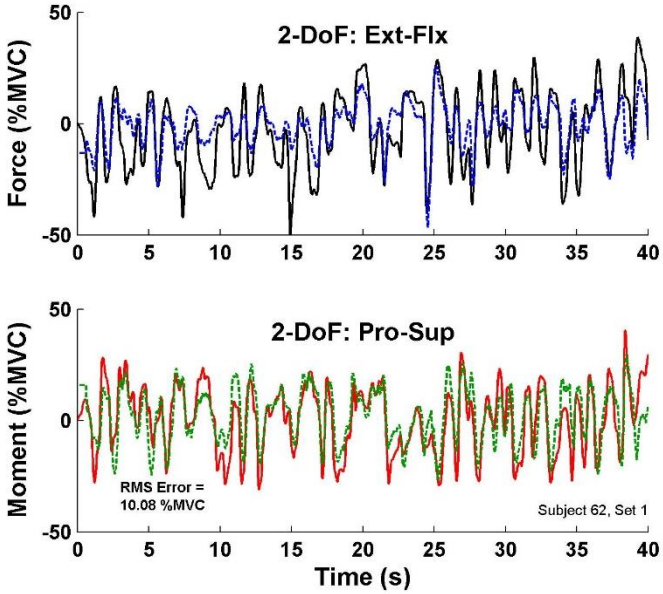

Fig. 5. **Contralateral, 2-DoF Model, Dynamic:** Example time-series plots of 2-DoF models, contralateral contractions, dynamic tracking with four electrodes. Key: solid black = actual Ext-Flx, dashed blue = estimated Ext-Flx, solid red = actual Pro-Sup, dashed green = estimated Pro-Sup. Training from both 1- and 2-DoF trials.

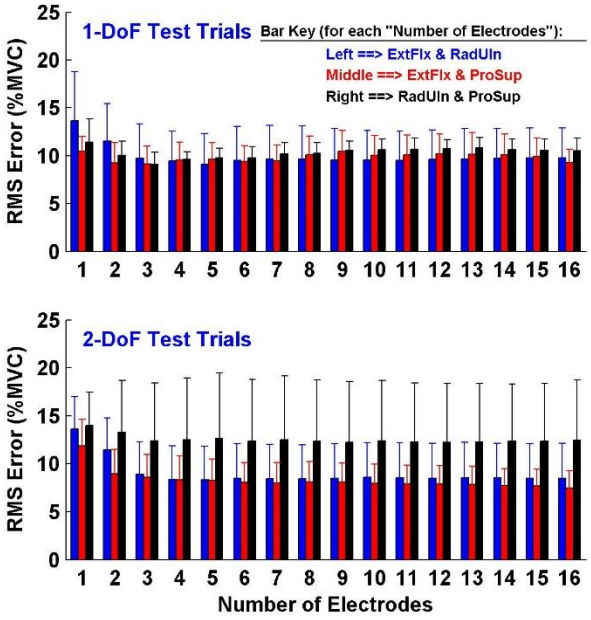

Fig. 6. **Contralateral, 2-DoF Model, Dynamic:** Comparison of (cross-validated) mean plus std. dev. results between contraction types for 2-DoF models vs. number of electrodes. Training from only 2-DoF trials.

TABLE I. **QUASI-STATIC TRIALS:** SUMMARY RESULTS (%MVC) OF BI-LATERAL MIRROR TRAINING COMPARISON OF IPSILATERAL VS. CONTRALATERAL EMG-FORCE ERRORS IN THREE SUBJECTS

Condition	Ipsi v. Contra	DoF(s)		
1-DoF Models (2 electrodes)		**Ext-Flx**	**Rad-Uln**	**Pro-Sup**
Assessed on 1-DoF trials	Ipsi:	5.1 ± 1.4	7.1 ± 2.1	8.5 ± 5.3
	Contra:	5.6 ± 2.0	11.1 ± 9.5	10.4 ± 3.3
2-DoF Models (4 electrodes)		**Ext-Flx & Rad-Uln**	**Ext-Flx & Pro-Sup**	**Rad-Uln & Pro-Sup**
Train with 1- DoF trials; Assess with 1-DoF trials	Ipsi:	5.5 ± 2.6	6.7 ± 2.5	7.3 ± 2.9
	Contra:	6.5 ± 3.8	6.1 ± 2.1	7.2 ± 4.7
Train with 1-DoF trials; Assess with 2-DoF trials	Ipsi:	9.6 ± 1.6	13.2 ± 4.4	17.5 ± 14.7
	Contra:	13.2 ± 6.6	11.2 ± 2.4	14.6 ± 2.5
Train with 1- and 2-DoF trials; Assess with 2-DoF trials	Ipsi:	6.8 ± 1.1	8.5 ± 1.5	9.6 ± 3.2
	Contra:	11.2 ± 7.4	8.9 ± 2.2	9.9 ± 4.7

TABLE II

DYNAMIC TRIALS, 1-DOF MODELS: SUMMARY RESULTS (MEAN ± STD. DEV % MVC RMS ERROR). PARENTHESES IN FINAL COLUMN INDICATE NUMBER OF ELECTRODES CORRESPONDING TO MINIMUM AVERAGE ERROR.

Motion	Ipsilateral				Contralateral			
	2 Electrodes	4 Electrodes	8 Electrodes	Electrodes with Min. Error	2 Electrodes	4 Electrodes	8 Electrodes	Electrodes with Min. Error
Ext-Flx	5.5 ± 0.8	5.3 ± 1.5	5.2 ± 1.7	(9) 5.1 ± 1.7	5.2 ± 2.8	5.0 ± 2.6	4.8 ± 2.1	(14) 4.7 ± 2.0
Rad-Uln	7.0 ± 4.5	6.5 ± 4.2	5.9 ± 3.8	(9) 5.9 ± 3.7	8.3 ± 4.8	8.1 ± 4.7	7.9 ± 5.1	(7) 7.4 ± 4.2
Pro-Sup	6.3 ± 2.2	5.4 ± 1.9	5.5 ± 1.3	(6) 5.2 ± 1.5	6.7 ± 2.1	6.6 ± 2.4	6.6 ± 2.4	(3) 6.4 ± 2.4

TABLE III

DYNAMIC TRIALS, 2-DOF MODELS: SUMMARY RESULTS (MEAN ± STD. DEV % MVC RMS ERROR). PARENTHESES IN FINAL COLUMN INDICATE NUMBER OF ELECTRODES CORRESPONDING TO MINIMUM AVERAGE ERROR.

Motion	Ipsilateral			Contralateral		
	4 Electrodes	8 Electrodes	Electrodes with Min. Error	4 Electrodes	8 Electrodes	Electrodes with Min. Error
Train with 1-DoF Trials						
Ext-Flx&Rad-Uln	9.8 ± 3.4	9.2 ± 3.7	(5) 9.0 ± 3.4	11.2 ± 4.1	10.9 ± 3.6	(12) 10.7 ± 3.4
Ext-Flx&Pro-Sup	9.2 ± 1.1	8.9 ± 1.7	(10) 8.7 ± 1.8	10.4 ± 3.1	9.6 ± 2.8	(13) 9.4 ± 2.8
Rad-Uln&Pro-Sup	16.9 ± 7.4	16.8 ± 7.4	(16) 14.8 ± 5.9	11.8 ± 4.0	12.4 ± 3.6	(6) 11.7 ± 3.3
Train with 2-DoF Trials						
Ext-Flx&Rad-Uln	7.2 ± 2.6	6.8 ± 3.1	(14) 6.7 ± 3.0	8.4 ± 4.3	8.4 ± 4.4	(5) 8.3 ± 4.2
Ext-Flx&Pro-Sup	7.1 ± 1.5	6.6 ± 1.6	(10) 6.2 ± 0.7	8.3 ± 3.0	8.1 ± 2.6	(16) 7.5 ± 2.2
Rad-Uln&Pro-Sup	12.4 ± 7.3	11.7 ± 8.8	(12) 10.6 ± 7.8	12.5 ± 7.9	12.3 ± 7.8	(12) 12.3 ± 7.5
Train with 1- and 2-DoF Trials						
Ext-Flx&Rad-Uln	8.0 ± 2.9	7.4 ± 2.9	(12) 7.1 ± 3.1	9.4 ± 4.0	8.5 ± 3.8	(14) 8.4 ± 3.8
Ext-Flx&Pro-Sup	7.9 ± 0.7	7.0 ± 1.5	(16) 6.9 ± 1.5	8.6 ± 2.9	7.8 ± 2.2	(16) 7.7 ± 2.2
Rad-Uln&Pro-Sup	12.9 ± 7.6	11.4 ± 6.1	(15) 11.1 ± 6.8	11.3 ± 5.5	11.2 ± 5.5	(6) 11.1 ± 5.3

9.4 Discussion

Under both quasi-static and dynamic contractions, the majority of error comparisons found that when comparing ipsilateral vs. contralateral training, errors were greater (by 6–56 %MVC) when contralateral training was used. Note that this result does not imply that forces produced by the two arms of the subjects varied by 6–56%. In particular, if the force on one side was a constant fraction of that of the other, the gains of the EMG-force models would appropriately adjust to correct this error entirely. Further, dynamic models (i.e., those used to model the dynamic trials) can adjust for systematic linear differences between the left- and right-side forces, at least those consistent with the systems available in our model (25th-order FIR filters). Hence, the differences in errors shown in Table I–III are most indicative of differences in contraction profiles (left- vs. right-side) and not absolute strength.

Accordingly, it would be interesting to simultaneously measure the forces produced by both arms, to better understand the ability of able-bodied subjects to match contralateral efforts. Regardless, subjects with limb absence likely have more difficulty in matching contralateral efforts than do able-bodied subjects, since limb-absent subjects also lack aspects of motor feedback (proprioception and force).

9.5 Conclusion

In summary, the trend in our results was for larger errors in contralateral-trained models than in ipsilateral-trained models. The average error differences in quasi-static 1-DoF trials varied from 6–56%, when measured in %MVC (effect size: 0.29–0.69). Differences were as large as 65% (effect size 1.04) in quasi-static 2-DoF trials (Ext-Flx & Rad-Uln). These results suggest that differences in contralateral contraction profiles account for some of the additional errors commonly found when training EMG-force models using bi-lateral mirrored contractions. Additional study in a larger able-bodied population is warranted, in which it would also be useful to simultaneously measure the forces produced by both wrists, providing a more complete comparison of the ability—and limitations—of subjects to match contraction profiles contralaterally. With the cases giving the better effect sizes of 1.04 and 0.69, this pilot study finds that, in a full study, paired comparisons at α=0.05 would require a sample size of 10 and 19, respectively, for 80% statistical power [25].

References

[1] P. Parker, K. Englehart, and B. Hudgins, "Myoelectric signal processing for control of powered limb prostheses," *J. Electromyo. Kinesiol.*, vol. 16, pp. 541–548, 2006.
[2] D. J. Atkins, D. C. Y. Heard, and W. H. Donovan, "Epidemilogic overview of individuals with upper-limb loss and their reported research priorities," *J. Prosthet. Orthot.*, vol. 8, pp. 2–11, 1996.
[3] T. A. Kuiken, G. A. Dumanian, R. D. Lipschutz, L. A. Miller, and K. A. Stubblefield, "The use of targeted muscle reinnervation for improved myoelectric prosthesis control in a bilateral shoulder disarticulation amputee," *Prosthet. Orthot. Int.*, vol. 28, pp. 245–253, 2005.
[4] T. A. Kuiken, G. Li, B. A. Lock, R. D. Lipschutz, L. A. Miller, K. A. Stubblefield, *et al.*, "Targeted muscle reinnervation for real-time myoelectric control of multifunction artificial arms," *J. Am. Med. Assoc.*, vol. 301, pp. 619–628, 2009.
[5] D. Graupe and W. K. Cline, "Functional separation of EMG signals via ARMA identification methods for prosthesis control purposes," *IEEE Trans. Sys. Man Cyber.*, vol. 5, pp. 252–259, 1975.
[6] B. Hudgins, P. Parker, and R. N. Scott, "A new strategy for multifunction myoelectric control," *IEEE Trans. Biomed. Eng.*, vol. 40, pp. 82–94, 1993.
[7] R. Boostani and M. H. Moradi, "Evaluation of the forearm EMG signal features for the control of a prosthetic hand," *Physiol. Meas.*, vol. 24, pp. 309–319, 2003.
[8] K. Englehart and B. Hudgins, "A robust, real-time control scheme for multifunction myoelectric control," *IEEE Trans. Biomed. Eng.*, vol. 50, pp. 848–854, 2003.
[9] M. A. Powell, R. R. Kaliki, and N. V. Thakor, "User training for pattern recognition-based myoelectric prostheses: Improving phantom limb movement consistency and distinguishability," *IEEE Trans. Neural Sys. Rehabil. Eng.*, vol. 22, pp. 522–532, 2014.
[10] P. Liu, D. R. Brown, E. A. Clancy, F. Martel, and D. Rancourt, "EMG-force estimation for multiple fingers," presented at the IEEE Sig. Proc. Med. Biol. Symp., 2013.
[11] S. Muceli and D. Farina, "Simultaneous and proportional estimation of hand kinematics from EMG during mirrored movements at multiple degrees-of-freedom," *IEEE Trans. Neural Sys. Rehabil. Eng.*, vol. 20, pp. 371–378, 2012.
[12] S. Muceli, N. Jiang, and D. Farina, "Extracting signals robust to electrode number and shift for online simultaneous and proportional myoelectric control by factorization algorithms," *IEEE Trans. Neural Sys. Rehabil. Eng.*, vol. 22, pp. 623–633, 2014.
[13] N. Jiang, K. B. Englehart, and P. A. Parker, "Extracting simultaneous and proportional neural control information for multiple-DOF prostheses from the surface electromyographic signal," *IEEE Trans. Biomed. Eng.*, vol. 56, pp. 1070–1080, 2009.
[14] N. Jiang, J. L. Vest-Nielsen, S. Muceli, and D. Farina, "EMG-based simultaneous and proportional estimation of wrist/hand kinematics in uni-lateral trans-radial amputees," *J. NeuroEng. Rehabil.*, vol. 9:42, 2012.
[15] A. Ameri, E. N. Kamavuako, E. J. Scheme, K. B. Englehart, and P. Parker, "Support vector regression for improved real-time, simultaneous myoelectric control," *IEEE Trans. Neural Sys. Rehabil. Eng.*, vol. 22, pp. 1198–1209, 2014.
[16] A. Fougner, O. Stavdahl, P. J. Kyberd, Y. G. Losier, and P. A. Parker, "Control of upper limb prosthesis: Terminology and proportional myoelectric Control—A review," *IEEE Trans. Neural Sys. Rehabil. Eng.*, vol. 20, pp. 663–677, 2012.
[17] J. L. Nielsen, S. Holmgaard, N. Jiang, K. B. Englehart, D. Farina, and P. Parker, "Simultaneous and proportional force estimation for multifunction myoelectric prostheses using mirrored bilateral training," *IEEE Trans. Biomed. Eng.*, vol. 58, pp. 681–688, 2011.
[18] A. Ameri, E. J. Scheme, E. N. Kamavuako, K. B. Englehart, and P. A. Parker, "Real-time, simultaneous myoelectric control using force and position-based training paradigms," *IEEE Trans. Biomed. Eng.*, vol. 61, pp. 279–287, 2014.
[19] H. J. M., F. Biebmann, N. Jiang, H. Rehbaum, D. Farina, F. C. Meinecke, *et al.*, "Linear and nonlinear regression techniques for simultaneous and proportional myoelectric control," *IEEE Trans. Neural Sys. Rehabil. Eng.*, vol. 22, pp. 269–279, 2014.
[20] E. A. Clancy and K. A. Farry, "Adaptive whitening of the electromyogram to improve amplitude estimation," *IEEE Trans. Biomed. Eng.*, vol. 47, pp. 709–719, 2002.
[21] P. Prakash, C. A. Salini, J. A. Tranquilli, D. R. Brown, and E. A. Clancy, "Adaptive whitening in electromyogram amplitude estimation for epoch-based applications," *IEEE Trans. Biomed. Eng.*, vol. 52, pp. 331–334, 2005.
[22] E. A. Clancy, O. Bida, and D. Rancourt, "Influence of advanced electromyogram (EMG) amplitude processors on EMG-to-torque estimation during constant-posture, force-varying contractions," *J. Biomech.*, vol. 39, pp. 2690–2698, 2006.
[23] L. Ljung, *System Identification: Theory for the User*. Upper Saddle River, NJ: Prentice-Hall, 1999, pp. 491–519.
[24] E. A. Clancy, L. Liu, P. Liu, and D. V. Moyer, "Identification of constant-posture EMG-torque relationship about the elbow using nonlinear dynamic models," *IEEE Trans. Biomed. Eng.*, vol. 59, pp. 205–212, 2012.
[25] G. W. Snedecor and W. G. Cochran, *Statistical Methods*, 7th ed., Iowa State, 1980, p. 104.

Appendix

A. 2016 ISEK Conference Abstract

Title:

Two Degrees of Freedom EMG-Force at the Wrist in Able-Bodied Subjects Using a Minimum Number of Electrodes: Pilot Testing of Limb-Absent Subjects

Authors:

Edward A. Clancy, Worcester Polytechnic Institute, ted@wpi.edu

Carlos Martinez-Luna, Liberating Technologies, Inc., carlos.martinez@liberatingtech.com

Marek Wartenberg, Worcester Polytechnic Institute, marek.wartenberg@wpi.edu

Todd R. Farrell, Liberating Technologies, Inc., Todd Farrell, todd.farrell@liberatingtech.com

Contact Name, affiliation/institution, e-mail:

Ted Clancy, ECE Dept., Worcester Polytechnic Institute, 100 Institute Rd., Worcester, MA, 10609 USA. Email: ted@wpi.edu.

Abstract:

BACKGROUND: Traditional hand-wrist prostheses provide proportional control of only 1 degree of freedom (DoF) at a time, requiring the user to mode-switch between them. Research using large numbers of electrodes on able-bodied subjects has related the EMG of the forearm muscles to two degrees of freedom at the wrist. Initial evaluation in limb-absent subjects also shows this relationship, albeit with higher errors. However, using such large numbers of electrodes in a commercial prosthesis is not presently practical. Hence, we studied the ability to extract EMG-force information using a minimum number of electrodes.

METHODS: For 10 able-bodied subjects, 16 conventional bipolar electrodes were mounted transversely about the proximal forearm. The hand was secured to a load cell which measured forces generated during wrist extension-flexion, radial-ulnar deviation and pronation-supination. A screen target produced slowly-moving (quasi-static) force targets along one of these three contraction

dimensions per trial, and also produced targets with equal levels of co-contraction for pairs of dimensions (2-DoF tasks). Effort ranged over 0–30% MVC. Linear, static, 1-DoF and 2-DoF models relating EMG amplitude to force were then trained, using regularized linear least squares. Initially, all 16 electrodes were used as inputs. Thereafter, backward stepwise selection of the training data sequentially reduced the number of electrodes. RMS error on a separate test trial was evaluated at each step.

RESULTS: For 1-DoF models, stepping down to fewer than two electrodes was unacceptable; and retaining more than two electrodes provided limited benefit. This result was expected and consistent with existing prosthesis practice. With 2 electrodes, the 1-DoF average error ranged from 6.5–9.5%, depending on the DoF; pronation-supination exhibited the highest errors. For 2-DoF tasks, there was little or no change in error stepping from 16 down to 4 electrodes. Errors generally increased progressively as the number of selected electrodes decreased from 4 to 1. With 4 electrodes, the 2-DoF error averaged 6.3–8.1%, depending on the DoFs. Minimum errors occurred when combining flexion-extension with ulnar-radial deviation.

This experiment was piloted with 4 unilateral limb-absent subjects. Force was measured from their sound side and mirrored contractions produced on the limb-absent side. Electrodes were mounted on the limb-absent side. For 1-DoF models using 2 electrodes, errors ranged from 12.8–18.3%, depending on the DoF. For 2-DoF models using 4 electrodes, errors ranged from 13.8–16.1%. Result trends matched those of the able-bodied subjects, but with higher errors overall.

CONCLUSION: These results are encouraging that as few as 4 conventional electrodes, optimally located about the forearm, could provide 2 DoFs of simultaneous, independent and proportional control with error rates similar to the 1-DoF approach currently used for commercial prosthesis control.